

อนุภาคนาโนโคโรซานตัวพาออก-ทรานส์-เรตินิล อะซิเตอท์: ลักษณะสมบัติและการปลดปล่อย  
แบบควบคุม



นางสาว มยุรา วิริยะศุภร

สถาบันวิทยบริการ  
วิทยานิพนธ์นี้เป็นส่วนหนึ่งของการศึกษาตามหลักสูตรปริญญาวิทยาศาสตรมหาบัณฑิต  
จุฬาลงกรณ์มหาวิทยาลัย  
สาขาวิชาเทคโนโลยีชีวภาพ

คณะวิทยาศาสตร์ จุฬาลงกรณ์มหาวิทยาลัย

ปีการศึกษา 2550

ลิขสิทธิ์ของจุฬาลงกรณ์มหาวิทยาลัย

CHITOSAN NANOPARTICLE AS ALL-TRANS-RETINYL ACETATE CARRIER  
: CHARACTERIZATION AND CONTROLLED RELEASE



Miss Mayura Wittayasuporn

สถาบันวิทยบริการ

จุฬาลงกรณ์มหาวิทยาลัย  
A Thesis Submitted in Partial Fulfillment of the Requirements  
for the Degree of Master of Science Program in Biotechnology

Faculty of Science

Chulalongkorn University

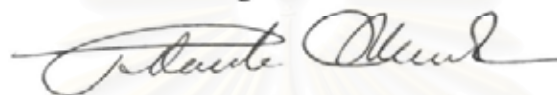
Academic Year 2007

Copyright of Chulalongkorn University

Thesis Title CHITOSAN NANOPARTICLE AS ALL-TRANS-RETINYL  
ACETATE CARRIER: CHARACTERIZATION AND CONTROLLED  
RELEASE  
By Miss Mayura Wittayasuporn  
Field of Study Biotechnology  
Thesis Advisor Associate Professor Supason Wanichweacharunguang, Ph.D.  
Thesis Co-advisor Associate Professor Sirirat Rengpipat, Ph.D.

---

Accepted by the Faculty of Science, Chulalongkorn University in Partial Fulfillment of  
the Requirements for the Master's Degree

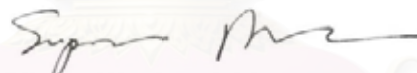


.....Dean of the Faculty of Science  
(Professor Piamsak Menasveta, Ph.D.)

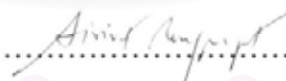
#### THESIS COMMITTEE



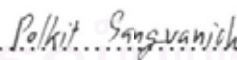
.....Chairman  
(Associate Professor Sirirat Kokpol, Ph.D.)



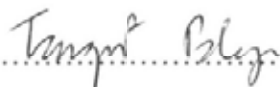
.....Thesis Advisor  
(Associate Professor Supason Wanichweacharunguang, Ph.D.)



.....Thesis CO-advisor  
(Associate Professor Sirirat Rengpipat, Ph.D.)



.....Member  
(Associate Professor Polkit Sangvanich, Ph.D.)



.....Member  
(Assistant Professor Tanapat Palaga, Ph.D.)

มยุรา วิหะศุภกร : อนุภาคนาโนโคโคซานตัวพาออล-ทรานส์-เรตินิล อะซิเตรท: ลักษณะสมบัติและการปลดปล่อยแบบควบคุม. (CHITOSAN NANOPARTICLE AS ALL-TRANS-RETINYL ACETATE CARRIER: CHARACTERIZATION AND CONTROLLED RELEASE) อ. ที่ปรึกษา: รศ. ดร. ศุภสร วนิชเวหารุ่งเรือง, อ. ที่ปรึกษา ร่วม: รศ.ดร.ศิริรัตน์ เร่งพิพัฒน์, 119 หน้า.

ในงานวิจัยนี้ได้ทำการสังเคราะห์อนุภาคเอมเพกฟทาโลอิลโคโคซาน และเอมเพก-4-เมทอกซีซินนาโมอิลฟทาโลอิลโคโคซานขึ้นจากนั้นนำอนุพันธ์โคโคซานทั้งสองมาเตรียมเป็นอนุภาคนาโนด้วยวิธีโซลเวนต์สเฟสเมเนตต์ ได้อนุภาคที่มีขนาดเฉลี่ย 50-60 นาโนเมตร และมีประจุลบ (- 23 ถึง -30 มิลลิโวลต์) การศึกษาสมบัติการต้านเชื้อแบคทีเรียของอนุภาคนาโนโคโคซานทั้งสองพบว่าสามารถยับยั้งการเจริญของแบคทีเรีย *Staphylococcus aureus* ATCC 25923 และ *Escherichia coli* ATCC 25922 ได้ การศึกษาค่าความเป็นพิษต่อเซลล์มนุษย์ของอนุภาคนาโนโคโคซานทั้งสองพบว่าอนุภาคทั้งสองชนิดไม่มีความเป็นพิษต่อเซลล์มะเร็งผิวหนังของมนุษย์ นอกจากนี้ได้ทำการกักเก็บออล-ทรานส์เรตินิลอะซิเตรทลงในอนุภาคทั้งสองการศึกษาพฤติกรรม การปลดปล่อยแบบควบคุมของออล-ทรานส์เรตินิลอะซิเตรทที่ถูกกักเก็บอยู่ในอนุภาคทั้งสองที่ภาวะความเป็นกรด-ด่างต่างๆพบว่า มีการปลดปล่อยออล-ทรานส์เรตินิลอะซิเตรทออกมามากที่สุดเมื่ออนุภาคอยู่ในภาวะที่เป็นกลาง

## สถาบันวิทยบริการ จุฬาลงกรณ์มหาวิทยาลัย

สาขาวิชา.....เทคโนโลยีชีวภาพ..... ลายมือชื่อนิสิต..... พ.ร.ร. วิหะศุภกร.....  
ปีการศึกษา.....2550.....ลายมือชื่ออาจารย์ที่ปรึกษา.....  
ลายมือชื่ออาจารย์ที่ปรึกษาร่วม.....

# # 4872416123: MAJOR BIOTECHNOLOGY

KEY WORD: DRUG DELIVERY/ CHITOSAN/ ANTIBACTERIAL/ ALL-TRANS  
RETINYL ACETATE

MAYURA WITTAYASUPORN: CHITOSAN NANOPARTICLE AS ALL-  
TRANS-RETINYL ACETATE CARRIER: CHARACTERIZATION AND  
CONTROLLED RELEASE. THESIS ADVISOR: ASSOC. PROF.  
SUPASON WANICHWEACHARUNGRUANG, Ph.D., THESIS  
COADVISOR: ASSOC. PROF. SIRIRAT RENGPIPAT, Ph.D. 119 pp.

In this work, mPEG-phthaloylchitosan (PPLC) and mPEG-4-methoxycinnamoylphthaloylchitosan (PCPLC) were synthesized. The PPLC and PCPLC were induced into nanoparticle by solvent displacement method. Their size and zeta potential were in the range of 50-60 nm and -23-30 mV, respectively. The antibacterial activity of mPEG-phthaloylchitosan (PPLC) and mPEG-4-methoxycinnamoylphthaloylchitosan (PCPLC) nanoparticles was evaluated by a turbidity method. Result showed that both nanoparticles could inhibit the growth of the *Staphylococcus aureus* ATCC 25923 and *Escherichia coli* ATCC 25922. Cytotoxicity evaluation of both nanoparticles indicated that both nanoparticles were not harmful to human melanoma skin cell lines. In addition, All-*trans* retinyl acetate (ATRA) was loaded into both nanoparticles. Study of the pH effect (pH 4, 7 and 10) on release behaviors of ATRA from particles was investigated by dialysis method. The results indicated that the ATRA release was maximum at neutral pH.

สถาบันวิทยบริการ  
จุฬาลงกรณ์มหาวิทยาลัย

Field of Study..... Biotechnology.....Student's signature...Mayura Wittayasuporn  
Academic Year.....2007.....Advisor's signature...  
Co-advisor's signature...  
Siri R. Rengpipat

## ACKNOWLEDGEMENTS

First of all, I would like to express my sincere appreciation and gratitude to my advisor, Associate Professor Dr. Supason Wanichweacharungruang and my Co-advisor, Associate Professor Dr. Sirirat Rengpipat for her helpful this research, valuable assistance and generous encouragement throughout the course of this research. Also thank for the valuable suggestions to Assistant Professor Dr. Tanapat Palaga for his helpful and comment in this research.

Gratefully thanks are extended to Graduate School, Chulalongkorn University and National Research Council of Thailand for granting financial support to fulfill this thesis.

Finally, I would like to special thank my family, Ms. Nattaporn Anumansirikul, Ms. Pakamas Vongtae and research group members for their helpful this research and encouragement throughout my entire education.



สถาบันวิทยบริการ  
จุฬาลงกรณ์มหาวิทยาลัย

# CONTENTS

	<b>Pages</b>
Abstract in Thai.....	iv
Abstract in English.....	v
Acknowledgements.....	vi
List of Schemes.....	x
List of Figures.....	xi
List of Tables.....	xv
List of Abbreviations.....	xix
CHAPTER I: INTRODUCTION.....	1
1.1 Chitin-chitosan.....	1
1.2 Chemical modification of chitosan .....	2
1.3 Antibacterial activity of chitosan.....	7
1.4 Drug delivery system of chitosan.....	8
1.4.1 Vehicles for drug delivery.....	9
1.4.2 Parameters affecting the release characteristics of drugs from chitosan micro/nanospheres.....	12
1.5 Retinol.....	13
1.6 Literature reviews.....	15
1.5 Research goals.....	19
CHAPTER II: EXPERIMENTAL.....	21
2.1 Materials and Chemicals.....	21
2.2 Instruments and Equipments.....	22
2.3 Synthesis of Phthaloylchitosan (PLC).....	23
2.4 Synthesis of poly(ethylene glycol) methyl ether terminated with carboxylic groups (mPEG-COOH).....	24
2.5 Synthesis of mPEG-Phthaloylchitosan (PPLC).....	25
2.6 Synthesis of mPEG-4-Methoxycinnamoylphthaloylchitosan (PCPLC).....	26
2.7 Antibacterial study.....	27
2.7.1 Preparation of bacteria.....	27

2.7.2 Determination of MIC.....	27
2.7.3 Determination of MBC.....	28
2.7.4 Survival of bacteria.....	28
2.8 Cytotoxicity study of mPEG–phthaloylchitosan (PPLC) and mPEG-4-methoxycinnamoyl-phthaloylchitosan nanoparticles (PCPLC).....	29
2.8.1 Cell culture and treatment.....	29
2.8.2 Assessment of cytotoxicity by MTT assay.....	29
2.9 Encapsulation of ATRA into nanoparticles.....	30
2.10 Differential scanning calorimetry.....	30
2.11 Morphology and zeta potential of chitosan nanoparticles...	30
2.12 <i>In vitro</i> release.....	31
CHAPTER III: RESULT AND DISCUSSION.....	32
3.1 Characterization of Phthaloylchitosan, mPEG- Phthaloylchitosan and mPEG-4-Methoxycinnamoyl phthaloylchitosan .....	32
3.1.1 Phthaloylchitosan.....	33
3.1.2 Poly(ethylene glycol)methyl ether terminated with Carboxylic Groups.....	36
3.1.3 mPEG-Phthaloylchitosan.....	37
3.1.4 mPEG-4-Methoxycinnamoylphthaloylchitosan.....	41
3.2 Antibacterial study.....	44
3.2.1 Determination of MIC and MBC.....	44
3.2.2 Survival of bacteria.....	46
3.3 Cytotoxicity study of mPEG–Phthaloylchitosan (PPLC) and mPEG-4-Methoxycinnamoylphthaloylchitosan nanoparticles (PCPLC).....	48
3.4. Encapsulation of all- <i>trans</i> retinyl acetate (ATRA) into nanoparticles.....	49
3.5 <i>In vitro</i> release.....	53
3.6 Differential scanning calorimetry.....	55
3.7 Morphology, size distribution and zeta potential of chitosan nanoparticles.....	62



CHAPTER IV: CONCLUSION.....	66
REFERENCES.....	68
APPENDICES.....	81
Appendix A.....	82
Appendix B.....	89
Appendix C.....	100
VITA.....	119



สถาบันวิทยบริการ  
จุฬาลงกรณ์มหาวิทยาลัย

## List of Schemes

Schemes	Pages
1.1 Deacetylation of chitin to chitosan.....	1
1.2 Acylation reaction.....	3
1.3 Phthaloylation reaction .....	3
1.4 Synthesis of cyclodextrin-linked chitosan.....	4
1.5 Grafting of poly(ethylene glycol) onto chitosan by reductive alkylation with PEG-aldehyde derivative.....	5
1.6 Chemical structure of <i>N</i> -methylene phosphoric chitosan.....	5
1.7 Strategy for the substitution of sugars to chitosan by reductive <i>N</i> - alkylation.....	6
1.8 <i>N</i> -carboxymethylation of chitosan.....	7
2.1 Synthesis of Phthaloylchitosan (PLC).....	23
2.2 Synthesis of poly(ethylene glycol) methyl ether terminated with carboxylic groups (mPEG-COOH).....	24
2.3 Synthesis of mPEG-Phthaloylchitosan (PPLC).....	25
2.4 Synthesis of mPEG-4-Methoxycinnamoylphthaloylchitosan (PCPLC).....	26
3.1 Synthesis of phthaloylchitosan, mPEG-Phthaloylchitosan and mPEG-4-Methoxycinnamoylphthaloylchitosan.....	32
3.2 Synthesis of Phthaloylchitosan.....	33
3.3 Synthesis of poly (ethylene glycol) methyl ether terminated with carboxylic groups (mPEG-COOH).....	36
3.4 Synthesis of mPEG-phthaloylchitosan.....	37
3.5 Synthesis of mPEG-4-methoxycinnamoylphthaloylchitosan.....	41

## List of Figures

Figures	Pages
1.1 EDTA grafted chitosan.....	8
1.2 Structure of liposome.....	9
1.3 Nanoemulsion: Lipid monolayer enclosing a liquid lipid core.....	10
1.4 Structure of micro/nanoparticle.....	11
1.5 Chemical structure of retinol and its derivatives.....	14
3.1 IR spectra (KBr) of a.) chitosan and b.) phthaloylchitosan.....	33
3.2 $H^1$ -NMR spectrum of Phthaloylchitosan (PLC) (DMSO deuterated with 0.05% TFA).....	34
3.3 UV absorption spectrum of phthaloylchitosan (PLC) in DMSO at concentration 60 ppm.....	35
3.4 IR spectra (KBr) of a.) mPEG and b.) mPEG-COOH.....	36
3.5 IR spectra (KBr) of a) chitosan, b) phthaloylchitosan and c) mPEG-phthaloylchitosan (PPLC).....	38
3.6 $H^1$ -NMR spectrum of mPEG–phthaloylchitosan (PPLC) (DMSO deuterated with 0.05% trifluoroacetic acid).....	39
3.7 UV absorption spectra of Phthaloylchitosan (PLC) and mPEG–phthaloylchitosan (PPLC) in DMSO at concentration 60 ppm.....	39
3.8 IR spectra (KBr) of a) chitosan, b) phthaloylchitosan and c) mPEG-4-methoxycinnamoyl phthaloylchitosan (PCPLC).....	42
3.9 $H^1$ -NMR spectrum of mPEG-4-methoxycinnamoylphthaloylchitosan (PCPLC, DMSO deuterated).....	43
3.10 UV absorption spectrum of mPEG-4-methoxycinnamoyl phthaloylchitosan (PCPLC) in DMSO at concentration 60 ppm.....	44
3.11 Absorbance difference between 0 h. and 24 h. of bacterial growth after treated with chitosan nanoparticles (PPLC and PCPLC), clindamycin. Control was the culture in Tryptic soy broth.....	47
3.12 The percentage reduction of bacteria after treated with chitosan nanoparticle and clindamycin.....	48

3.13	Cytotoxic effect induced by PPLC and PCPLC on A375 cell line. Cells were incubated with nanoparticles for 72 h. at a concentration of 0.25, 0.025 and 0.0025 mg/ml. ....	49
3.14	TEM photographs of (a) unencapsulated PPLC nanoparticle and (b) ATRA-encapsulated PPLC nanoparticle at concentration 600 ppm.....	50
3.15	TEM photographs of (a) unencapsulated PCPLC nanoparticle and (b) ATRA-encapsulated nanoparticle at concentration 600 ppm.....	51
3.16	NMR spectrum of ATRA loaded mPEG-phthaloylchitosan nanoparticles. (PPLC, DMSO deuterated with 0.05% trifluoroacetic acid).....	51
3.17	NMR spectrum of ATRA loaded mPEG-4-methoxycinnamoyl phthaloylchitosan nanoparticles. (PCPLC, DMSO deuterated with 0.05% trifluoroacetic acid).....	52
3.18	SEM photographs of unencapsulated PPLC nanoparticle (a), 10% ATRA-loaded PPLC nanoparticle (b), 25% ATRA-loaded PPLC nanoparticle (c) and 50% ATRA-loaded PPLC nanoparticle (d) at concentration 600 ppm.....	56
3.19	SEM photographs of unencapsulated PCPLC nanoparticle (a), 10% ATRA-loaded PCPLC nanoparticle (b), 25% ATRA-loaded PCPLC nanoparticle (c) and 50% ATRA-loaded PCPLC nanoparticle at concentration 600 ppm.....	57
3.20	Size distribution profiles of mPEG–phthaloylchitosan (PPLC) nanoparticles and 10%, 25% and 50% ATRA-loaded PPLC nanoparticles at concentration 600 ppm.....	58
3.21	Size distribution profiles of mPEG-4-methoxycinnamoyl phthaloylchitosan (PCPLC) nanoparticles and 10%, 25% and 50% ATRA-loaded PPLC nanoparticles at concentration 600 ppm.....	59
3.22	Zeta potential profiles of mPEG–phthaloylchitosan (PPLC) and mPEG-4-methoxycinnamoylphthaloylchitosan (PCPLC) nanoparticles at concentration 600 ppm.....	59

3.23	TEM photograph of PPLC before (a.) and after 10% ATRA (b.), 25% ATRA (c.) and 50% ATRA (d.) to polymer encapsulation at 600 ppm.....	60
3.24	TEM photograph of PCPLC before (a.) and after 10% ATRA (b.), 25% ATRA (c.) and 50% ATRA (d.) to polymer encapsulation at 600 ppm.....	61
3.25	Size and morphology of 10,000 ppm PPLC nanoparticles: a) before and b) after autoclave at 110 °C, 10 minute, 1 bar/sq inch.....	61
3.26	Size and morphology of 10,000 ppm PCPLC: a) before and b) after autoclave at 110 °C, 10 minute, 1 bar/sq inch.....	62
3.27	<i>In vitro</i> release profile of ATRA from the PPLC nanoparticles in PBS at pH 4, pH 7 and pH 10 for 72 h.....	63
3.28	<i>In vitro</i> release profile of ATRA from the PCPLC nanoparticles in PBS at pH 4, pH 7 and pH 10 for 72 h.....	64
A.1	Calibration curve of all- <i>trans</i> retinyl acetate in ethanol solution.....	82
A.2	UV absorption spectra of all- <i>trans</i> retinyl acetate was adhered at the outside of mPEG-phthalylchitosan nanoparticle in ethanol solution.....	82
A.3	UV absorption spectra of all- <i>trans</i> retinyl acetate adhered at the outside of mPEG-4-methoxycinnamoylphthaloylchitosan nanoparticle in ethanol solution.....	85
B.1	NMR spectrum of phthaloylchitosan (DMSO deuterated with 0.05% trifluoroacetic acid).....	89
B.2	NMR spectrum of mPEG-phthaloylchitosan (DMSO deuterated with 0.05% trifluoroacetic acid).....	90
B.3	NMR spectrum of mPEG-4-Methoxycinnamoylphthaloylchitosan (DMSO deuterated with 0.05% trifluoroacetic acid).....	91
B.4	First run differential scanning calorimetry (DSC) curve of all- <i>trans</i> retinyl acetate.....	92
B.5	Second run differential scanning calorimetry (DSC) curve of chitosan.....	93

B.6	Second run differential scanning calorimetry (DSC) curve of mPEG-phthaloylchitosan nanoparticle.....	94
B.7	Second run differential scanning calorimetry (DSC) curve of mPEG-phthaloylchitosan non-nanostructure.....	95
B.8	Second run differential scanning calorimetry (DSC) curve of ATRA-encapsulated mPEG-phthaloylchitosan nanoparticle.....	96
B.9	Second run differential scanning calorimetry (DSC) curve of mPEG-4-methoxycinnamoylphthaloylchitosan nanoparticle.....	97
B.10	Second run differential scanning calorimetry (DSC) curve of mPEG-4-methoxycinnamoylphthaloylchitosan non-nanostructured.....	98
B.11	Second run differential scanning calorimetry (DSC) curve of ATRA-encapsulated mPEG-4-methoxycinnamoylphthaloylchitosan nanoparticle.....	99
C.1	Growth curve of Gram-positive bacteria <i>Staphylococcus aureus</i> ATCC 25923 in Tryptic soy broth.....	101
C.2	Log CFU of Gram-positive bacteria, <i>Staphylococcus aureus</i> ATCC 25923 in Tryptic soy agar.....	101
C.3	Growth curve of Gram-negative bacteria, <i>Escherichia coli</i> ATCC 25922 in Tryptic soy broth.....	103
C.4	Log CFU of Gram-negative bacteria, <i>Escherichia coli</i> ATCC 25922 in Tryptic soy agar.....	103

## List of Tables

Tables	Pages
3.1	MIC and MBC ( $\mu\text{g}/\text{mL}$ ) of chitosan solution, chitosan nanoparticles and clindamycin against bacteria tester..... 45
3.2	Drug loading (% loading) and encapsulation efficiency percentages (%EE) of 600 ppm ATRA-encapsulated PPLC and PCPLC nanoparticles..... 53
3.3	Thermal properties of chitosan (CS), mPEG-phthaloylchitosan (PPLC), mPEG-4-methoxycinnamoyl phthaloylchitosan (PCPLC), and their ATRA-loaded and unloaded nanoparticles.....54
3.4	The percentage of ATRA released total and release rate of ATRA from PPLC nanoparticle..... 64
3.5	The percentage of ATRA released total and release rate of ATRA from PCPLC nanoparticle.....65
C.1	Growth rate of Gram-positive bacteria <i>Staphylococcus aureus</i> ATCC 25923 in Tryptic soy broth..... 100
C.2	Growth rate of Gram-negative bacteria, <i>Escherichia coli</i> ATCC 25922 in Tryptic soy broth..... 102
C.3	Growth of Gram-positive bacteria, <i>Staphylococcus aureus</i> ATCC 25923 after treated with mPEG-phthaloylchitosan nanoparticle (PPLC) for 24 h at various concentrations..... 104
C.4	Growth of Gram-positive bacteria, <i>Staphylococcus aureus</i> ATCC 25923 after treated with mPEG-4-methoxycinnamoylphthaloylchitosan nanoparticle (PCPLC) for 24 h at various concentrations..... 104
C.5	Growth of Gram-positive bacteria, <i>Staphylococcus aureus</i> ATCC 25923 after treated with chitosan for 24 h at various concentrations..... 105
C.6	Growth of Gram-positive bacteria, <i>Staphylococcus aureus</i>

	ATCC 25923 after treated with clindamycin for 24 h at various concentrations.....	105
C.7	Growth of untreated Gram-positive bacteria, <i>Staphylococcus aureus</i> ATCC 25923 after incubated for 24 h.....	106
C.8	Growth of <i>Staphylococcus aureus</i> ATCC 25923 after tested with mPEG-phthaloylchitosan by a loopful on Tryptic soy agar.....	106
C.9	Growth of <i>Staphylococcus aureus</i> ATCC 25923 after tested with mPEG-4-methoxycinnamoylphthaloylchitosan by a loopful on Tryptic soy agar.....	107
C.10	Growth of <i>Staphylococcus aureus</i> ATCC 25923 after tested with chitosan by a loopful on Tryptic soy agar.....	107
C.11	Growth of <i>Staphylococcus aureus</i> ATCC 25923 after tested with clindamycin by a loopful on Tryptic soy agar.....	108
C.12	Growth of Gram-negative bacteria, <i>Escherichia coli</i> ATCC 25922 after treated with mPEG-phthaloylchitosan nanoparticle (PPLC) for 24 h at various concentrations.....	108
C.13	Growth of Gram-negative bacteria, <i>Escherichia coli</i> ATCC 25922 after treated with mPEG-4- methoxycinnamoylphthaloylchitosan nanoparticle (PCPLC) for 24 h at various concentrations.....	109
C.14	Growth of Gram-negative bacteria, <i>Escherichia coli</i> ATCC 25922 after treated with chitosan for 24 h at various concentrations.....	109
C.15	Growth of Gram-negative bacteria, <i>Escherichia coli</i> ATCC 25922 after treated with clindamycin for 24 h at various concentrations.....	110
C.16	Growth of untreated Gram-negative bacteria, <i>Escherichia coli</i> ATCC 25922 after incubated for 24 h.....	110
C.17	Growth of <i>Escherichia coli</i> ATCC 25922 after tested with mPEG-phthaloylchitosan by a loopful on Tryptic soy agar.....	111



C.18	Growth of <i>Escherichia coli</i> ATCC 25922 after tested with mPEG-4-methoxycinnamoyl-phthaloylchitosan by a loopful on Tryptic soy agar.....	111
C.19	Growth of <i>Escherichia coli</i> ATCC 25922 after tested with chitosan by a loopful on Tryptic soy agar.....	112
C.20	Growth of <i>Escherichia coli</i> ATCC 25922 after tested with clindamycin by a loopful on Tryptic soy agar.....	112
C.21	Growth of Gram-positive bacteria, <i>Staphylococcus aureus</i> ATCC 25923 after treated with mPEG-phthaloylchitosan nanoparticle (PPLC) for 24 h at concentration 2500 µg/mL.....	113
C.22	Growth of Gram-positive bacteria, <i>Staphylococcus aureus</i> ATCC 25923 after treated with mPEG-4-Methoxycinnamoylphthaloylchitosan nanoparticle (PCPLC) for 24 h at concentration 5000 µg/mL .....	113
C.23	Growth of Gram-positive bacteria, <i>Staphylococcus aureus</i> ATCC 25923 after treated with clindamycin for 24 h at concentration 250 µg/mL .....	114
C.24	Growth of untreated Gram-positive bacteria, <i>Staphylococcus aureus</i> ATCC 25923 after incubated for 24 h.....	114
C.25	Log CFU/mL of Gram-positive bacteria, <i>Staphylococcus aureus</i> ATCC 25923 after treated with mPEG-phthaloylchitosan nanoparticle (PPLC) at concentration 2500 µg/mL for 24 h.....	114
C.26	Log CFU/mL of Gram-positive bacteria, <i>Staphylococcus aureus</i> ATCC 25923 after treated with mPEG-4-methoxycinnamoylphthaloylchitosan nanoparticle (PCPLC) at concentration 5000 µg/mL for 24 h.....	115
C.27	Log CFU/mL of Gram-positive bacteria, <i>Staphylococcus aureus</i> ATCC 25923 after treated with clindamycin at concentration 250 µg/mL for 24 h.....	115
C.28	Log CFU/mL of untreated Gram-positive bacteria, <i>Staphylococcus aureus</i> ATCC 25923 after incubated for 24 h.....	115

C.29	Growth of Gram-negative bacteria, <i>Escherichia coli</i> ATCC 25922 after treated with mPEG-phthaloylchitosan nanoparticle (PPLC) for 24 h at concentration 5000 µg/mL .....	116
C.30	Growth of Gram-negative bacteria, <i>Escherichia coli</i> ATCC 25922 after treated with mPEG-4- methoxycinnamoylphthaloylchitosan nanoparticle (PCPLC) for 24 h at concentration 5000 µg/mL .....	116
C.31	Growth of Gram-negative bacteria, <i>Escherichia coli</i> ATCC 25922 after treated with clindamycin for 24 h at concentration 2500 µg/mL.....	117
C.32	Growth of untreated Gram-negative bacteria, <i>Escherichia coli</i> ATCC 25922 after incubated for 24 h.....	117
C.33	Log CFU/mL of untreated Gram-negative bacteria, <i>Escherichia coli</i> ATCC 25922 after treated with mPEG-phthaloylchitosan nanoparticle (PPLC) at concentration 5000 µg/mL for 24 h.....	117
C.34	Log CFU/mL of untreated Gram-negative bacteria, <i>Escherichia coli</i> ATCC 25922 after treated with mPEG-4- methoxycinnamoylphthaloylchitosan nanoparticle (PCPLC) at concentration 5000 µg/mL for 24 h.....	118
C.35	Log CFU/mL of untreated Gram-negative bacteria, <i>Escherichia coli</i> ATCC 25922 after treated with clindamycin at concentration 2500 µg/mL for 24 h.....	118
C.36	Log CFU/mL of untreated Gram-negative bacteria, <i>Escherichia coli</i> ATCC 25922 after incubated for 24 h.....	118

## List of Abbreviations

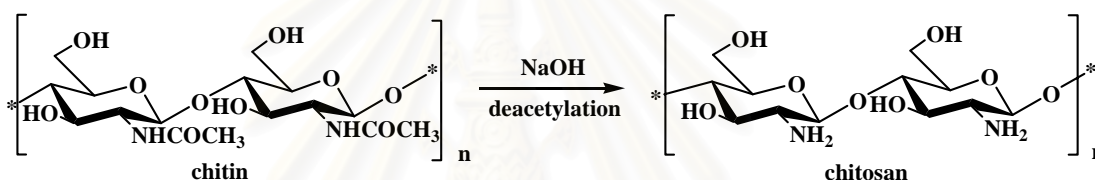
°C	degree Celsius
cm <sup>-1</sup>	per centimeter (s)
cm <sup>-1</sup>	unit of wavenumber (IR)
MW	molecular weight
nm	nanometer (s)
Hz	hertz
mJ	millijoule
mW	milliwatt
mV	millivolt
IR	Infrared
h	hour
min.	minute
g	gram (s)
mL	milliliter (s)
NMR	nuclear magnetic resonance
SEM	Scanning electron microscope
TEM	Transmission electron microscope
%	Percent
λ	wavelength
ppm	parts per million
UV	ultraviolet
ATRA	all- <i>trans</i> retinyl acetate
EDCI	1-(3-dimethylaminopropyl)-3-ethylcarbodiimide hydrochloride
DMSO	dimethyl sulfoxide
DMF	dimethyl formamide
PLC	Phthaloylchitosan
PPLC	mPEG-Phthaloylchitosan
PCPLC	mPEG-4-Methoxycinnamoylphthaloylchitosan

# CHAPTER I

## INTRODUCTION

### 1.1 Chitin-chitosan

Chitin is a linear polymer of *N*-acetyl-2-amino-2-deoxy-deglucopyranose units linked  $\beta$ -(1-4) bonds. It is distributed widely in nature as the skeletal material of crustaceans, insects and as a component of cell walls of bacteria and fungi [1]. When the degree of deacetylation of chitin reaches about 50%, it becomes soluble in aqueous acidic media and is called chitosan [2].



**Scheme 1.1** Deacetylation of chitin to chitosan

Thus, chitosan is a linear polymer of glucosamine and *N*-acetylglucosamine units linked by 1-4 glucosidic bonds [3]. Much attention has been paid recently to chitin and chitosan in agricultural, food, industrial, and medical fields such as biomedicine, pharmacology, and biotechnology due to their biological activities including biocompatibility, biodegradability, nontoxicity, mucoadhesivity, bacteriostatic activities [1-5]. Therefore, chitin and chitosan are interesting functional polysaccharides as well as abundant resources. The presence of amino groups in chitin and chitosan is highly advantageous for providing unique biological and chemical functions and for conducting chemical modification reactions. Reactive functional groups in chitosan include an amino group at C-2 as well as both primary and secondary hydroxyl groups at the C-3, and C-6 positions [6-8]. These groups allow various chemical modifications of chitosan such as acylation, *N*-phthaloylation, tosylation, alkylation, Schiff base formation, reductive alkylation, *O*-carboxymethylation, *N*-carboxyalkylation, silylation, and graft copolymerization [2-9]. Chemical modifications of these groups resulted in the production of numerous

useful derivatives for specific applications. Chitosan has limited application because it is insoluble in neutral, alkaline media and most organic solvents. Recently researchers have shown that improved water solubility and bioactivities properties could be found in modified chitosan [6-11].

The most important fields of chitosan must be recognized are cosmetics (especially for hair care in relation to electrostatic interactions) and the pharmaceutical and biomedical applications. Chitosan and its derivatives have been used for drug delivery applications include oral, nasal, parenteral and transdermal administration, and gene delivery. Chitosan derivatives had been used for gene transfection. *N*-alkylated chitosan were prepared, it shown that transfection efficiency increases upon elongating the alkyl side chains [12]. In addition, Chitosan has also been used as a potential carrier for prolonged delivery of drugs, macromolecules and targeted drug delivery. Magnetic chitosan microspheres used in targeted drug delivery are expected to be retained at the target site capillaries under the influence of an external magnetic field [13].

Another point to note is biological activity in regard to agriculture since chitosan exhibits antiviral and antiphage activities. It inhibits the growth of bacteria and bacterial infection, and stimulates the natural defenses in plants. A mechanism has been proposed via the "octadecanoid pathway" [14].

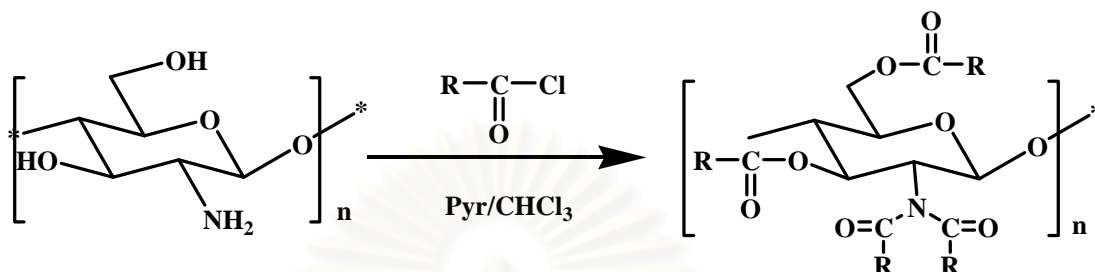
## **1.2 Chemical modification of chitosan**

Although chitosan would be expected to attract even more numerous applications because it is cheap, biocompatible, biodegradable and non-toxic, but its use limit only dissolved in acetic media owing to its compact crystalline structure. Until now, much work has been reported to solve this problem by modified chitosan.

### *Acylation*

A variety of acylation reactions are possible with both chitin and chitosan. Acylation with long chain aliphatic carboxylic acid chlorides such as hexanoyl, dodecanoyl, and tetradecanoyl chlorides give derivatives with a degree of acylation of 3. Such a thoroughly acylated product is soluble in chloroform [15]. IR and thermal analyses data have revealed that chitosan with a higher degree of deacetylation was more

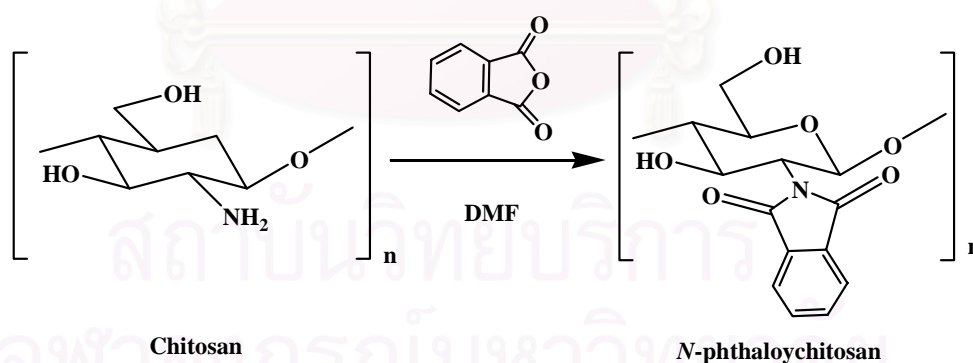
susceptible for acylation owing to a decrease in hydrogen bonding. Acylation of chitosan with a cyclic ester (lactone) such as  $\beta$ -propiolactone or  $\gamma$ -butyrolactone in an appropriate solvent gives derivatives having *N*-hydroxyalkanoyl groups [16].



**Scheme 1.2** Acylation reaction

### *N*-phthaloylation

The amino functionalities of the water-soluble chitosan can be protected with the phthalimido group, and deprotection to regenerate free amino group. In addition, phthaloylchitosan is soluble in organic solvents. The phthaloylation reaction can be accomplished by treating a chitosan suspension in DMF with excess phthalic anhydride at 120-130 °C. The resulting fully -phthaloylated chitosan was soluble in DMSO [6].

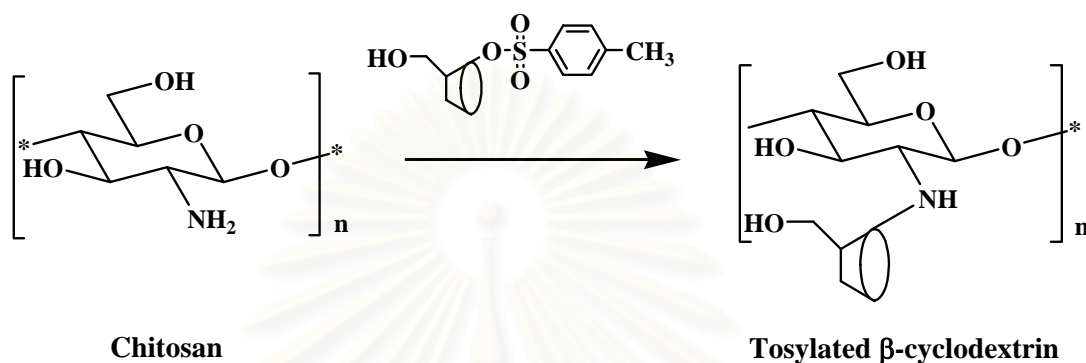


**Scheme 1.3** *N*-Phthaloylation reaction

### *Cyclodextrin-linked chitosans*

The cyclic oligosaccharides, namely  $\alpha$ - $\beta$ - $\gamma$ -cyclodextrins (CD), are important because of their ability to encapsulate hydrophobic molecules in their toroidal hydrophobic cavity, whose selectivity depends on the number of glucose units (respectively 6, 7, 8 D-glucose units) [17-19]. Cyclodextrin-linked chitosan is interesting for the viewpoint of pharmaceuticals, including drug delivery, cosmetics, and analytical

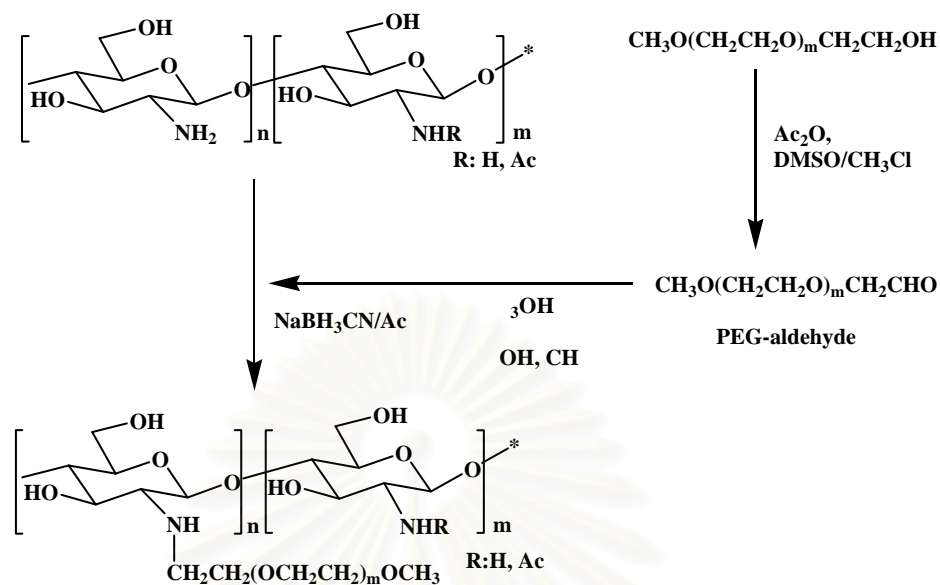
chemistry. Tosylated  $\beta$ -CD is also useful to link chitosan at the 2-position of CD, as reported by Chen et al. They applied the tosylated  $\beta$ -CD linked chitosan for slow release of radioactive iodine ( $^{131}\text{I}_2$ ) in rats [20].



**Scheme 1.4** Synthesis of cyclodextrin-linked chitosan

#### *Chitosan-grafted copolymers.*

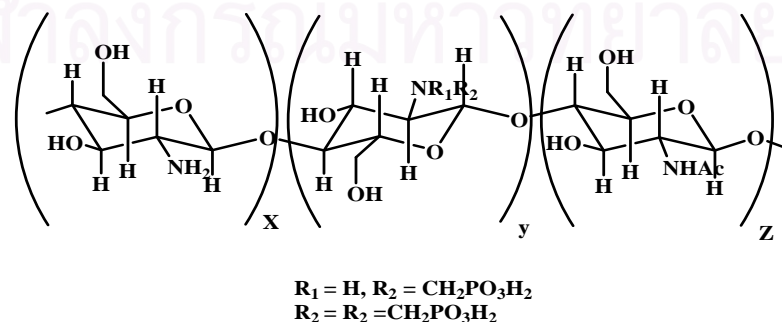
Modification chitosan with a polymer may have the advantage, because modification with a hydrophilic polymer would be expected to result in hydrophilic chitin or chitosan while keeping the fundamental skeleton intact. Some approaches for grafting of hydrophilic polymer onto chitin and chitosan were reported as a technique to improve affinity to water or organic solvents [21-23]. Poly(ethylene glycol) (PEG) is a unique polymer widely used as a pharmacological product of preferable hydrophilicity and biocompatibility with low biodegradability. Harris *et al.* published a report on the synthesis of PEG-chitosan derivative by the modification of chitosan with reductive alkylation of amino group by PEG-aldehyde (Scheme 1.4) [24]. One of the most explored chitosan derivatives is poly(ethylene glycol)-grafted chitosan, which has the advantage of being water soluble, depending on the degree of grafting: higher molecular weight PEG at low DS gives higher solubility than low molecular weight PEG [25].



**Scheme 1.5** Grafting of poly(ethylene glycol) onto chitosan by reductive alkylation with PEG-aldehyde derivative.

#### *N*-methylene phosphonic chitosans.

These interesting anionic derivatives (*N*-methylene phosphonic chitosans), with some amphoteric character were synthesized under various conditions and proved to have good complexing efficiency for cations such as  $\text{Ca}^{2+}$ , and those of transition metals (Cu (II), Cd (II), Zn (II) etc.) [26, 27]. The complexation provides corrosion protection for metal surfaces [28]. *N*-methylene phosphonic chitosans were also modified and grafted with alkyl chains to obtain amphiphilic properties that have potential applications in pharmaceutical and cosmetics field.

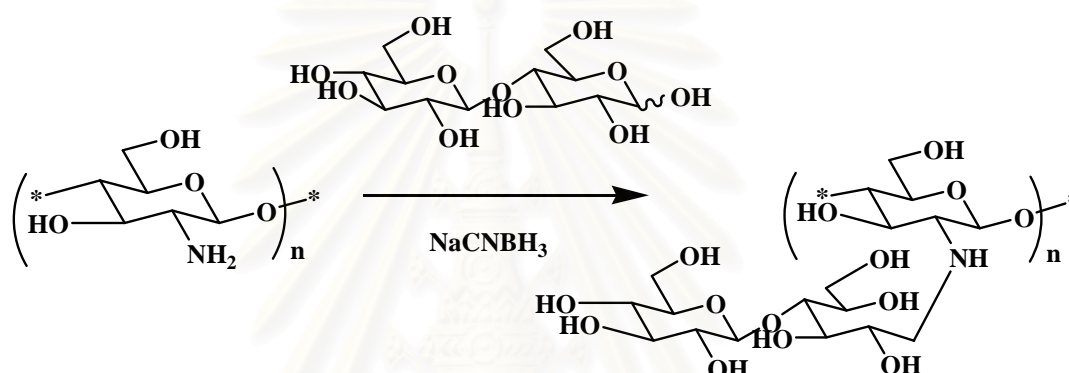


**Scheme 1.6** Chemical structure of *N*-methylene phosphoric chitosan



### Alkylated chitosans.

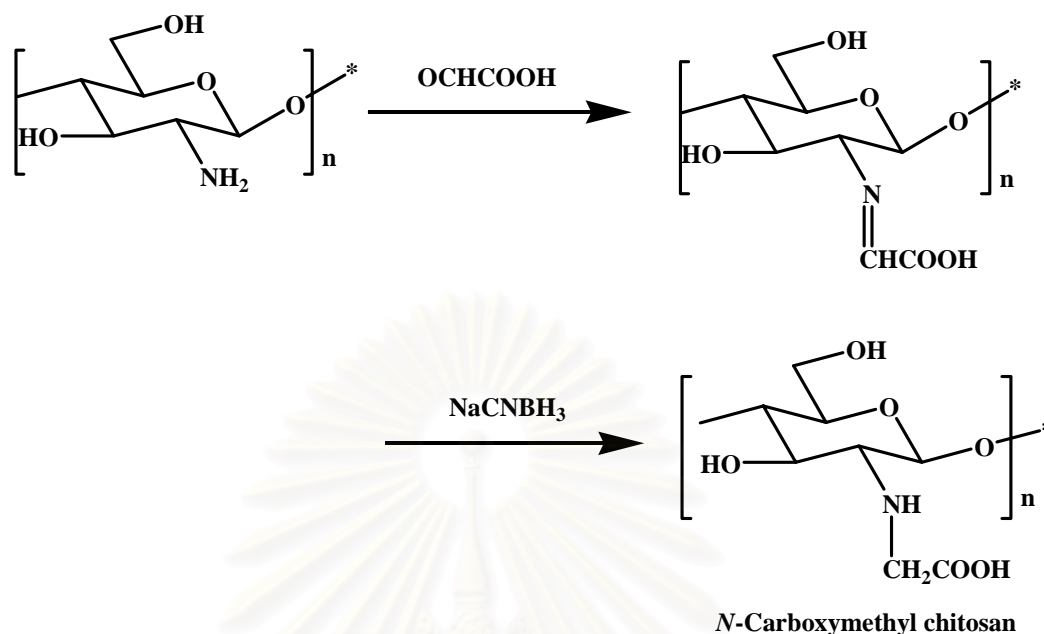
Alkylated chitosans are very important as amphiphilic polymers based on polysaccharides. The first derivative having these characteristics was a C-10-alkyl glycoside branched chitosan with a high degree of substitution (DS = 1.5), which gelled when heated over 50 °C [29]. Yalpani and Hall modified chitosan with sugars by reductive alkylation of chitosan with a series of reducing sugars. The obtained branched derivatives were soluble in water and organic solvent [30, 31].



**Scheme 1.7** Strategy for the substitution of sugars to chitosan by reductive *N*-alkylation

### *O*-and *N*-carboxymethylchitosan

The introduction of carboxy groups to chitin and chitosan derivatives leads to the anionic or amphoteric properties. Carboxymethylation of chitin with monochloro acetic acid in strong alkali conditions is a convenient method for the introduction of carboxyl groups at C-6 hydroxyl groups of chitin [32-33]. When chitosan is reacted with monochloro acetic acid in the same condition, *N,O*-carboxymethylated derivatives are obtained [34-35]. Reduction of the Schiff base formed by chitosan and aldehyde group of glyoxylic acid gives *N*-carboxymethyl chitosan derivative [36]. These derivatives are water-soluble and are attracting much attention as metal collecting materials [37-38] and biomaterials for a blood anticoagulant [39].



**Scheme 1.8** *N*-carboxymethylation of chitosan.

### 1.3 Antibacterial activity of chitosan

After the discovery of the antimicrobial activity of chitosan, many researchers have continued studies in this field. The mechanism behind this activity can be summarized as follows [40]:

(1) The cationic nature of chitosan interacting with the predominantly anionic cell wall components (lipopolysaccharides and proteins) of the microorganism, which results in the leakage of intracellular components due to changes in permeability barrier; preventing nutrients from entering the cell.

(2) Oligomeric chitosan penetrates into the cells of microorganisms and prevents the growth of cells by preventing the transformation of DNA into RNA.

Grafted chitosan presents interesting properties for wound-healing applications, because chitosan derivatives can exhibit enhanced bacteriostatic activity with respect to pure chitosan. Ethylene diamine tetraacetic acid (EDTA) grafted onto chitosan (Figure 1.1) increases the antibacterial activity of chitosan by complexing magnesium that under normal circumstances stabilizes the outer membrane of Gram-negative bacteria [41]. The increase in chitosan antimicrobial activity is also observed with carboxymethyl-chitosan, which makes essential transition metal ions unavailable for bacteria [43] or binds to the negatively charged bacterial surface to disturb the cell

membrane [42]. Therefore, the grafted chitosans are used in woundhealing systems, such as carboxymethyl-chitosan for the reduction of periodontal pockets in dentistry [43] and chitosan grafted with EDTA as a constituent of hydro- and hydro alcoholic gels for topical use [41].

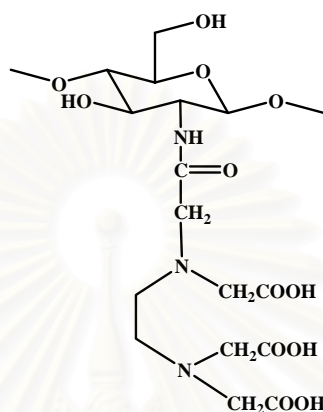


**Figure 1.1** EDTA grafted chitosan

To enhance the antibacterial potency of chitosan, thiourea chitosan was prepared by reacting chitosan with ammonium thiocyanate followed by its complexing with  $\text{Ag}^+$ . The thiourea chitosan- $\text{Ag}^+$  was against bacteria and molds [44].

#### 1.4 Drug delivery system of chitosan

Chitosan has been used as a carrier for various active agents including drugs and biologics due to its physicochemical and biological properties. It is extremely important that chitosan be hydro-soluble and positively charged. These properties enable it to interact with negatively charged polymers, macromolecules and polyanions on contact in an aqueous environment. It has the special feature of adhering to mucosal surfaces, a fact that makes it a useful polymer for mucosal drug delivery [45-48]. Chitosan has interesting biopharmaceutical characteristics such as pH sensitivity, biocompatibility and low toxicity [49-50]. Moreover, chitosan is metabolised by certain human enzymes, especially lysozyme, and is considered as biodegradable [51]. Due to these favorable properties, the interest in chitosan and its derivatives as excipients in drug delivery has been increased in recent years.

### 1.4.1 Vehicles for drug delivery

#### *Liposome*

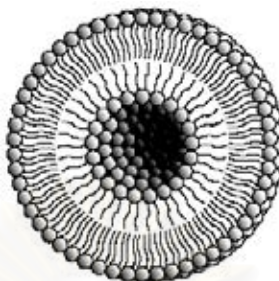


**Figure 1.2** Structure of liposome

Liposomes have been used as drug delivery systems since the 1960s [52]. Liposomes are defined as vesicles in which an aqueous volume is entirely surrounded by a phospholipid membrane [53]. Liposome size can vary from 30 nm to several micrometers, and can be uni- or multilamellar. Liposome properties have been extensively investigated and can vary substantially with desired size, lipid composition, surface charge, and method of preparation. Interest in liposomes is directed upon their vesicular structure limited by one or more outer protecting shell(s) consisting of lipids arranged in a bilayer configuration and upon their ability to interact with living cells in one of four ways: adsorption, endocytosis, lipid exchange and fusion. Depending on the method of preparation [54–56]. Sethi et al. describes various methods of liposome preparation and subsequent liposomal properties affecting drug activity [57]. Liposomes have been administered in a variety of ways but intravenous injection is the most practical route. The intracellular penetration of liposomes is effected through endocytosis when they should become localized in endosomes where degradation by phospholipases takes place [58]. A number of studies applied various surface modification approaches to classical liposomes to increase their circulation half-lives for effective passive targeting or sustained drug action. These approaches include incorporation of linear dextrans [59], sialic acid-containing gangliosides [60], and lipid derivatives of hydrophilic polymers such as PEG [61, 62], poly-*N*-vinylpyrrolidones [63] and polyvinyl alcohol [64], to provide steric stabilization around the liposomes for protection from the mononuclear phagocytic system (MPS) uptake.

As described above, liposomes have a great potential in the area of drug delivery. However, some of the problems limiting the manufacture and development of liposomes have been stability issues, batch to batch reproducibility, sterilization method, low drug entrapment, particle size control, production of large batch sizes and short circulation half-life of vesicles [65].

### *Emulsion system*

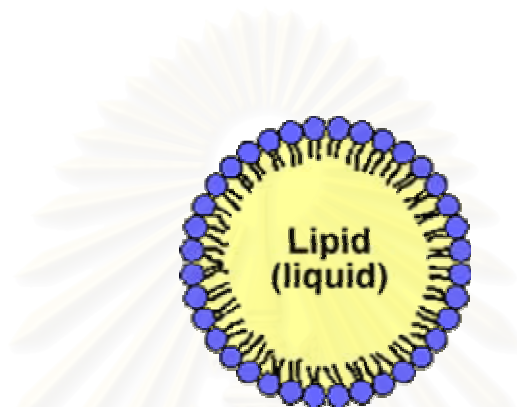


**Figure 1.3** Nanoemulsion: Lipid monolayer enclosing a liquid lipid core.

Nanoemulsions are dispersions of oil and water where the dispersed phase droplets are in the nanosize range and stabilized with a surface active film composed of surfactant and co-surfactant [66-69]. Nanoemulsions are transparent or translucent systems that have a dispersed-phase droplet size range of typically 20 to 200 nm [70], although in earlier cases these systems have also been called microemulsions. Nanoemulsions are attractive as pharmaceutical formulations because they form spontaneously, are thermodynamically stable, and optically transparent. The nanosize range of the droplets prevent creaming or sedimentation from occurring on storage and droplet coalescence. Structure of the nanoemulsion can affect the rate of drug release. *In vivo* pharmacokinetics of injectable nanoemulsions of vincristine have been investigated [71]. The researchers also found lower acute toxicity when animals were given vincristine microemulsion compared to free vincristine. This illustrated that nanoemulsions have the ability to decrease toxicity of anticancer agents by increased targeting to tumor sites. Another group of researchers incorporated poly(lactide-co-glycolide) to paclitaxel microemulsion for controlled release of paclitaxel [72]. Paclitaxel release rate was found to be retarded with increasing

molecular weight of poly(lactide-co-glycolide). However, the emulsion system also had stability problem such as changes in colour and phase separation.

#### *Micro/nanoparticle*



**Figure 1.4** Structure of micro/nanoparticle

Conveying the greater interest in liposomes with their membrane-like composition. However, the stability of liposomes is often contested and other types of carriers are studied in order to have better control over the delivery of drugs. Owing to their polymeric nature, nanoparticles may be more stable than liposomes in biological fluids and during storage. Kreuter and Speiser [73] succeeded in preparing polyacrylamide nanoparticles in the presence of antigens whilst developing a vaccine adjuvant. Nanoparticles can further be subclassified according to their composition: namely polymer-based, lipid-based, and ceramic-based materials, albumin nanoparticles and nanogels [53]. Polymer-based nanoparticles are made from copolymers to increase circulation half-life and reduce mononuclear phagocytic system (MPS) uptake and inactivation. Nanoparticles of decreasing surface hydrophobicity have lower amounts of adsorbed plasma proteins and opsonins on their surfaces [74]. Poly(lactic acid) (PLA) poly(glycolic acid) (PGA), PLGA, poly-ε-caprolactone, and poly(methyl methacrylate) nanoparticles are the most widely studied because they are biocompatible and approved for human administration [75-84]. For instance, PLA and PLGA degrade by hydrolysis to lactic acid and glycolic acid metabolites that are eliminated via natural pathways in the body.

#### 1.4.2 Parameters affecting the release characteristics of drugs from chitosan micro/nanospheres

Parameters determine the drug release behavior from chitosan microspheres include concentration and molecular weight of the chitosan, the type and concentration of crosslinking agent, variables like stirring speed, type of oil, additives, crosslinking process used and drug chitosan ratio.

##### *Effect of molecular weight of chitosan*

Drug release studies from chitosan microspheres have generally shown that the release of the drug decreases with an increase in molecular weight of chitosan. Shiraishi et al. [85] investigated the effect of molecular weight of chitosan hydrolysate on the release and absorption rate of indomethacin from gel beads. The release rate of indomethacin was found to decrease with increasing molecular weight of chitosan. Similar results were obtained when oxytetracycline release from acylated chitosan microspheres was studied. It was observed that the release decreased with increasing molecular weight of chitosan [86]. Similarly, Al-Helw et al. [87] reported that release of phenobarbitone from crosslinked chitosan microspheres was slower from high molecular weight chitosan when compared to medium and low molecular weight chitosan. However, Genta et al. [88] reported that the fastest ketoprofen dissolution profile from chitosan microspheres was obtained from medium molecular weight chitosan. This may be attributed to swelling behavior of chitosan microspheres. An increase in molecular weight of chitosan leads to increase in viscosity of the gel layer, which influences the diffusion of the drug as well as erosion of the microspheres.

##### *Effect of concentration of chitosan*

Nishioka et al. [89] reported that the rate of cisplatin release reduced with the increasing concentration of chitosan in glutaraldehyde cross-linked chitosan microsphere.

#### *Effect of drug content in the microspheres*

A number of reports have shown that the release of drugs from microspheres increases with increase in drug content in the chitosan microspheres [90]. However, contrary results have also been reported. Akbuga and Durmaz [91] reported that furosemide release from chitosan microspheres followed the Higuchi matrix model. As the amount of furosemide incorporated increased, furosemide release was also increased. While Bodmeier et al. [92] reported that the release of sulfadiazine (a water insoluble drug) decreased with increase in drug content in the chitosan microspheres.

#### *Effect of density of crosslinking*

The crosslinking density has a remarkable effect on the release of drugs from the microspheres. Jameela et al. [93] revealed that highly crosslinked microspheres released only 35% of the progesterone in 40 days compared to 70% release from lightly crosslinked microspheres. Mitoxantrone released from chitosan microspheres, was also controlled by the extent of crosslinking. The crosslinking was carried out using glutaraldehydesaturated toluene [94]. Only about 25% of the drug was released over 36 days from highly crosslinked microspheres. Ko et al. [95] prepared felodipine loaded chitosan microparticles with tripolyphosphate (TPP) by ionic crosslinking. On examining the morphologies of TPP–chitosan microparticles with scanning electron microscopy, it was observed that as pH of TPP solution decreased and molecular weight of chitosan increased, microparticles had more spherical shape and smooth surface. Chitosan microparticles prepared with lower pH or higher concentration of TPP solution resulted in slower felodipine release from microparticles. With decreasing molecular weight and concentration of chitosan solution, release of the drug was increased. The release of drug from TPP–chitosan microparticles decreased when crosslinking time increased.

### **1.5 Retinol**

The retinoids are a class of chemical compounds structurally related to vitamin A and comprised of natural and synthetic analogs [96]. Animal-derived foods contain preformed Vitamin A predominantly as retinyl esters. Plant-derived foods contain pro-Vitamin A carotenoids, such as  $\beta$ -carotene. The majority of preformed Vitamin A



and pro-Vitamin A carotenoids are converted to all-trans-retinol (Vitamin A alcohol) by a series of reactions in both the intestinal lumen and mucosa. Once absorbed by the enterocyte, retinol is re-esterified and packaged with other dietary lipids into chylomicrons for transport to the liver. The liver is the major site of retinoid storage and processing in the body [97].

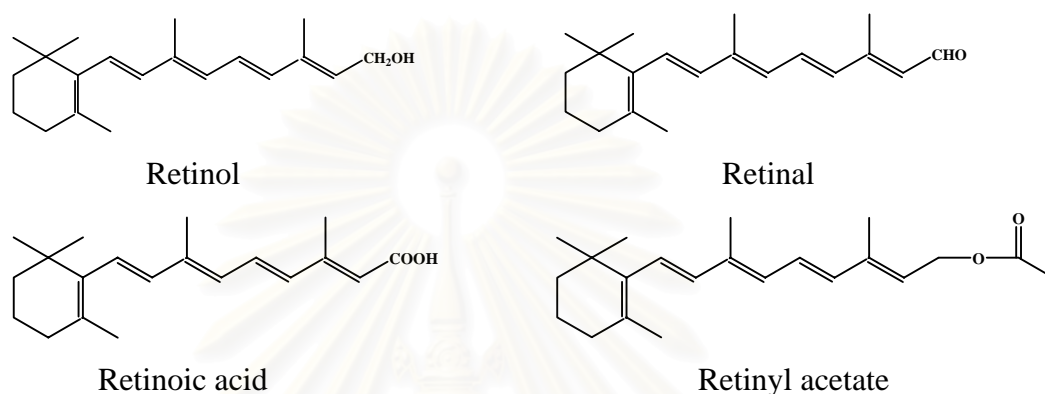


**Figure 1.5** Chemical structure of retinol and its derivatives.

Vitamin A and its derivatives, the retinoids, regulate the growth, survival, and differentiation of many cell types. Interest has recently been focused on the use of vitamin A acid (retinoic acid) for the treatment of dermatological diseases such as acne and psoriasis [96]. To date, much of the research conducted on Vitamin A and retinoids in the nervous system has focussed on embryonic or early postnatal brain development. It is now well established that retinoids regulate genes which control neuronal differentiation, neurite outgrowth, and the patterning of the anteroposterior axis of the neural tube. These effects likely account for the teratogenic effects of Vitamin A [98, 99]. More recently, evidence has emerged that retinoid signalling may also be required for several aspects of adult brain function [100].

Since this time, more than 2,500 retinoids have been synthesized and biologically tested. The compounds with the most promising therapeutic index have been subject to clinical trials. Within the first generation of retinoids, all-trans retinoic acid (tretinoin) and 13-cis retinoic acid (isotretinoin) were identified as promising candidates [96], the second generation of retinoids included the aromatic retinoids etretinate (ethyl 9-(4-methoxy-2,3,6-trimethyl-phenyl)- 3,7-dimethyl-nona- 2,4,6,8-tetraenoate) and acitretin (9-(4-methoxy-2,3, 6-trimethyl-phenyl)- 3,7-dimethyl-nona-

2,4,6,8- tetraenoic acid) and the third generation produced the polyaromatic arotinoids with or without polar end groups [96]. These compounds were found useful in the treatment of various dermatological conditions, such as acne, psoriasis and other disorders of keratinization and lichen ruber planus [101, 102]. In addition, some of them clearly showed activity in the treatment of malignant diseases [101-106]. At pharmacological doses, retinoids induce a variety of effects associated with cancer prevention such as suppression of *in vitro* cell transformation, inhibition of carcinogenesis in various organs in animal models and a decrease in the occurrence of second primary tumors for epithelial malignancies [107, 108]

## 1.6 Literature reviews

### *Chitosan as a material for drug delivery*

Chitosan and its derivatives have drawn attention as a drug delivery vehicle. Because of chitosan shows interesting biological properties such as biodegradability, biocompatibility, mucoadhesivity and antibacterial activity.

In 2001, Kevin A. Janes *et al.* [109], prepared chitosan nanoparticles by ionotropic gelation with sodium tripolyphosphate (TPP). The positive charge of DOX complexing with the polyanion, dextran sulfate and was loaded into nanoparticles. The effects of doxorubicin (DOX) encapsulation and/or release on cytotoxic activity relative to free DOX were studied. The evaluation of the activity of DOX-loaded nanoparticles in cell cultures indicated that those containing dextran sulfate were able to maintain cytostatic activity relative to free DOX, while DOX complexed to chitosan before nanoparticle formation showed slightly decreased activity. Additionally, confocal studies showed that DOX was not released in the cell culture medium but entered the cells while remaining associated to the nanoparticles.

In 2002, Ko *et al.* [110], prepared chitosan microparticle with tripolyphosphate (TPP) by ionic crosslinking. The particle sizes of TPP-chitosan microparticles were 500 to 710 nm. felodipine as a model drug were loaded into TPP-chitosan and their release behavior were studied. Chitosan microparticles prepared with lower pH or higher concentration of TPP solution resulted in slower felodipine release from microparticles. With decreasing MW and concentration of chitosan

solution, release behavior was increased. The release of drug from TPP-chitosan microparticles decreased when cross-linking time increased.

In 2006, Prego C. *et al.* [111], modified chitosan with poly(ethylene glycol) (PEG) (0.5% and 1% pegylation degree). Their properties were investigated. Chitosan-PEG nanocapsules and the control PEG-coated nanoemulsions were obtained by the solvent displacement technique. Their size was in the range of 160–250 nm. The presence of PEG, whether alone or grafted to chitosan, improved the stability of the nanocapsules in the gastrointestinal fluids. Finally, the results of the *in vivo* studies showed the capacity of chitosan-PEG nanocapsules to enhance and prolong the intestinal absorption of salmon calcitonin. Additionally, they indicated that the pegylation degree affected the *in vivo* performance of the nanocapsules.

In 2006, Jian Du *et al.* [112], prepared polyelectrolyte beads based on carboxymethyl Konjac glucomannan (CKGM) and chitosan (CS) via electrostatic interaction. The pH effect on bovine blood proteins (BSA) release from the beads were studied at pH 1.2, 5.0 and 7.4. The result shown that the amount of BSA released at medium condition (pH 5.0) was relatively low, only about 65% of protein released within 3 h. However, during the same length of time, at pH 1.2 and pH 7.4 the amounts of BSA released increased 81% and 73%, respectively.

In 2006, Opanasopit, P. *et al.* [113] prepared *N*-phthaloylchitosan-grafted poly(ethylene glycol) methyl ether (mPEG)(PLC-g-mPEG) and camptothecin (CPT) was loaded into micelles by dialysis method. Their *in vitro* release behaviors were studied in phosphate-buffered saline (PBS) at pH 7.4 for 96 hours by dialysis method. Release of CPT from the micelles was sustained. When compared to the unprotected CPT, CPT-loaded PLC-g-mPEG micelles were able to prevent the hydrolysis of the lactone group of the drug.

In 2006, Dong-Gon Kim *et al.* [114], prepared retinol-encapsulated chitosan nanoparticles with ultrasonication at an output power of 50W for 10 cycles of 2 s on ice. Retinol-encapsulated chitosan nanoparticle has a spherical shape and its particle sizes were around 50–200 nm according to the drug contents. Particle size was increased according to the increase of drug contents.

In 2006, Francesca Maestrelli *et al.* [115] prepared nanoparticles made of chitosan and cyclodextrins using the ionotropic gelation method. Two hydrophobic

drugs, triclosan and furosemide, were selected as models for complexation with the cyclodextrin and further entrapment in the chitosan nanocarrier. These results led to the conclusion that the drug–cyclodextrin complex was efficiently retained in the nanoparticulate structure. The *in vitro* release profile observed for these nanoparticles was characterized by an initial fast release followed by a delayed release phase.

In 2007, Yuan *et al.* [116], prepared chitosan microsphere cross-linked with genipin (Methyl (1*R*,2*R*,6*S*)-2-hydroxy-9-(hydroxymethyl)-3-oxabicyclo[4.3.0]nona-4,8-diene-5-carboxylate) and albumin was loaded into chitosan microsphere. The degree of cross-linking, swelling and the release of albumin from the microspheres was determined. Swelling ratios decreased significantly from 119.2% in the uncross-linked condition to 108.8% at 16 h cross-linking time. The release of albumin was reduced with as little as 4 h cross-linking time to 30.9% of uncross-linked microspheres for up to 24 days and by as much as 52.3-60.0% for up to 31 days with 8-16 h cross-linking time. Using genipin concentrations of 1.0 to 2.0 mM for 4 h, greatly reduced albumin release to only 12.4% to 27.1% on day 24.

In 2007, Yin-Song Wang *et al.* [117], prepared nanoparticles by cholesterol-modified chitosan conjugate with succinyl linkages (CHCS). Epirubicin (EPB), as a model anticancer drug, was physically entrapped inside CHCS self-aggregated nanoparticles. EPB-loaded CHCS self-aggregated nanoparticles were almost spherical in shape and their size increased from 338.2 to 472.9 nm with the EPB-loading content increasing from 7.97% to 14.0%. The release behavior of EPB from CHCS self-aggregated nanoparticles was studied *in vitro* by dialysis method. The results showed that EPB release rate decreased with the pH increase of the release media. In phosphate buffered saline (PBS, pH 7.4), the EPB release was very slow and the total release amount was about 24.9% in 48 h.

In 2007, Bao-Lin Guo and Qing-Yu Gao [118], prepared semi-interpenetrating networks (semi-IPN) polyampholyte hydrogels using carboxymethylchitosan and poly(N-isopropylacrylamide) with N,N'-methylenebisacrylamide (BIS) as the crosslinking agent. Coenzyme A (CoA) was loaded into hydrogels and its release behavior were studied. The result showed that within 24 h at 37 °C, the cumulative release ratio of CoA was 22.6% at pH 2.1 and 89.1% at pH 7.4. The release rate of CoA was higher at 37 °C than 25 °C in a pH 7.4 buffer solution. An increased release

rate of CoA was observed with the content of increased carboxymethylchitosan in the hydrogel at 25 °C in pH 7.4 solution.

In 2007, Opanasopit, P. *et al.* [119], prepared amphiphilic grafted copolymer *N*-phthaloylchitosan-grafted poly(ethylene glycol) methyl ether (PLC-g-mPEG) using chitosan with four different degrees of deacetylations (DD) (80, 85, 90 and 95%). All-*trans* retinoic acid (ATRA) was incorporated into PLC-g-mPEG by dialysis method. The particle sizes of ATRA incorporated into micelles were about 80–160 nm depending on the initial drug-loaded and %DD of chitosan. It was found that %DD of chitosan, was a key factor in controlling the incorporation efficiency, stability of the drug-loaded micelles and drug release behavior. As the %DD increased, the incorporation efficiency and ATRA-loaded micelles stability increased.

#### *Antimicrobial activity of chitosan*

Owing to chitosan was polycationic compound. Therefore, they have interested as potential antibacterial agent.

In 2004, Lifeng Qi *et al.* [120], prepared chitosan nanoparticles by chitosan cross-linked with tripolyphosphate (TPP). Copper was loaded into chitosan nanoparticles. The antibacterial activity of chitosan nanoparticles and copper-loaded chitosan nanoparticles against *E. coli*, *S. choleraesuis*, *S. Typhimurium*, and *S. aureus* was determined by turbidity method. The antibacterial activity of chitosan nanoparticles and copper-loaded nanoparticles are significantly higher than that of chitosan and doxycycline (positive control).

In 2005, Yang *et al.* [121], studied the antibacterial activity of *N*-alkylated disaccharide chitosan derivatives against *Escherichia coli* and *Staphylococcus aureus*. The effect of degree of substitution (DS) with disaccharide and the kind of disaccharide present in the molecule on antibacterial activity were investigated. The kind of disaccharide linked to the chitosan molecule, a DS of 30-40%, in general, exhibited the most pronounced antibacterial activity against both organism. *E. coli* and *S. aureus* were most susceptible to cellobiose chitosan derivative (DS 30-40%) and maltose chitosan derivative (DS 30-40%), respectively.

In 2005, Yanfei Peng *et al.* [122], synthesized hydroxypropyl chitosan (HPCS) derivatives from chitosan and propylene epoxide. Antimicrobial activities of the

HPCS derivatives were evaluated by the Kirby–Bauer disc diffusion method and the microtube dilution broth method. The HPCS derivatives exhibited no inhibitory effect on two bacterial strains (*Escherichia coli* and *Staphylococcus aureus*). However, some inhibitory effect was found against *Coniella diplodiella*, *Fusarium oxysporum*, *Altwenaria mali*, and *Physaclospora piricola*.

In 2006, Nan Liu *et al.* [123], investigated the effect of molecular weight ( $5.5 \times 10^4$  to  $15.5 \times 10^4$  Da) and concentration of chitosans on antibacterial activity using *Escherichia coli* by the optical density method. All of the chitosan samples with MW from  $5.5 \times 10^4$  to  $15.5 \times 10^4$  Da showed antimicrobial activities at the concentrations higher than 200 ppm. The growth of *E. coli* was promoted by chitosan at concentration lower than 200 ppm. At the concentration range from 50 to 100 ppm, the antibacterial activity of low MW chitosan is higher than that of the high MW samples.

In 2006, Hamit Camer *et al.* [124], prepared poly(N-vinylimidazole) grafted onto chitosan in dilute acetic acid solution via ceric ion initiation. The antibacterial activity of poly(N-vinylimidazole) grafted chitosan was investigated by standard disc agar diffusion method. The grafted polymer exhibited against the growth of *Pseudomonas aeruginosa*, *Escherichia coli*, *Bacillus subtilis* and *Staphylococcus aureus*. Grafted polymer showed that increasing degree of grafting of poly(N-vinylimidazole) increase the antibacterial activity.

In 2007, Ning-lin Zhou *et al.* [125], prepared silver-chitosan, silver-chitosan/clay, and polymer/silver-chitosan/clay nanocomposites by intercalation reaction. Their antibacterial activity was investigated by Inhibition Ring Test. Result shows that the nanocomposite could inhibit *Escherichia coli* (ATCC 25922), *Pseudomonas aeruginosa* (ATCC 27853), *Staphylococcus aureus* (ATCC 25923) and *Candida albicans* (ATCC 14053).

## 1.7 Research goals

The objectives of this research can be summarized as follows:

1. To entrap cosmetic active into chitosan nanoparticles.
2. To study release behavior of cosmetic active from chitosan nanoparticles.
3. To investigate the antimicrobial activity of chitosan nanoparticles.

4. To study cytotoxicity of chitosan nanoparticles.



สถาบันวิทยบริการ  
จุฬาลงกรณ์มหาวิทยาลัย

## **CHAPTER II**

### **EXPERIMENTAL**

#### **2.1. Materials and Chemicals**

##### *Chemical synthesis and characterize*

Chitosan (MW of 110,000) was purchased from seafresh Chitosan (Lab), Co., (Bangkok, Thailand). *N,N'*-Dimethyl formamide (DMF) and dimethyl sulfoxide (DMSO) were purchased from Labscan (Bangkok, Thailand). 1-Ethyl-3-(3-dimethylaminopropyl) carbodiimide (EDCI) and 4-methoxycinnamic acid were purchased from Acros Organics (Geel, Belgium). 1-Hydroxy benzotriazole (HOBT) was purchased from Beijing Beiqing Chuangye Sci. & Tech. Development Co., Ltd. (Beijing, China). Methoxy poly(ethylene glycol) methyl ether (mPEG) MW of 5,000 was purchased from Fluka Chemical company (Buchs, Switzerland). Phthalic anhydride was purchased from Carlo Erba Reagent (Milan, Italy). Pyridine and all-*trans* retinyl acetate (ATRA) were provided from Sigma chemical Co. Ltd (St. Louis, MO, USA.). Dialysis tubing cellulose membranes (MWCO 12,400 Dalton, size 76 mm x 49 mm) used for dialysis experiments were purchased from Sigma-Aldrich Co. (Steinheim, Germany).

##### *Media culture for antibacterial study*

Tryptic soy broth (TSB) and Tryptic soy agar (TSA) were purchased from Difco laboratories (Detroit, MI, USA). Clindamycin was purchased from RPC International Co., LTD (Bangkok, Thailand).

##### *Media culture and chemical reagent for cytotoxic study*

RPMI 1640 media, fetal bovine serum, 100 mM sodium pyruvate, HEPES (4-(2-hydroxyethyl)-1-piperazineethane sulfuric acid) (free acid 1 M solution (238.3 g/L)) and Trypsin-EDTA, were obtained from Hyclone (Utah, USA). 3-(4,5-Dimethylthiazo-2-yl)-2,5-diphenyl tetrazolium bromide (MTT) and Gentamycin were purchased from Biobasic Inc. (Ontario, Canada).



## 2.2 Instruments and Equipments

### *Chemical synthesis and characterization*

The  $^1\text{H}$ -NMR spectra were obtained in deuterated dimethylsulfoxide ( $\text{DMSO-}d_6$ ) using Varian Mercury spectrometer which operated at 400.00 MHz (Variance Company, USA). The FT-IR spectra were recorded on a Nicolet Fourier Transform Infrared spectrophotometer: Impact 41.0 (Nicolet Instruments Technologies, Inc. WI, USA). Ultraviolet absorption spectra were obtained with the aids of an HP 8453 UV/VIS spectrophotometer (Agilent Technologies, CA, USA) using 1 cm-pathlength quartz cell.

Size distribution and zeta potential were obtained with zetasizer nano series instrument (Zs, Malvern instruments, United Kingdom). Thermogram of each samples were obtained with differential scanning calorimeter: DSC 204 (Netzsch Group, Selb, Germany). Centrifugation was performed on Allegra 64R high speed centrifuge (Beckman Coulter, Inc., Japan). Transmission electron microscope (TEM) and scanning electron microscope (SEM) photographs were obtained from JEM-2100 (JEOL, Japan) and JSM-6400 (JEOL, Japan), respectively.

### *Antibacterial determination*

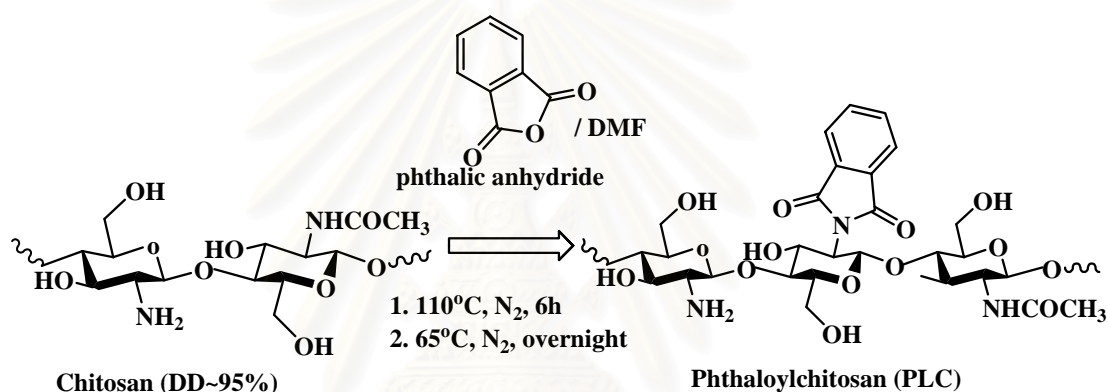
The solutions were sterilized with autoclave SS-352 model (Tomy company, USA). Laminar flow clean V6 used for experiments was supplied from Lab service company (Bangkok, Thailand). Bacteria were incubated in incubator shaker SK-737 (Amerex Instruments, CA, USA) and incubator Modell 800 (Mettmert company, Schwabach, Germany). Spectrophotometer genesys 20 for experiment was supplied from Thermo spectronic (NY, USA). The pH value of media was obtained with pH meter Mettler Toledo (S-20K, China). Micropipett P10, P20, P100, P1000 and P5000 used for experiment were furnished from Gilson company, Inc. (Ohio, USA). The solutions were mixed with Vortex mixer G-560E (Scientific industries, Inc., NY, USA).

### *Cytotoxic experiment*

The cell lines A-375 used in cytotoxic study were harvested with Rotofix 32 centrifuge (Hettich, Kirchleugern, Germany). Pipet-aid used for experiment was furnished from Drummond (USA). Melanoma cell line was maintained in 5%  $\text{CO}_2$  incubator 311 (Thermoelectron corporation, USA). Larminar flow carbinet H1 used for experiment was supplied from Lab service LTD part (Bangkok, Thailand). Water

bath used for experiment was purchased from Memmert (Schwabach, Germany). Tissue culture 96 well plates for the MTT assay was furnished from Nunc™ Brand products (Roskilde, Denmark). Inverted microscope for experiment was supplied from Olympus (London, United Kingdom). Hemocytometer for cell count was purchased from Boeco (Hamburg, Germany). Tissue culture flask (25 cm<sup>3</sup>) for the cell culture was supplied from Corning incorporated (MA, USA).

### 2.3. Synthesis of Phthaloylchitosan (PLC)

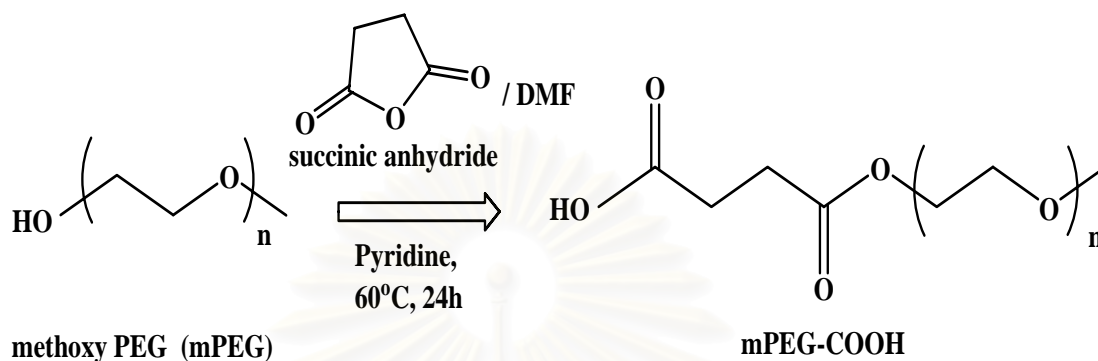


Scheme 2.1

Phthaloylchitosan was synthesized according to Scheme 2.1. In short, three gram (0.01 moles) of chitosan (MW 110,000 Da) were reacted with 13.623 g (0.09 moles) of phthalic anhydride in 20 mL of DMF at 110 °C under nitrogen for 6 h. Then the temperature was reduced to 60 °C for 12 h. The solution was precipitated in ice water and the precipitate was washed with methanol to give a dark brown solid product of Phthaloylchitosan (PLC)

**Phthaloylchitosan (PLC):** dark brown powder. yield: 81%. FTIR (KBr, cm<sup>-1</sup>): 1,771 and 1710 (C<sub>2</sub>O<sub>2</sub>N<sub>2</sub>, phthalimido group), 1710 (C=O, ester), 721, 1388 and 1650 (aromatic ring) and 3,472 (OH). <sup>1</sup>H-NMR (400 MHz, DMSO-*d*<sub>6</sub> with 0.05% TFA, δ, ppm): 2.0 (s, 3H, NCOCH<sub>3</sub>) 2.7-4.7 (m, 6H, H2-H6 of pyranose ring), 5.1 (br, 1H, H1 of pyranose ring) and 7.57-7.66 (m, 18H, Ar-H of phthaloyl group). UV-VIS (DMSO) λ max: 280 nm.

## 2.4 Synthesis of poly(ethylene glycol) methyl ether terminated with carboxylic groups (mPEG-COOH)

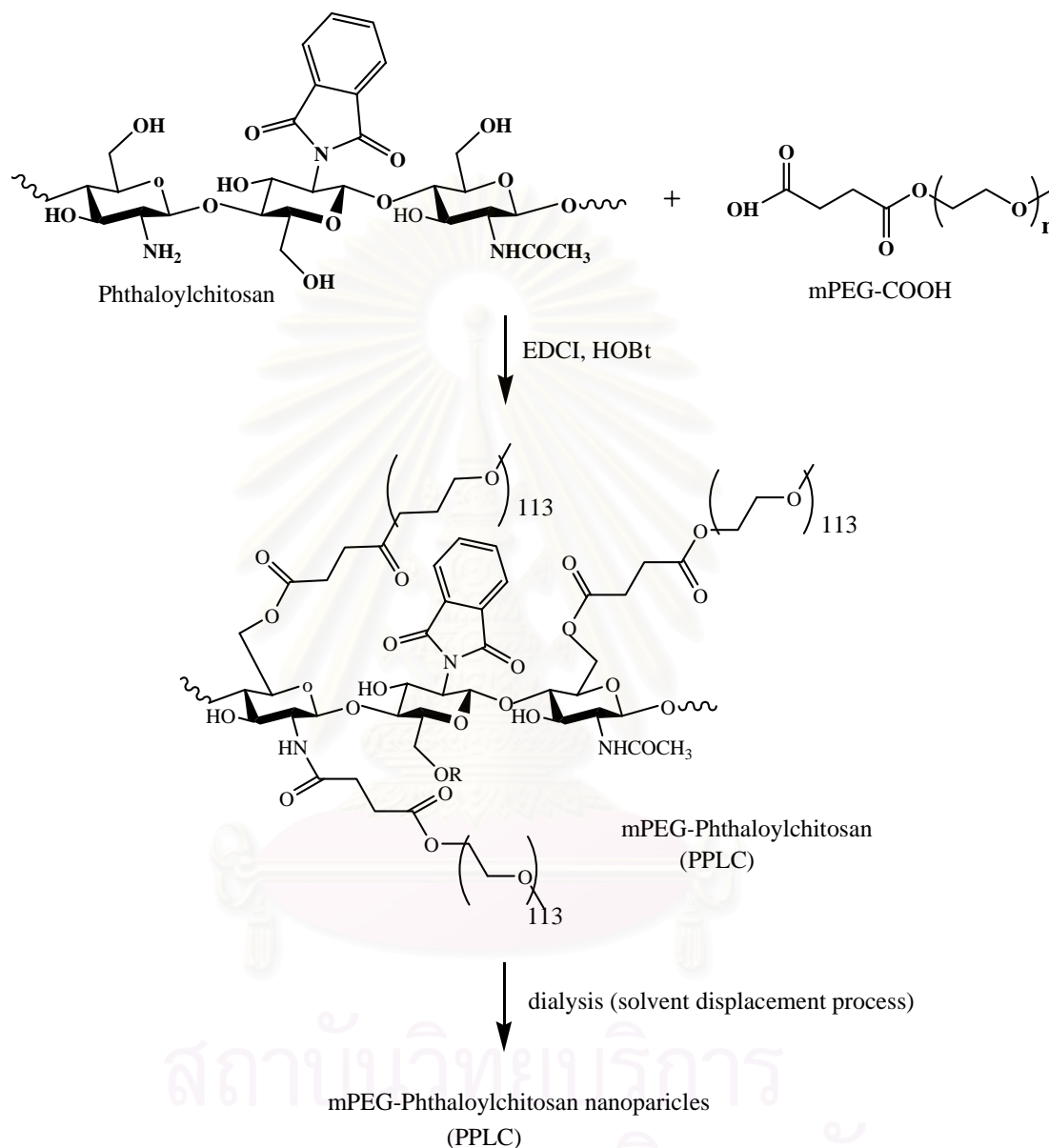


**Scheme 2.2**

Three grams ( $0.6 \times 10^{-3}$  moles) of poly (ethylene glycol) methyl ether (mPEG, MW 5,000) were reacted with 0.06 g ( $0.6 \times 10^{-3}$  moles) of succinic anhydride in 1 mL of DMF at 60°C for 17 h. Pyridine was added as catalyst. The mixture was precipitated into diethyl ether and the product was collected. The product was centrifuged and dried to obtain a white powder of poly(ethylene glycol) methyl ether terminated with carboxylic groups (mPEG-COOH, Scheme 2.2).

**Poly(ethylene glycol) methyl ether terminated with carboxylic groups (mPEG-COOH):** white powder. FTIR (KBr,  $\text{cm}^{-1}$ ): 3,447 (OH), 2,888 (C–H stretching), 1,736 (C=O of succinyl group), and 1,111 (C–O–C of PEG).  $^1\text{H}$  NMR (400 MHz, DMSO- $d_6$  with 0.05% TFA,  $\delta$ , ppm): 2.8 (t, 4H, HOOC-CH $_2$ -), and 3.4 (t, 452H, O-CH $_2$ - in PEG).

## 2.5 Synthesis of mPEG–Phthaloylchitosan (PPLC)



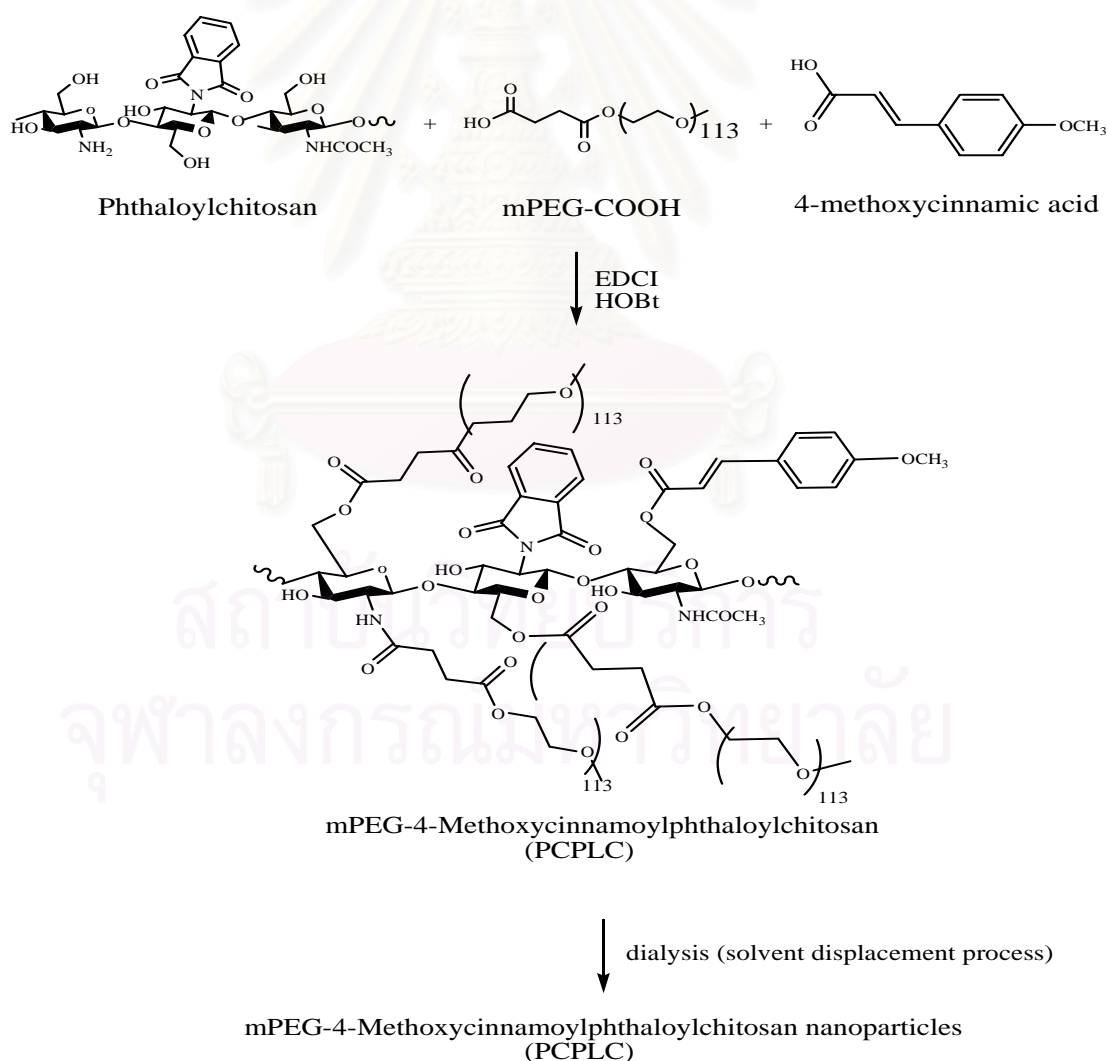
**Scheme 2.3**

mPEG–Phthaloylchitosan (PPLC) was synthesized according to Scheme 2.3. Briefly, one gram of compound PPLC was reacted with 7.56 g ( $0.1 \times 10^{-2}$  moles) of mPEG-COOH in the presence of 0.602 g ( $0.4 \times 10^{-2}$  moles) of HOBt as catalyst in 20 mL of DMF. The reactions was left overnight. Then this clear mixture solution was cooled to 4 °C and EDCI (0.85 g,  $0.4 \times 10^{-2}$  moles) was added and the mixture was

maintained at 4 °C for 1 h. before being left at room temperature for 12 h. The mixture was dialyzed against water and the centrifuged solid product was washed with methanol to obtain white powder of mPEG–phthaloylchitosan (PPLC).

**mPEG–Phthaloylchitosan (PPLC):** white powder. yield: 75 %. FTIR (KBr,  $\text{cm}^{-1}$ ): 3477 (OH), 2882 (C-H stretching), 1778 and 1710 (C=O anhydride), 1710 (C=O ester), and 721 (aromatic ring).  $^1\text{H-NMR}$  (400 MHz,  $\text{DMSO-}d_6$  with 0.05% TFA,  $\delta$ , ppm): 3.50 (t, 41H,  $-\text{OCH}_2\text{CH}_2\text{O}-$  of PEG), 2.72-4.74 (br, 14H, H2-H6 of glucosamine), 5.1 (br, 2H, H1 of pyranose ring) and 7.5-7.7 (m, 19H, Ar-H of phthaloyl group). UV-VIS (DMSO)  $\lambda$  max: 330 and 346 nm.

## 2.6 Synthesis of mPEG-4-Methoxycinnamoylphthaloylchitosan (PCPLC)



**Scheme 2.4**

mPEG-4-Methoxycinnamoylphthaloylchitosan (PCPLC) was synthesized according to Scheme 2.4. PLC (1 g) was reacted with 4-methoxycinnamic acid (0.3312 g,  $1.8 \times 10^{-3}$  moles) in 50 mL DMF. HOBt (0.6028 g,  $0.4 \times 10^{-2}$  moles) was added as catalyst and stirred at room temperature until the solution became clear. EDCI (0.9586 g,  $0.5 \times 10^{-2}$  moles) was added into the reaction. The mixture was maintained at  $4\text{ }^{\circ}\text{C}$  for 1 h before being left at room temperature for 12 h. After that, the mPEG-COOH (7.5836 g,  $1.5 \times 10^{-3}$  moles) was added into the mixture. Then EDCI (0.7668 g,  $0.4 \times 10^{-2}$  moles) was added and the mixture was stirred overnight at room temperature. The mixture was dialyzed against water to eliminate DMF and the centrifuged down product was washed with methanol to obtain pale brown particle of mPEG-4-methoxycinnamoyl phthaloylchitosan (PCPLC).

**mPEG-4-methoxycinnamoylphthaloylchitosan (PCPLC):** pale brown powder. yield: 57 %. FTIR (KBr,  $\text{cm}^{-1}$ ): 1773 (C=O of ester) and 1618 (C=C).  $^1\text{H-NMR}$  (400 MHz,  $\text{DMSO-}d_6$  with 0.05% TFA,  $\delta$ , ppm): 2.7-5.50 (s, 3H,  $\text{OCH}_3$ , t, 24H of PEG and br, 125H of pyranose ring), 6.4 (d, 1H, Ar-CH=), 6.94 and 7.59 (d, 4H, Ar-H of cinnamoyl group), 7.48-7.72 (m, 2H, Ar-H of cinnamoyl group, 1H, Ar- $\text{HC}=\text{CH-COOR}$  and 149H, Ar-H of phthaloyl group).

## 2.7 Antibacterial study

### 2.7.1 Preparation of bacteria

*Staphylococcus aureus* (*S. aureus*) ATCC 25923 and *Escherichia coli* (*E. coli*) ATCC 25922 were obtained from the Department of Medical Sciences, Ministry of Public Health. *E. coli* and *S. aureus* were grown in Tryptic soy broth (TSB, Difco, USA) in shake flasks at  $37^{\circ}\text{C}$  in incubator shaker for 7 hour prior to harvesting. After the incubation, the concentration of the bacteria was adjusted to approximately  $10^8$  CFU/mL.

### 2.7.2 Determination of MIC

The minimum inhibitory concentration (MIC) of chitosan and chitosan nanoparticles (PPLC and PCPLC) was determined by turbidimetric method [120]. In this method, Test tubes each containing 2.0 mL of Tryptic soy broth (TSB, Difco, USA) were autoclaved for 15 min at  $121\text{ }^{\circ}\text{C}$ . The pH of the TSB was adjusted to 6.0. Chitosan

nanoparticles could be well-distributed in distilled water. Chitosan or chitosan nanoparticles were autoclaved for 10 min at 110 °C and chitosan nanoparticles were sonicated after sterilized. Two milliliter of chitosan solution or chitosan nanoparticles suspension was added to 2.0 mL of TSB. After mixing, two milliliter of the mixture was transferred to the second tube, and subsequent performing. Hence, each tube contained a test sample solution with half of the concentration of the previous tube. The tubes were inoculated under aseptic conditions with 20 µL of the freshly prepared bacteria suspension. The positive control was given with clindamycin, and blank control tubes were only contained Tryptic soy broth. After mixing, the tubes were incubated at 37 °C for 24 h. Tubes with were recorded the visible signs of growth or turbidity at 600 nm. The absorbance difference between 0 h and 24 h of the same tube was calculated. The absorbance difference of chitosan or chiosan nanoparticles was compared with the absorbance difference of blank control and positive control. The lowest concentration of chitosan and chitosan nanoparticles that inhibited the growth of bacteria was considered as the minimum inhibitory concentration or MIC. All the experiments were performed in triplicate.

### **2.7.3 Determination of minimum bactericidal concentration (MBC)**

The minimum bactericidal concentration (MBC), or the lowest concentration of chitosan or chitosan nanoparticles that kills 99.9% of the bacteria [120], was determined by assaying the live organisms in those tubes from the MIC test that showed no growth. A loopful from each of those tubes were inoculated on Tryptic soy agar (TSA, Difco, USA) After 24 h of incubation at 37 °C, bacteria growth was determined. If no growth was observed in any tube, the result was interpreted as MBC. All the experiments were performed in triplicate.

### **2.7.4 Survival of bacteria**

*E. coli* and *S. aureus* were grown in TSB in shake flasks for 7 hours at 37°C in incubator shaker. The bacteria suspensions were diluted with sterilized 0.85% normal saline to 10<sup>5</sup> CFU/mL. The antibacterial activity was determined by turbidity method as described above. After incubated at 37 °C for 24 hours, the bacteria suspensions were diluted ten-fold serial with 0.85% normal saline solution. The survival bacteria

were counted by the spread-plate method. 100  $\mu$ l portions from the diluted bacteria suspension were removed and quickly spreaded on TSA. After inoculation, the plates were incubated at 37 °C for 24 h, and the colonies were counted. Triplicated plates from one dilution were performed. The reduction of bacteria was calculated according to the following equation:

$$\text{Reduction (\%)} = (\log A - \log B) / \log A \times 100$$

Where A and B are the number of bacteria cells from the control and tester plates, respectively.

## **2.8 Cytotoxicity study of mPEG–phthaloylchitosan (PPLC) and mPEG-4-methoxycinnamoylphthaloylchitosan nanoparticles (PPLC).**

### **2.8.1 Cell culture and treatment**

Human melanoma A-375 cell line (ATCC CRL-1619™) was obtained from the American Type culture collection (Manassas, VA. USA). Cells were maintained in RPMI 1640 media supplemented with 10% fetal bovine serum (Hyclone, UT, USA), 10 mM HEPES , 100 mM sodium pyruvate and 100 mg/mL gentamycin. Cells were maintained at 37°C in a humidified atmosphere of 5% CO<sub>2</sub> in air. Cells were harvested using 0.25% trypsin-EDTA. Media were changed every other day. For cytotoxicity test, cells were seeded in 96-well plates at a concentration of 1x10<sup>4</sup> cells/mL and cultured for 4-6 h. at 37 °C to allow for adherence before being treated with nanoparticles. After cells adhered to culture plate, 5  $\mu$ L of nanoparticles dispersed into water at final concentrations 0.25, 0.025 and 0.0025 mg/mL, were added and cells were incubated at 37°C for 72 h before subjecting to MTT assay.

### **2.8.2 Assessment of cytotoxicity by MTT assay**

Cells were treated with nanoparticles as described above and 10  $\mu$ L of MTT reagent in PBS (final concentration of 0.5mg/mL) was added to the cell at the last 4 hours of incubation. After incubation for 72 hours at 37 °C, medium was carefully removed and 100  $\mu$ L of 0.04 N HCl-isopropanol was added to dissolve formazan crystals. Absorbances (Abs) were measured at 540 nm in microplate reader (Bio-Tek instrument). Cell viability was calculated using the follow equation:

$$\text{Cell viability (\%)} = (\text{Abs test cells} / \text{Abs control cells}) \times 100$$



Cell viability of untreated cell was set as 100%, and water was used as negative control. All the experiments were performed in triplicate.

### **2.9. Encapsulation of ATRA into nanoparticles.**

ATRA was encapsulated into nanoparticles by performing the polymeric self-assembly in the presence of ATRA. Briefly, PPLC or PCPLC (0.06 g) and ATRA (0.006, 0.015 and 0.03 gram) were dissolved in 10 mL of DMF. The mixture was stirred at room temperature until completely dissolved. The mixture was then placed into a dialysis bag and dialyzed against deionized water (Milli-Q). Aqueous suspension of the nanoparticles was then centrifuged at 20,000 rpm for 1 h and then very quickly rinsed with ethanol to remove the ATRA adhered at the outside of particles. The amount of ATRA loaded into nanoparticles was determined by analyzing this washing ethanol together with the dialysate, using UV absorption spectrophotometer at 325 nm. The % drug loading and encapsulation efficiency were calculated using equation (1) and (2), respectively.

$$\% \text{ drug loading} = \frac{\text{weight of drug in nanoparticle}}{\text{weight of nanoparticle}} \times 100 \quad (1)$$

$$\% \text{ encapsulation efficiency} = \frac{\text{total amount of ATRA} - \text{free ATRA}}{\text{total amount of ATRA}} \times 100 \quad (2)$$

Free ATRA = amount of ATRA found in dialysate and washing ethanol.

### **2.10 Differential scanning calorimetry**

DSC was performed using a Netzsch DSC 204 Phoenix. Four to ten milligrams of the dry samples were accurately weighed into aluminum cups and sealed. A small hole was done at the top of the cup in order to allow the release of water. An empty cup was used as reference. The experiment consisted of two runs. The first one from -100 to 130 or 150 °C and the second one from -100 to 350 °C. The experiments were run at a scanning rate of 10 K/min.

### **2.11 Morphology and zeta potential of chitosan nanoparticles**

Particle size distribution and the zeta potential of unloaded-chitosan nanoparticles (PPLC and PCPLC) and ATRA-loaded chitosan nanoparticles at concentration 600

ppm were determined using Zetasizer nano series (Malvern Instruments). The morphology of PLLC and PCPLC nanoparticles at concentration 600 ppm were determined with scanning electron microscope (SEM) and transmission electron microscope (TEM).

The effect of autoclave on morphology and particle size of nanoparticles was also studied. This was carried out by autoclaving the 10,000 ppm aqueous suspension of mPEG-phthaloylchitosan and mPEG-4-methoxycinnamoylchitosan at 110 °C, 1 bar/sq inch for 10 min. The autoclaved suspensions and un-autoclaved suspensions were subjected to scanning electron microscope (SEM) analyses.

### **2.12 *In vitro* release**

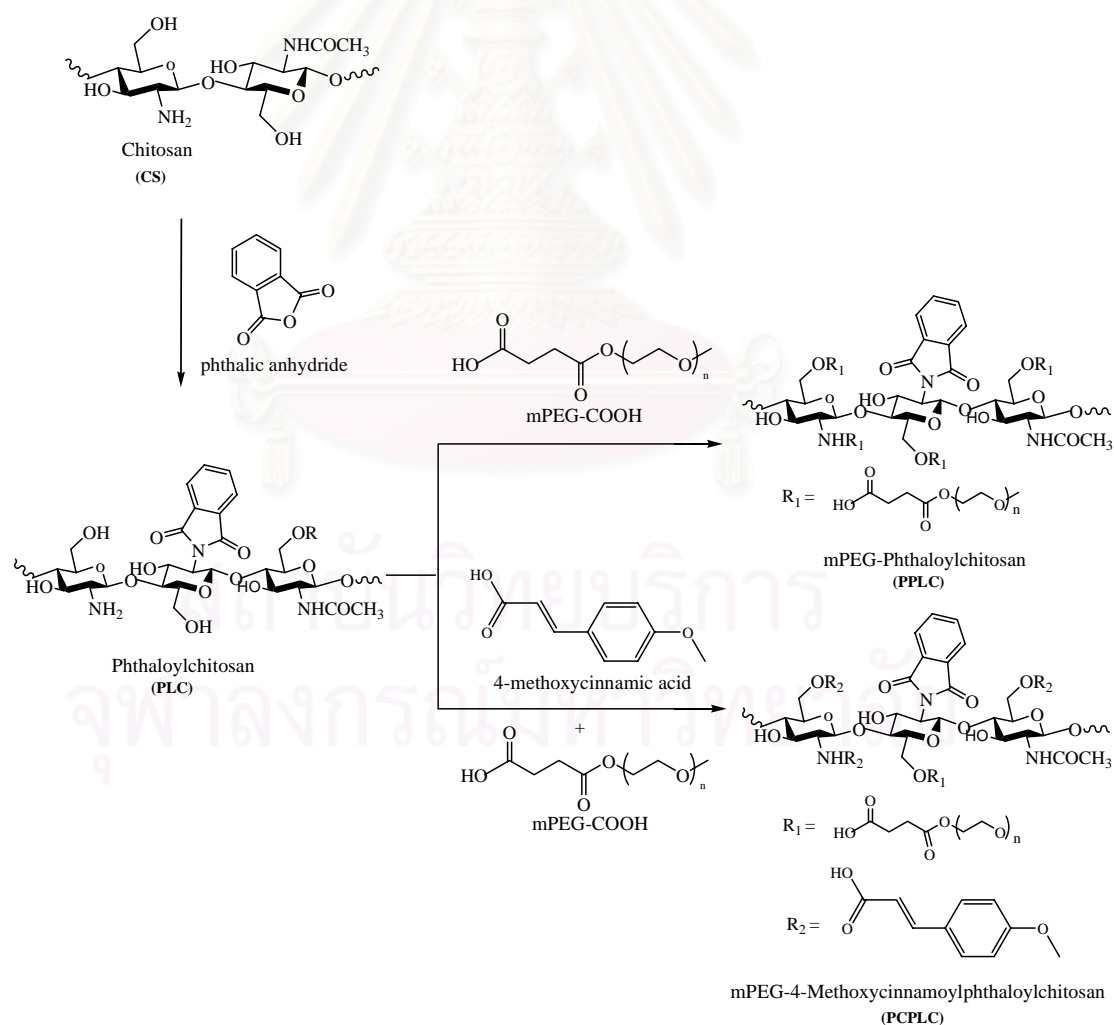
Release of ATRA from ATRA-loaded nanoparticles was measured using a dialysis method [119]. One hundred milliliters of the release medium (ethanol/tween-20/water, 10:15:75 (v/v/v) pH 4, 7 and 10) were added in the beaker. One milliliter of ATRA-loaded nanoparticles was placed into a dialysis bag and the bag was then immersed into the medium. The experiment was carried out at the room temperature. During the experiments, the medium (3 mL) was withdrawn at 1, 2, 4, 6, 24, 30, 48, 54 and 72 h with the replacement of the same volume of fresh medium. The amount of released ATRA was determined by UV spectroscopy at 325 nm using a calibration curve. The calibration curve was constructed from a series of ATRA solutions prepared in ethanol at concentrations of 0, 0.5, 1, 3, 5, 7 and 9 ppm. The results are expressed as the percentage cumulative release of ATRA. The experiments were done in duplicate.

## CHAPTER III

### RESULT AND DISCUSSION

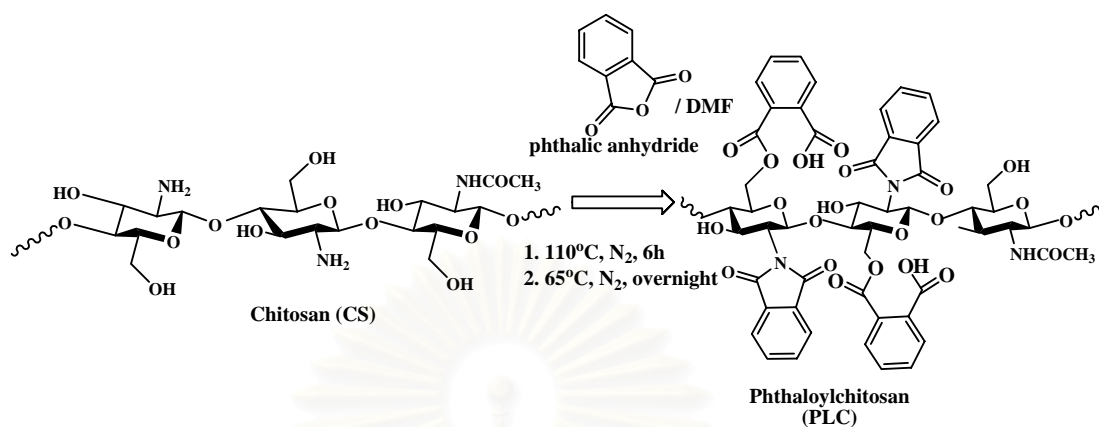
#### 3.1 Characterization of Phthaloylchitosan (PLC), mPEG-Phthaloylchitosan (PPLC) and mPEG-4-Methoxycinnamoylphthaloylchitosan (PCPLC).

Chemical modification of chitosan has been carried out as shown in Scheme 3.1. The obtained products mPEG-phthaloylchitosan and mPEG-4-methoxycinnamoyl phthaloylchitosan (PPLC and PCPLC) were induced into nanoparticles by solvent displacement process. The PPLC and PCPLC nanoparticles prepared in the experiment were soluble in DMF and DMSO but formed a colloid in water, ethanol and methanol.



Scheme 3.1

### 3.1.1 Phthaloylchitosan (PLC)



**Scheme 3.2** Synthesis of phthaloylchitosan

The phthaloylchitosan (PLC) was synthesized by reacting chitosan with phthalic anhydride in DMF. The obtained product was completely dissolved in DMSO and DMF. IR spectrum (KBr) of the product shows two absorption bands ( $1782\text{ cm}^{-1}$  and  $1710\text{ cm}^{-1}$ ) assignable to the phthalimido functionality. A band at  $1710\text{ cm}^{-1}$  (ester) also indicates O-phthaloylation. Three absorption bands ( $723$ ,  $1384$  and  $1646\text{ cm}^{-1}$ ) belonging to aromatic ring of phthalimido group onto chitosan (see Figure 3.1).

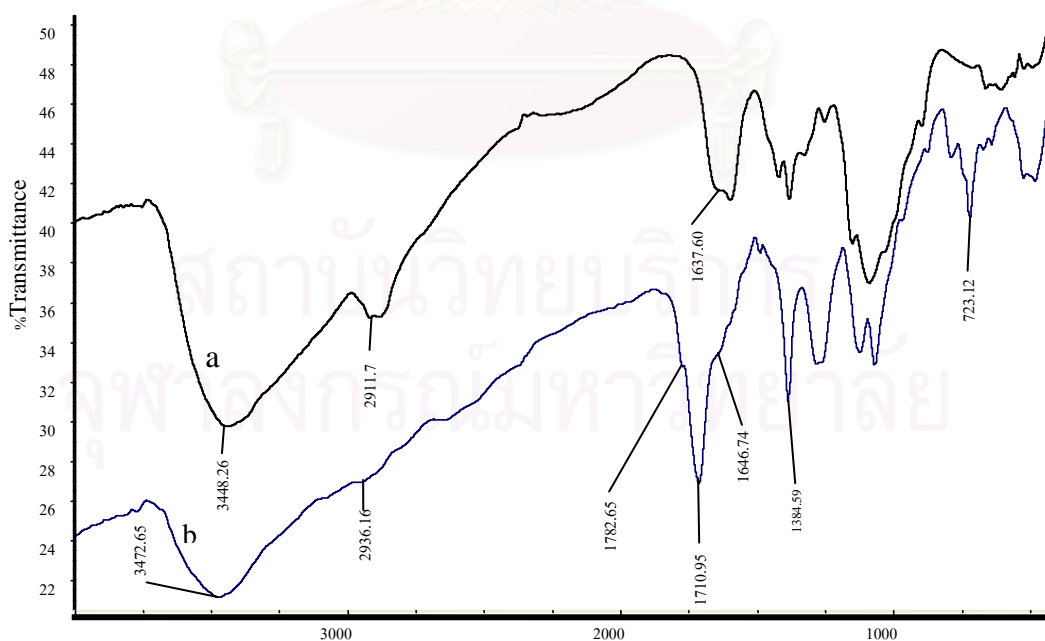


**Figure 3.1** IR spectra (KBr) of a.) chitosan and b.) phthaloylchitosan

The grafted polymer was characterized by  $^1\text{H-NMR}$  (in  $\text{DMSO-}d_6$ ), which clearly indicated the presence of phthaloyl moieties by the appearance of signals at 7.47-7.68 ppm (18H, Ar-H of the phthaloyl groups). Substitution degree of 220 % was determined from integration of the phthaloyl protons against protons of the glucosamine backbone (2.7-5.8 ppm, 7H, 1H-6H of glucosamine). Interference from HOD peak at 3.3 ppm could be avoided by adding a small amount of trifluoroacetic acid into the sample just prior to the NMR analysis, shifting the HOD peak to ~10-11 ppm.  $^1\text{H-NMR}$  of PLC shows insignificant amount of the *N*-acetyl signal (s, 2.0 ppm  $\text{NCOCH}_3$ ) indicating less than 1% substitution of *N*-acetyl functionality. From these results, it was concluded that the phthalimido group was successfully grafted onto chitosan. Furthermore, experiments were done to obtain UV absorption properties ( $\lambda_{\text{max}}$ ,  $\epsilon$ ) of this product. As show in Figure 3.3, in DMSO, the product gave only slight absorption in the UVB.

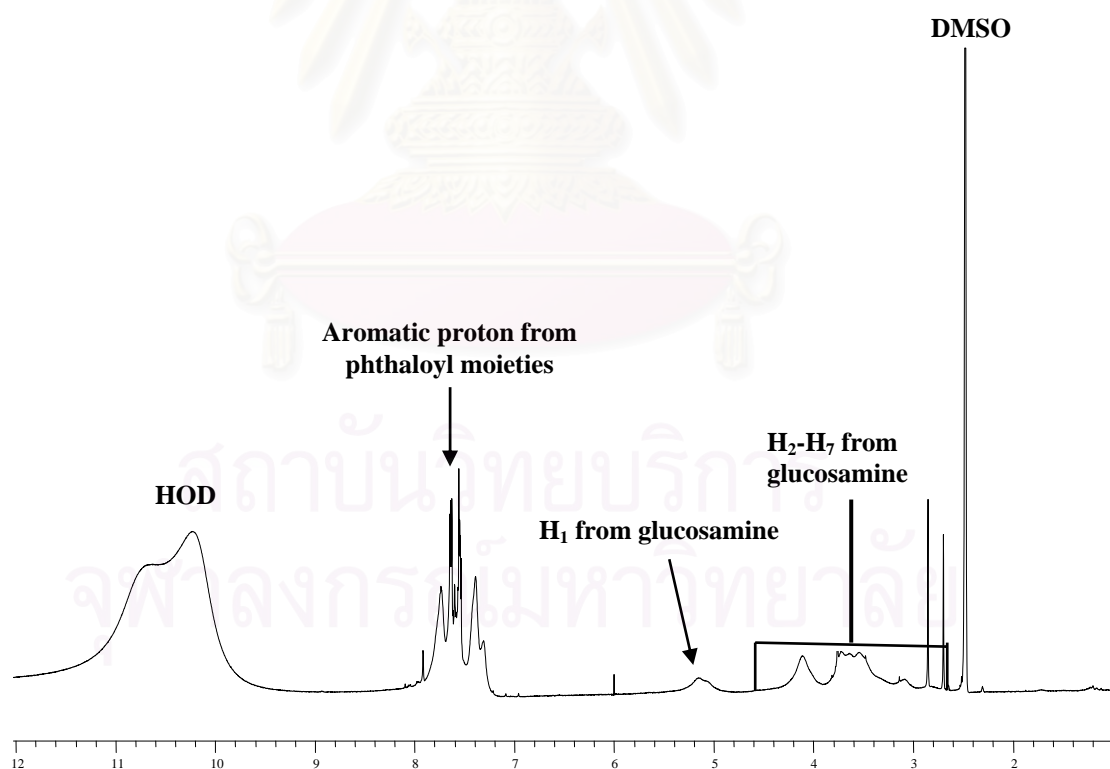


**Figure 3.2**  $^1\text{H-NMR}$  spectrum of phthaloylchitosan (PLC,  $\text{DMSO}$  deuterated with 0.05% trifluoroacetic acid).

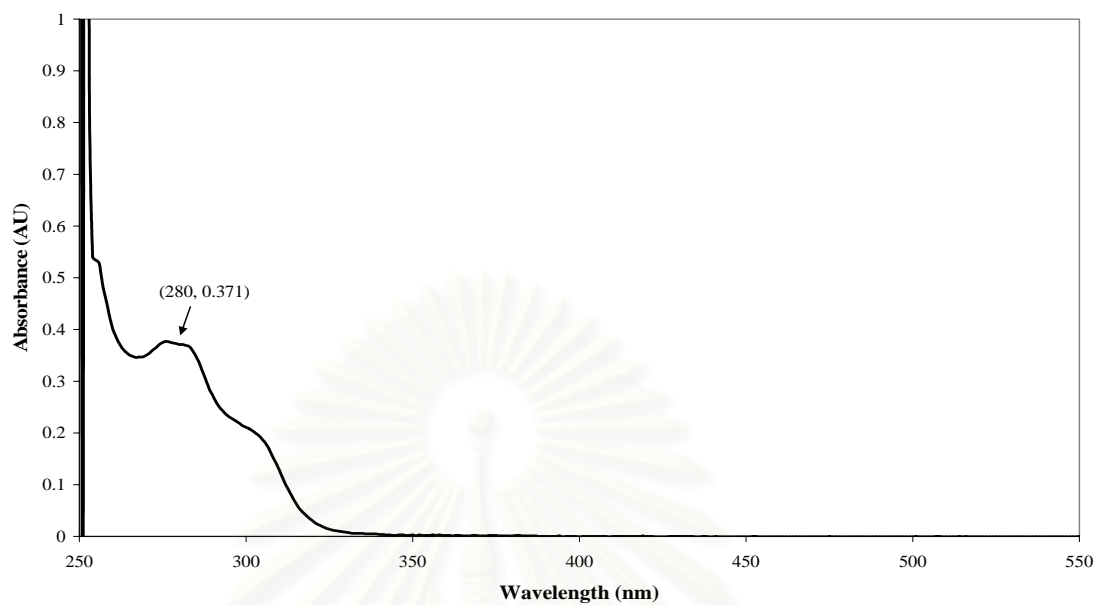
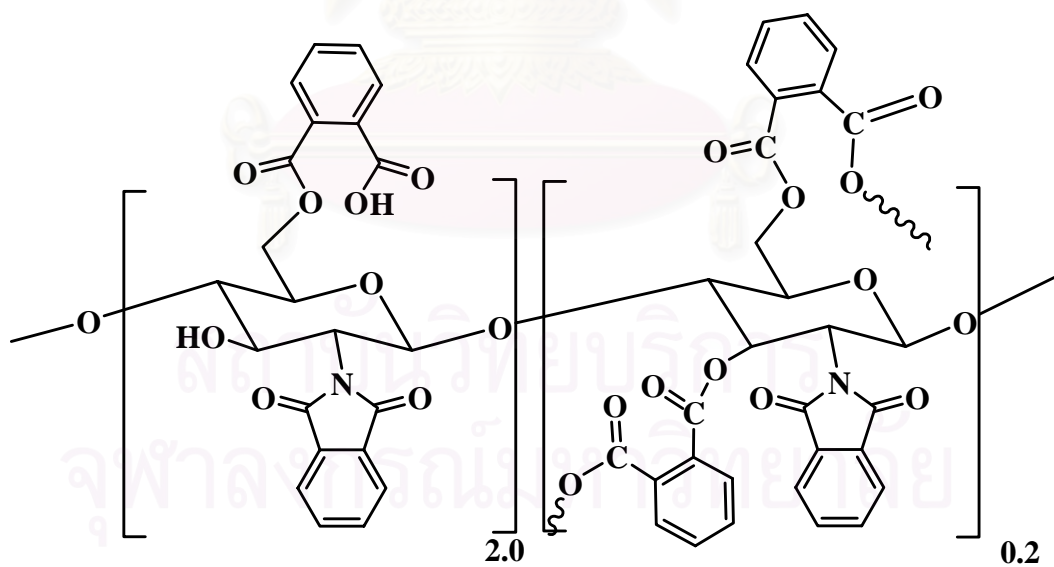
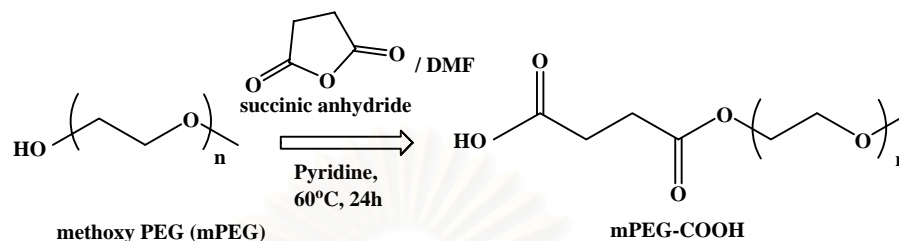


**Figure 3.3** UV absorption spectrum of phthaloylchitosan (PLC) in DMSO at concentration 60 ppm.

The general structure of the phthaloylchitosan is as followed.



### 3.1.2 Poly (ethylene glycol) methyl ether terminated with carboxylic groups (mPEG-COOH)



**Scheme 3.3** Synthesis of poly (ethylene glycol) methyl ether terminated with carboxylic groups (mPEG-COOH).

The mPEG-COOH was prepared by reacting poly (ethylene glycol) methyl ether with succinic anhydride in DMF using pyridine as catalyst. The product was obtained by precipitating with diethyl ether. The IR spectrum of mPEG-COOH shows absorption bands ( $1110\text{ cm}^{-1}$  and  $1149\text{ cm}^{-1}$ ) assignable to the ether bond (C-O-C) of mPEG. A peak at  $1735\text{ cm}^{-1}$  indicates carbonyl functionality. A peak at  $2884\text{ cm}^{-1}$  was methylene group on PEG. From these result, it was concluded that the terminal hydroxyl group of mPEG has been replaced with succinyl moiety (see Figure 3.4).

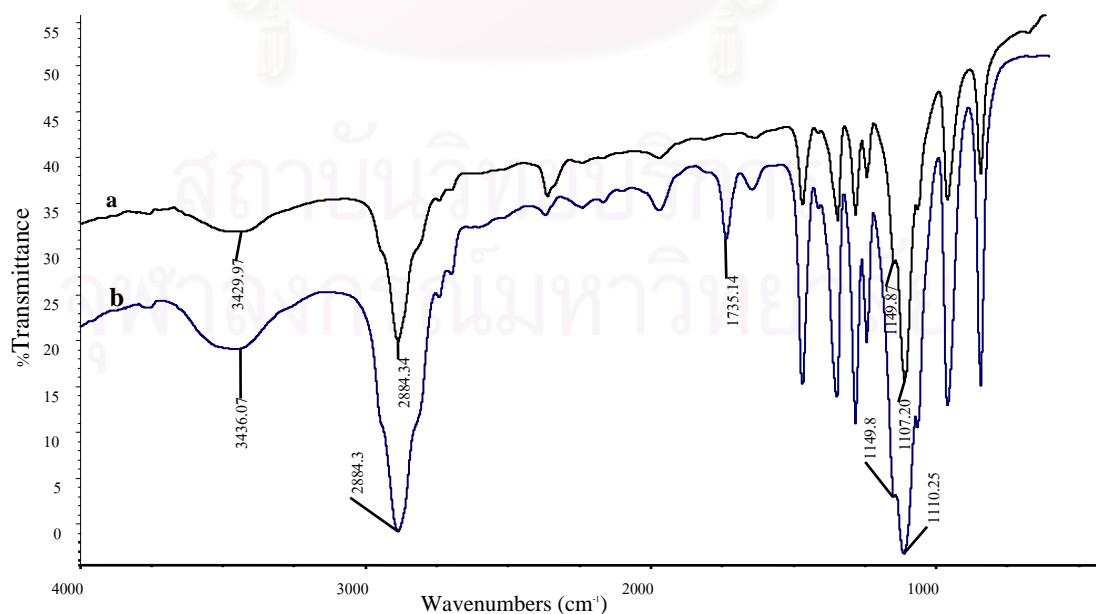
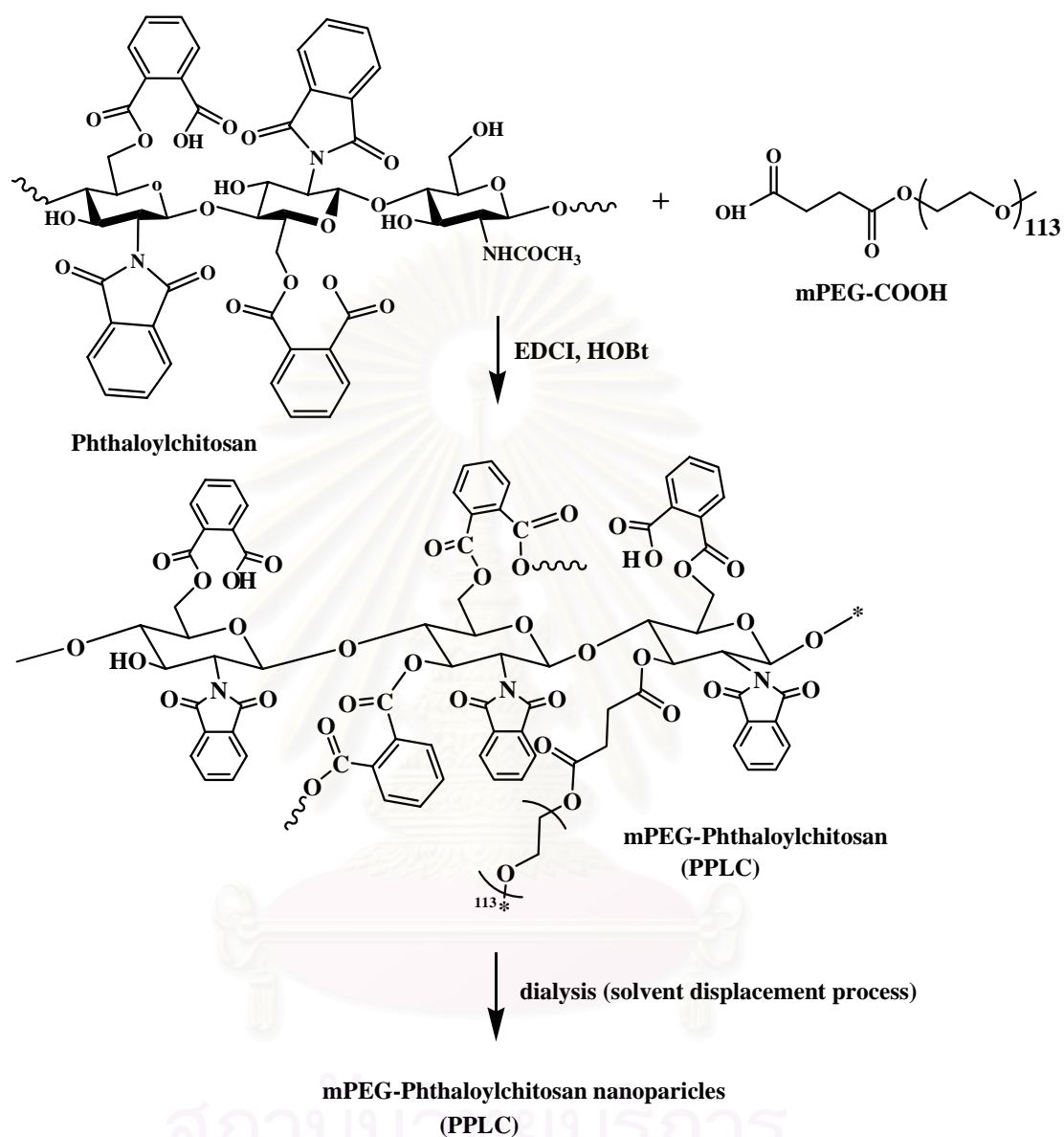


**Figure 3.4** IR spectra (KBr) of a.) mPEG and b.) mPEG-COOH.

## 3.1.3 mPEG-Phthaloylchitosan (PPLC)



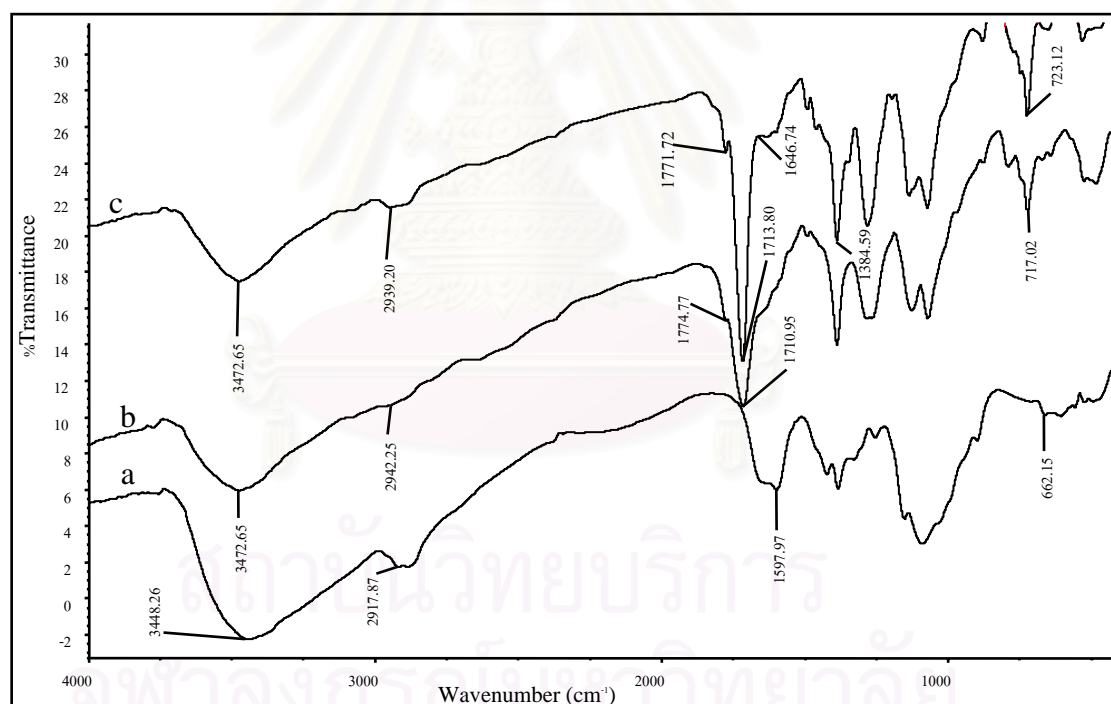
**Scheme 3.4** Synthesis of mPEG-phthaloylchitosan.

The mPEG-phthaloylchitosan (PPLC) was synthesized by reacting phthaloylchitosan with mPEG-COOH in DMF in the presence of HOBt and EDCI. The solution was reacted overnight at room temperature. The IR spectrum of the PPLC shows two absorption bands ( $1713\text{ cm}^{-1}$  and  $1771\text{ cm}^{-1}$ ) assignable to the carbonyl group of anhydride. A medium absorption peak at  $2939\text{ cm}^{-1}$  assignable to the methylene group



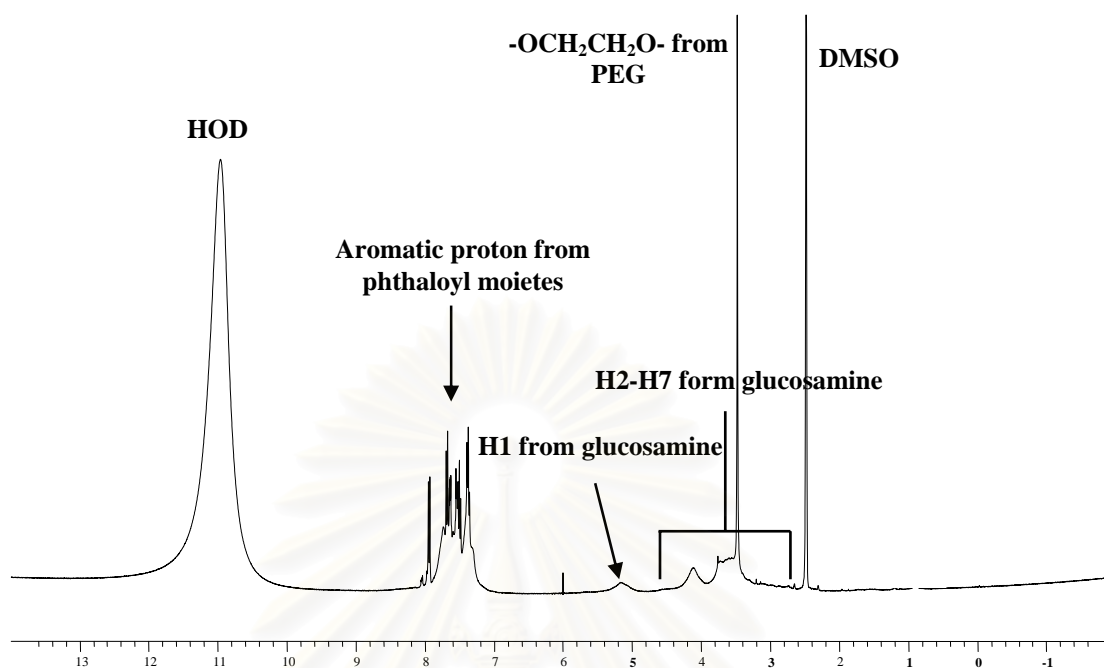
and three absorption bands (723, 1384 and 1646  $\text{cm}^{-1}$ ) referred to aromatic ring of phthalimido group onto chitosan (see Figure 3.5).

The PEG grafted phthaloylchitosan was characterized by  $^1\text{H-NMR}$  (in  $\text{DMSO-}d_6$ ), which clearly indicated the presence of PEG moieties by the appearance of sharp signal at 3.5 ppm (41H,  $-\text{OCH}_2\text{CH}_2\text{O}-$  of PEG). Substitution degree of 8.70% of PEG was obtained by integration the peaks area at 2.7-5.8 ppm which represented 7H from each pyranose ring of chitosan and 452H from each PEG unit against phthaloyl protons at 7.47-7.68 ppm (19H, Ar-H of the phthaloyl group) or against the H1 proton of the glucosemine at 5.1 ppm. The resonances from HOD peak at 3.3 ppm could be avoided by adding a small amount of trifluoroacetic acid into the sample just prior to the NMR analysis, shifting the HOD peak to  $\sim 10\text{-}12$  ppm (see in Figure 3.6).

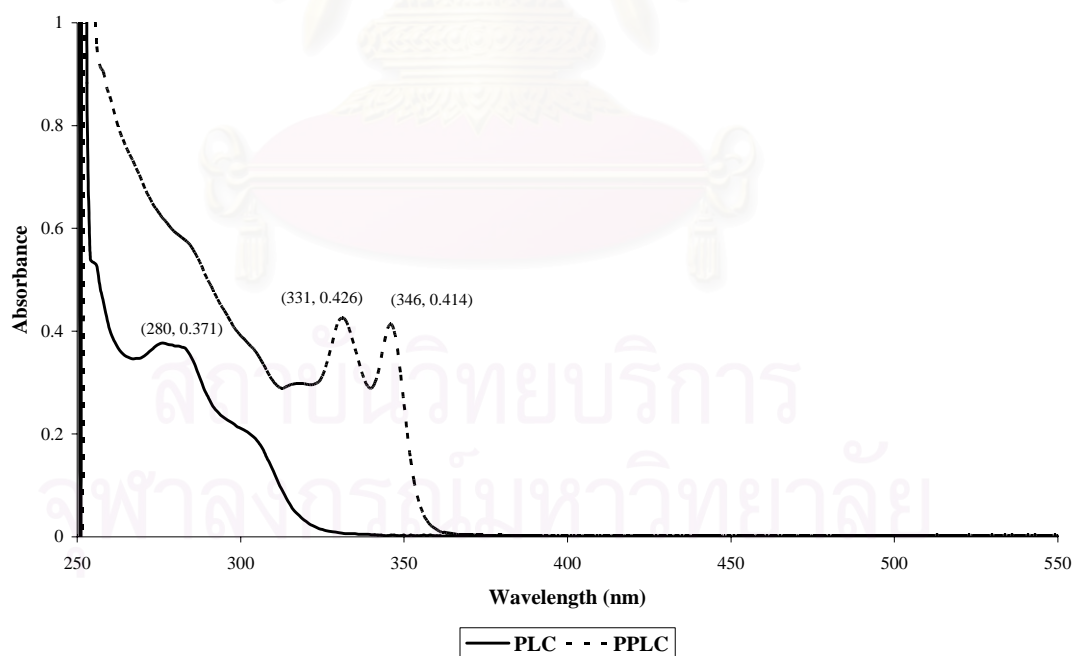


**Figure 3.5** IR spectra (KBr) of a.) chitosan, b.) phthaloylchitosan and c.) mPEG-phthaloylchitosan (PPLC).

As shown in Figure 3.7, the product gave two new absorption bands,  $\lambda_{\text{max}}$  of 332 nm and 347 nm in DMSO. After grafting mPEG-COOH onto phthaloylchitosan, the product possesses UVA absorption property.

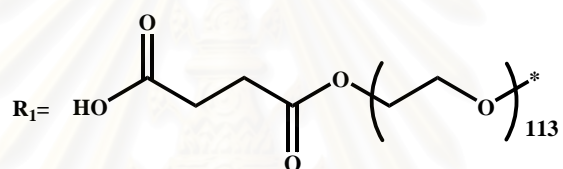
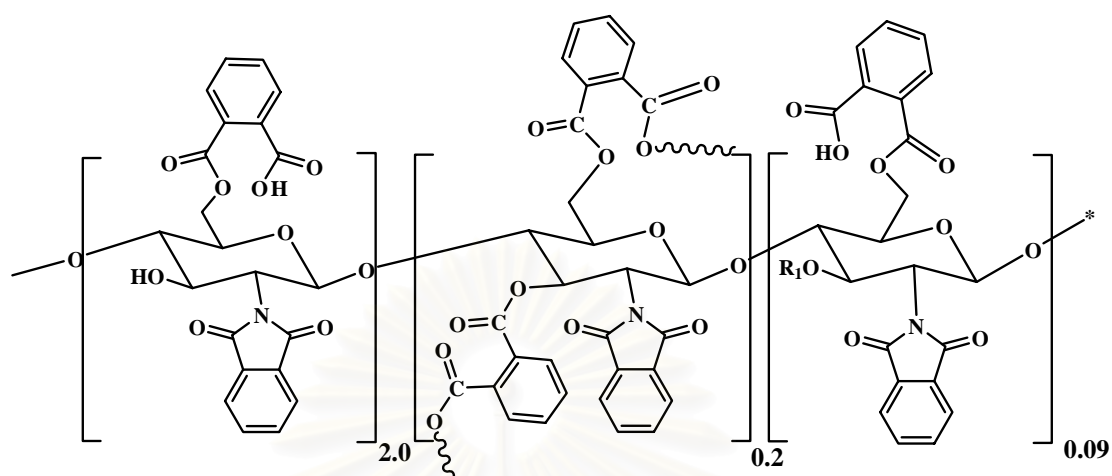


**Figure 3.6**  $^1\text{H}$ -NMR spectrum of mPEG-phthaloylchitosan (PPLC) (DMSO deuterated with 0.05% trifluoroacetic acid).

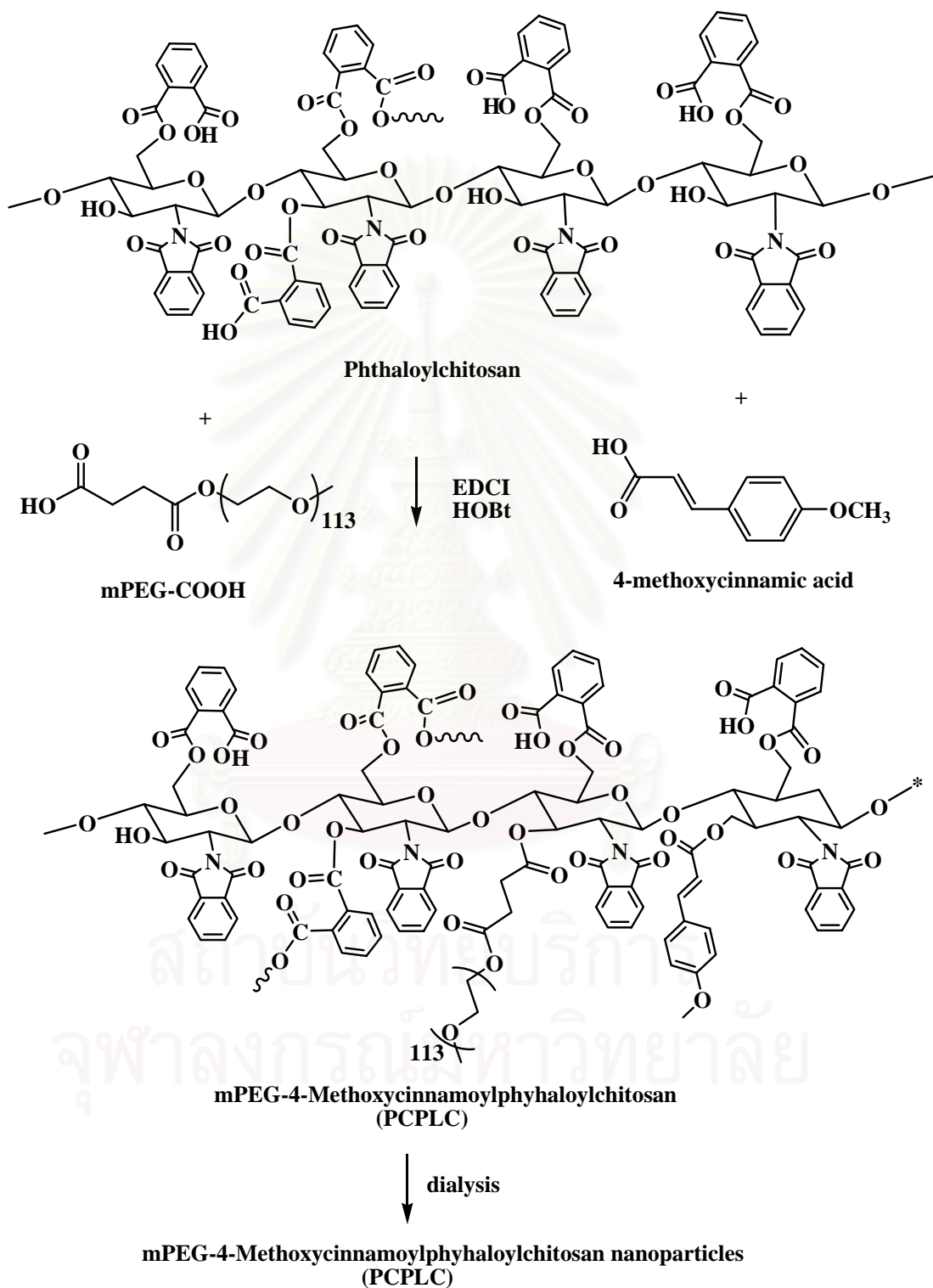


**Figure 3.7** UV absorption spectra of phthalolchitosan (PLC) and mPEG-phthaloylchitosan (PPLC) in DMSO at concentration 60 ppm.

The general structure of mPEG-phthaloylchitosan is as followed.



สถาบันวิทยบริการ  
จุฬาลงกรณ์มหาวิทยาลัย

3.1.4 mPEG-4-Methoxycinnamoylphthaloylchitosan (PCPLC)

Scheme 3.5 Synthesis of mPEG-4-methoxycinnamoylphthaloylchitosan

Grafting of 4-methoxycinnamic acid and mPEG-COOH onto phthaloylchitosan was carried out as shown in Scheme 3.5. The reaction gave 81% yield and exhibited pale brown solid appearance. The IR spectrum of the PCPLC shows two absorption bands ( $1716\text{ cm}^{-1}$  and  $1771\text{ cm}^{-1}$ ) and peak at  $1771\text{ cm}^{-1}$  (ester) assignable to the phthalimido functionality. An absorption peak shows at  $1619\text{ cm}^{-1}$  ( $\text{C}=\text{C}$  of cinnamoyl group) assignable to cinnamoyl functionality. The absorption peak shows at  $2933\text{ cm}^{-1}$  assignable to the methylene group and three absorption bands ( $726$ ,  $1384$  and  $1646\text{ cm}^{-1}$ ) referred to aromatic ring of phthalimido group (see in Figure 3.8).

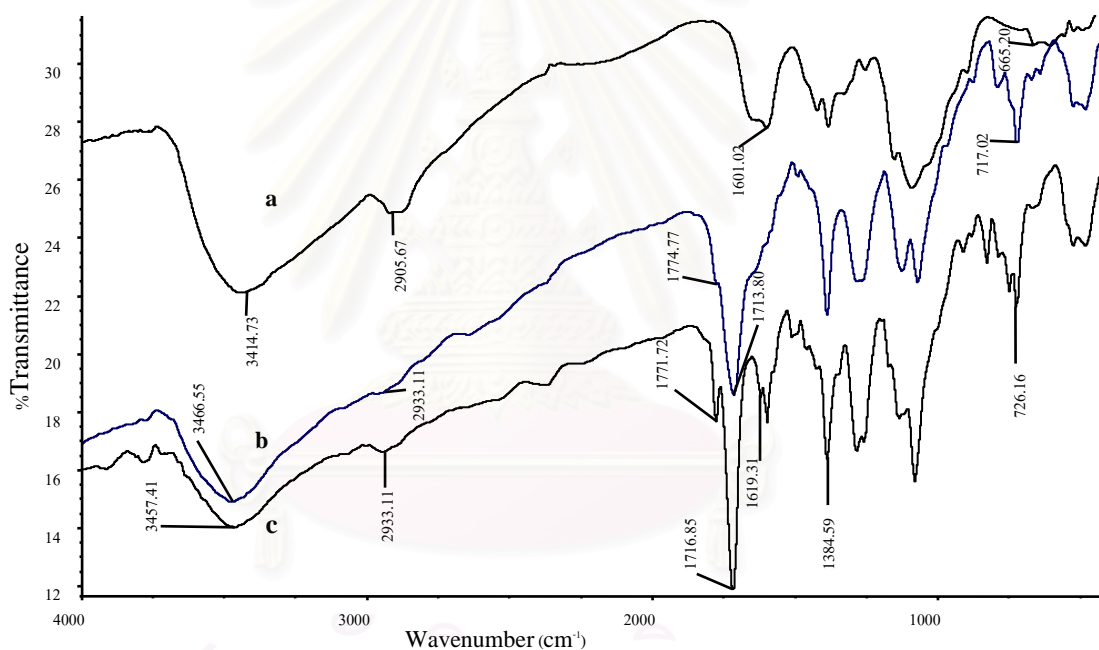


**Figure 3.8** IR spectra (KBr) of a) chitosan, b) phthaloylchitosan and c) mPEG-4-methoxycinnamoylphthaloylchitosan (PCPLC).

The grafted polymer was characterized by  $^1\text{H-NMR}$  (in  $\text{DMSO-}d_6$ ), which clearly indicated the presence of cinnamoyl moieties by the appearance of the resolved sharp doublet signals at  $6.4\text{ ppm}$  ( $1\text{H}$ ,  $J=16$ ,  $400\text{Hz}$ ,  $\text{Ar-CH}=\text{CH-COOR}$  of the cinnamoyl group). Substitution degree of PEG ( $0.55\%$ ) and cinnamoyl ( $13.33\%$ ) were estimated by integration the peak area at  $6.4\text{ ppm}$  which represented of  $1\text{H}$  ( $1\text{H}$ ,  $\text{Ar-CH}=\text{CH-COOR}$ ) from cinnamoyl group against the  $\text{H1}$  peak of the glucosamine at

5.1 ppm. The substitution degree of PEG could be estimated by integration the peak area at 2.7-5.50 ppm (3H of OCH<sub>3</sub>, 24H of PEG and 7H of glucosamine) (excluding the 3H of cinnamoyl group unit and 7H of glucosamine unit) against the H1 peak of the glucosamine at 5.1 ppm. The resonances from HOD peak at 3.3 ppm could be avoided by adding a small amount of trifluoroacetic acid into the sample just prior to the NMR analysis, shifting the HOD peak to ~11-12 ppm (see in Figure 3.9).

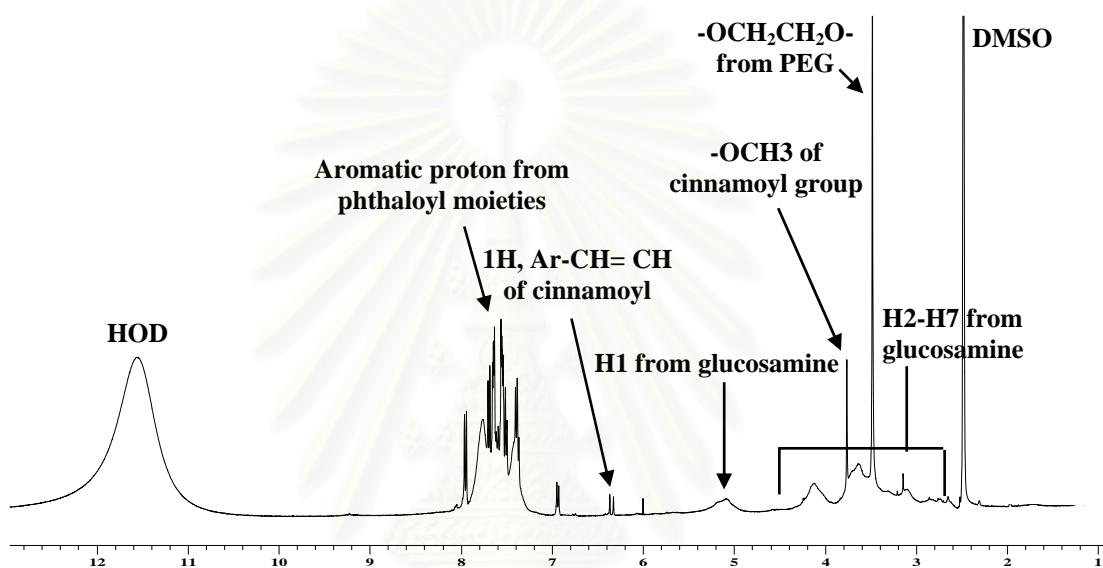


**Figure 3.9**  $^1\text{H}$ -NMR spectrum of mPEG-4-methoxycinnamoylphthaloylchitosan (PCPLC, DMSO deuterated with 0.05% trifluoroacetic acid).

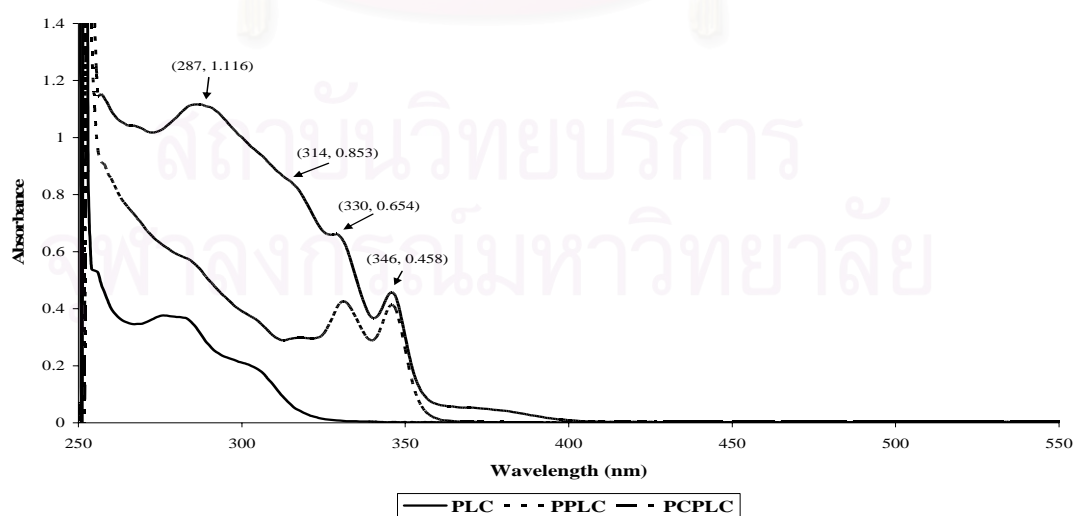
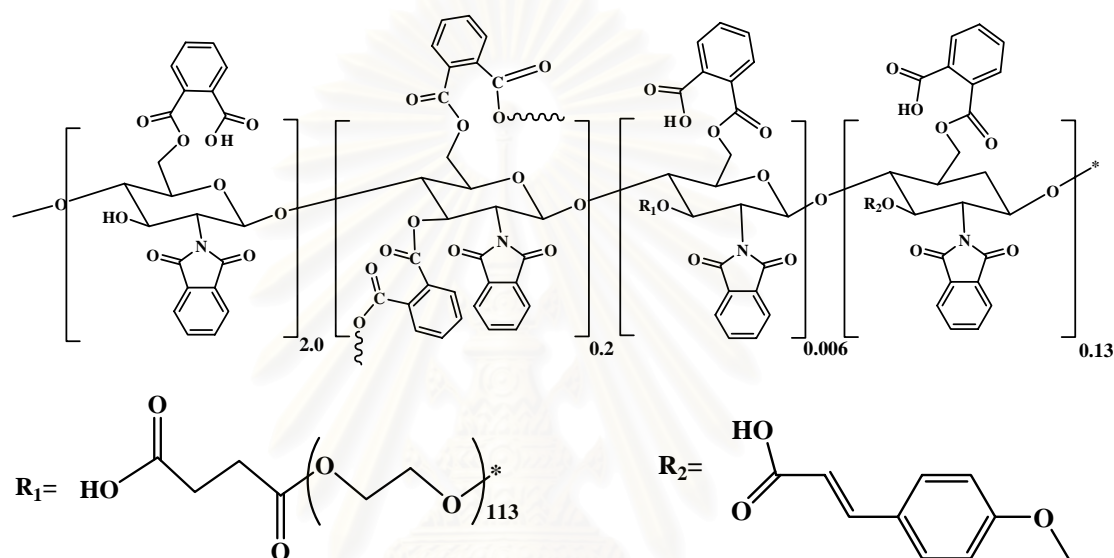


**Figure 3.10** UV absorption spectrum of mPEG-4-methoxycinnamoyl phthaloylchitosan (PCPLC) in DMSO at concentration 60 ppm.

As shown in Figure 3.10, UV absorption spectrum of mPEG-4-methoxycinnamoylphthaloylchitosan gave four absorption bands;  $\lambda_{\max}$  of 290 nm referred to phthaloylchitosan, 313 nm belonging to 4-methoxycinnamic acid, and 330 nm and 346 nm belonging to mPEG in DMSO. The general structure of mPEG-4-cinnamoylphthaloylchitosan is as followed.



## 3.2 Antibacterial study

### 3.2.1 Determination of MIC and MBC

An experiment has been carried out to compare the antibacterial activity of mPEG-phthaloylchitosan (PPLC) and mPEG-4-methoxycinnamoylphthaloylchitosan (PCPLC) nanoparticles, chitosan solution and clindamycin. The study was carried out against *S. aureus* and *E. coli*, using the turbidimetric method [120]. The results of the MIC (minimum inhibitory concentration) values are shown in Table 3.1. The MIC was the lowest absorbance difference between 0 h and 24 h at 600 nm ( $A_{600}$ ), when absorbance difference  $\leq 0.100$ . The inhibition effect of chitosan solution and chitosan nanoparticles at different concentrations against the growth of *E. coli* and *S. aureus* were examined. It could be concluded that the PPLC and PCPLC nanoparticles significantly inhibited the growth of the Gram-positive bacteria *S. aureus* and Gram-negative bacteria *E. coli*. The *S. aureus* cultured medium showed the absorbance difference of 0.062 even when the PPLC concentration was as small as 2500  $\mu\text{g/mL}$ ,

comparing to 1.122 of the control. The *S. aureus* cultured medium showed the absorbance difference of 0.622 when treated with the PCPLC concentration was 2500  $\mu\text{g/mL}$ . These results concluded that the PPLC and PCPLC nanoparticles could inhibit the growth of *S. aureus*. The chitosan solution and the clindamycin gave the absorbance differences of -0.632 and 0.062 at concentrations of 625 and 16  $\mu\text{g/mL}$ , respectively, when treated with *S. aureus*. In the case of Gram-negative bacteria *E. coli*, the absorbance difference was 0.095 when treated with PPLC at concentration 5000  $\mu\text{g/mL}$ . The absorbance difference for PCPLC at the same concentration was 0.192, comparing to 1.199 of the control. While the medium cultured with *E. coli* showed the absorbance differences of -0.197 and 0.012 for the chitosan solution at the concentration of 156  $\mu\text{g/mL}$  and clindamycin at the concentration 500  $\mu\text{g/mL}$ , respectively.

**Table 3.1** MIC and MBC ( $\mu\text{g/mL}$ ) of chitosan solution, chitosan nanoparticles and clindamycin against *S. aureus* and *E. coli*.

Bacteria	Chitosan solution		PPLC		PCPLC		Clindamycin	
	MIC	MBC	MIC	MBC	MIC	MBC	MIC	MBC
<i>S. aureus</i>	625	1250	2500	-	> 2500	-	16	250
<i>E. coli</i>	156	1250	5000	-	> 5000	-	500	2500

These results concluded that the chitosan nanoparticles (PPLC and PCPLC) had less antibacterial activity than the chitosan solution and clindamycin. The result agrees with previous works reported by Yang et al. (2005). They investigated the antibacterial properties of native chitosan and *N*-alkylated chitosan derivatives with disaccharide. They indicated that the chitosan exhibited a higher antibacterial activity against either *E. coli* or *S. aureus* than chitosan derivative at pH 6.0 [121]. It was suggested that a main factor for the antibacterial activity could be due to the positively charged amino groups at C-2 in the chitosan molecule [6, 10]. They could interact with the predominantly anionic molecules on the bacteria surface. This interaction could change the permeability of the cell membrane of the bacteria, resulting in a leakage of intercellular components, and then caused the death of the cell [126]. At the position C-2 in the PPLC and PCPLC molecules interacted with phthalimido



group and polymer. This is the reason why the grafting chitosan (PPLC and PCPLC) had antibacterial activity less than native chitosan. When compared the antibacterial activity between PPLC and PCPLC nanoparticles, from these results shown that the PPLC had more antibacterial activity than PCPLC. Because of at the C-2, C-3 and C-6 of PCPLC nanoparticle was grafted with polymer (phthalimido group, PEG and cinnamoyl group) more than the PPLC nanoparticle (only grafted with PEG). It's possible the protonate of methylene group on PEG interact with the negatively charge cell wall of the bacterial. Therefore the PPLC and PCPLC nanoparticle had the antibacterial activity.

From the data in Table 3.1, it was concluded that the inhibitory activity of chitosan, clindamycin and PPLC and PCPLC nanoparticles against Gram-positive bacteria were more potent than the Gram-negative bacteria. This may be a result of differences in the cell structure of the Gram-negative bacteria and the Gram-positive bacteria. Cell walls of the Gram-positive bacterium are fully composed of peptide polyglycogen. The peptidoglycan layer is composed of networks with plenty of pores, which allow foreign molecules to come into the cell without difficulty. Thus, nanoparticles may be able to penetrate into the cells by this route. But the cell wall of *E. coli*, a typical Gram-negative bacterium is made up of a thin membrane of peptide polyglycogen and an outer membrane constituted of lipopolysaccharide, lipoprotein and phospholipids. Because of the bilayer structure, the outer membrane possesses greater potential barrier against foreign molecules [126], making it more difficult for nanoparticles to enter [123].

### 3.2.2 Survival of bacteria

The cell count of *S. aureus* and *E. coli* were tested by spread-plate method. The initial number of bacterial for this experiment was  $10^5$  CFU/mL and test with the PPLC and PCPLC nanoparticle at concentration 2500  $\mu\text{g/mL}$  and 5000  $\mu\text{g/mL}$ . As describe above (Figure 3.11) the *S. aureus* cultured medium showed the absorbance difference of 0.060 at concentration of 2500  $\mu\text{g/mL}$  after treated with PPLC for 24 h, comparing to 1.042 of the control. In the same way, the *E. coli* cultured medium showed the absorbance difference of 0.088 after treated with PPLC at concentration 5000  $\mu\text{g/mL}$ ,

comparing to 1.145 of the control. From these results (Figure 3.11), it was indicated that the grafting chitosan (PPLC and PCPLC) could inhibit the growth of bacteria.

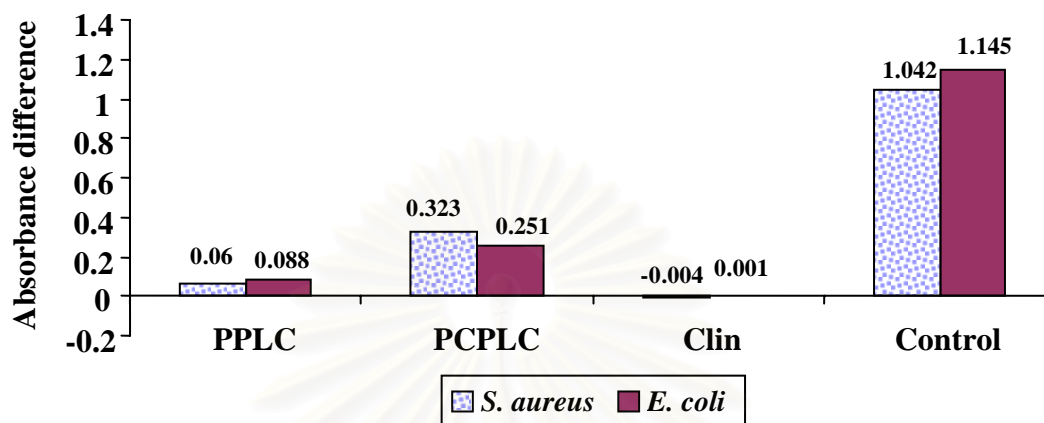


**Figure 3.11** Absorbance difference between 0 h. and 24 h. of bacterial growth after treated with chitosan nanoparticles (PPLC and PCPLC), clindamycin. Control was the culture in Tryptic soy broth.

The reduction percentages of *S. aureus* and *E. coli* after treated with chitosan nanoparticle and clindamycin are shown in Figure 3.12. The Gram-positive bacteria, *S. aureus* in control tube was  $3.25 \times 10^{14}$  CFU/mL (data shown in Appendix C, Table C.28) whereas the population of *S. aureus* when treated with PPLC and PCPLC were  $3.36 \times 10^8$  and  $3.43 \times 10^8$  CFU/mL, respectively (see in Appendix C, Table C.25 and C.26). Reduction percentages of *S. aureus* population after treated with PPLC, PCPLC, and clindamycin were 41.25, 41.18 and 100%, respectively. The reduction percentages of *E. coli* population after treated with PPLC, PCPLC and clindamycin was 35.05, 28.31 and 100%, respectively. These results indicated that although the nanoparticles have antibacterial activity towards both Gram-positive bacteria and Gram-negative bacteria, the both particles showed stronger antimicrobial activity on the Gram-positive bacteria.

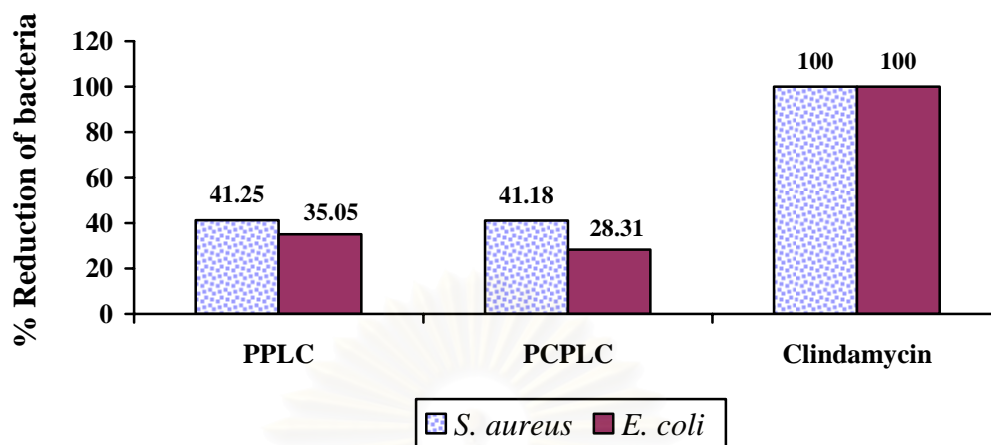


**Figure 3.12** The percentage reduction of bacteria after treated with chitosan nanoparticle and clindamycin.

### 3.3 Cytotoxicity study of mPEG–Phthaloylchitosan (PPLC) and mPEG-4-Methoxycinnamoylphthaloylchitosan nanoparticles (PCPLC).

The cytotoxic activities of PPLC and PCPLC nanoparticles were determined by MTT assay. MTT is a classical but still the most commonly used colorimetric method for determining cell growth, via measuring metabolic activity in the viable cells. The melanoma A-375 cell line was chosen for cytotoxicity experiment. Cell were incubated for 72 h at the density of  $1 \times 10^4$  cell/well with PPLC and PCPLC nanoparticles at concentrations of 0.25, 0.025 and 0.0025 mg/mL. Cell viability was identified using the MTT assay on the third day of culture. If the % viability of melanoma cell is less than 50%, it indicated that nanoparticles are toxic. From Figure 3.13, the % viability of cell lines were  $> 85\%$  after treated with PPLC and PCPLC nanoparticles at all concentration. These results indicated that the PPLC and PCPLC nanoparticles are not cytotoxic toward A-375 cells. Thus the PPLC and PCPLC nanoparticles are non-toxic and cell compatible. The result disagrees with previous work done by Qi and coworker (2005) [128]. They investigated the cytotoxic activities of chitosan nanoparticles and copper (II)-loaded chitosan nanoparticle. Chitosan nanoparticles and copper-loaded chitosan nanoparticles revealed cytotoxic activities against various tumor cell lines. They suggested that the surface charge of chitosan derivatives was the major factor affecting its cytotoxic activity due to the electrostatic interaction between the negatively charged groups of the tumor cells and

the positively charged amino groups of the chitosan [129]. The negative surface charge of PLLC and PCPLC nanoparticles may help explain the difference between their result and this work. Since the material tested in this work are different in chemical structure and surface charge from their work. In addition, different cell line used to test cytotoxicity may be another tester in discrepancy.

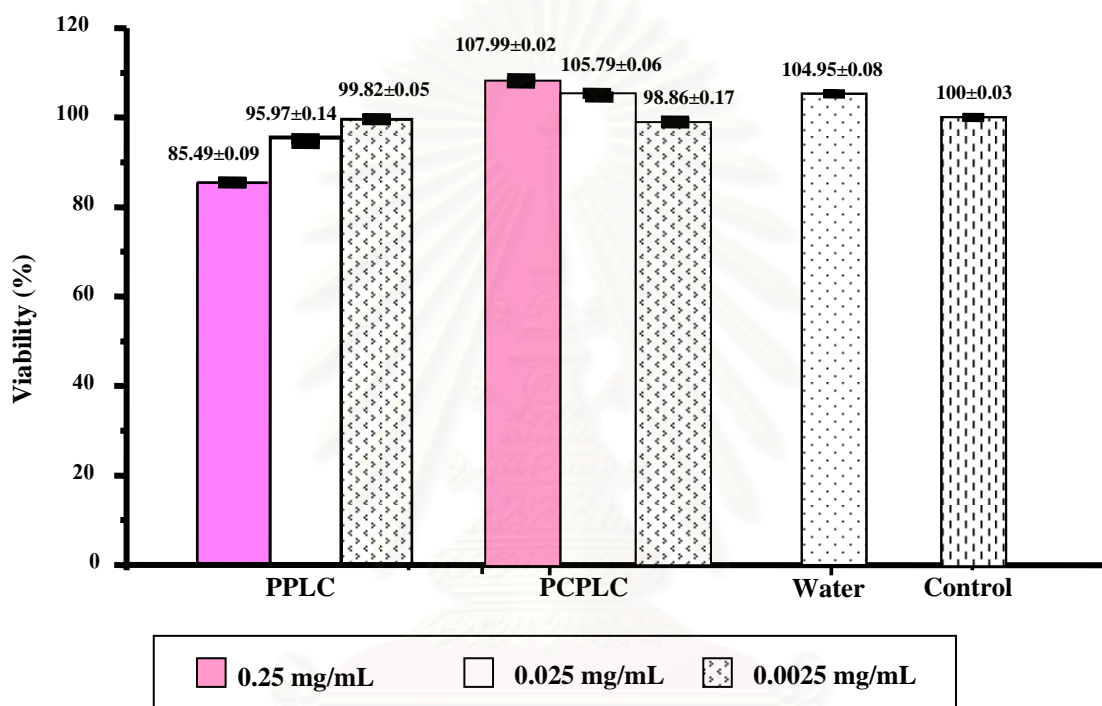


**Figure 3.13** Cytotoxic effect induced by PLLC and PCPLC on A-375 cell line. Cells were incubated with nanoparticles at a concentration of 0.25, 0.025 and 0.0025 mg/ml, for 72 h.

### 3.4. Encapsulation of all-*trans* retinyl acetate (ATRA) into nanoparticles.

In recent years, there has been much interest in the use of vitamin A and its derivative for the treatment of dermatological diseases such as acne and psoriasis. Unfortunately, some drawbacks such as poor water solubility, photostability and local irritating reactions strongly limit the topical use of vitamin A. To solve the problem, in this work, encapsulation of ATRA into nanoparticles (PLLC and PCPLC) was carried out. Encapsulation of ATRA was carried out by performing the dialysis of 0.6 % (w/v) PLLC or PCPLC solution (10 mL DMF) in a presence of 6, 15 and 30 mg

ATRA against water at pH 7. The obtained suspension of ATRA-encapsulated-nanoparticles in water was centrifuged (60 min at 20,000 g) and quickly washed with ethanol to remove ATRA on the outer sphere. Encapsulation efficiency was determined by quantitating amounts of ATRA recovered in the dialysate and in the washing EtOH, using UV absorption spectroscopy with the aid of calibration curves. The % encapsulation efficiency as calculated using equation (1)

$$\% \text{ encapsulation efficiency (\%EE)} = \frac{\text{total amount of ATRA- free ATRA}}{\text{total amount of ATRA}} \times 100 \quad (1)$$

Free ATRA = amount of ATRA found in dialysate and washing ethanol.

As can be seen in the TEM photographs (Figure 3.14 and 3.15), the PPLC and PCPLC particles are spherical and after ATRA encapsulation, the particles are bigger and the core shell is very apparent. This obvious core-shell appearance is probably a result of ATRA encapsulation. Darkness core indicates a presence of ATRA when the lighter shell represents polymer material.

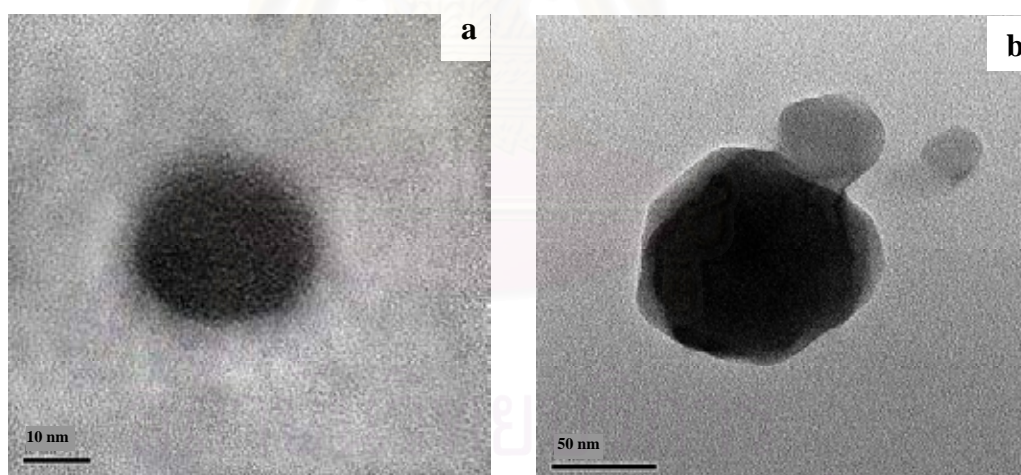


**Figure 3.14** TEM photographs of (a) unencapsulated PPLC nanoparticle and (b) ATRA-encapsulated PPLC nanoparticles at 600 ppm.

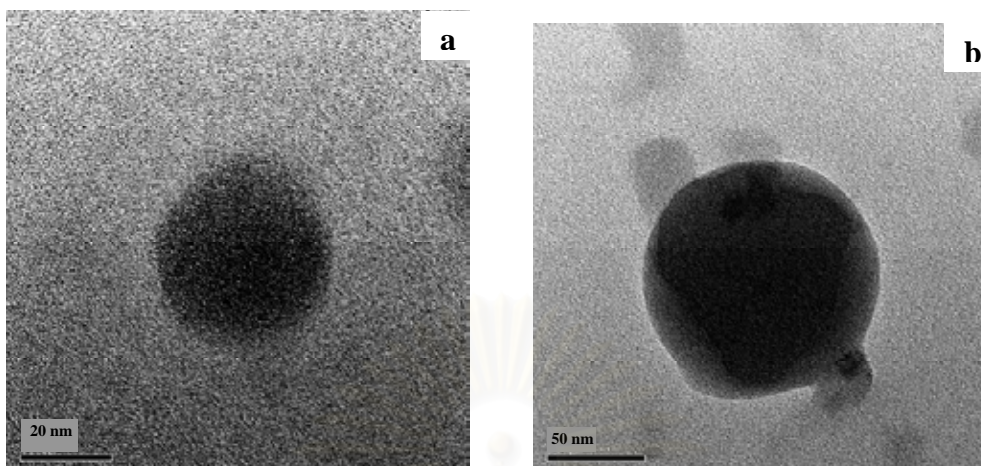


**Figure 3.15** TEM photographs of (a) unencapsulated PCPLC nanoparticle and (b) ATRA-encapsulated nanoparticles at 600 ppm.

In addition, the ATRA loaded PPLC and PCPLC nanoparticles were analyzed with NMR. The resonances from methyl proton peaks at 1.23 and 1.98 ppm of the ATRA molecule confirm successful encapsulation of ATRA into both nanoparticles (see in Figure 3.16 and 3.17)

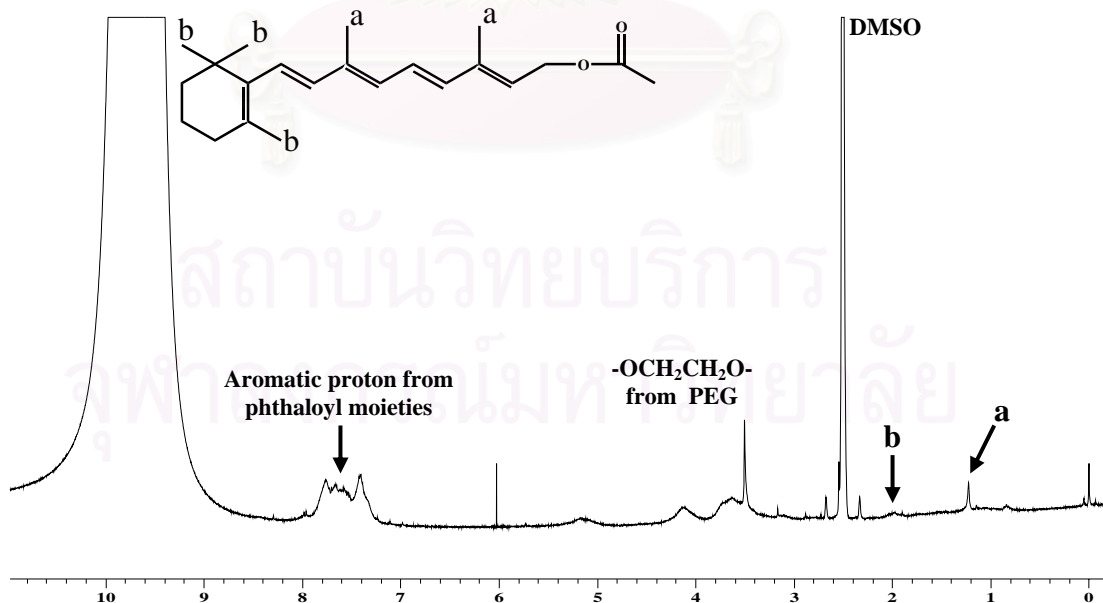


**Figure 3.16** NMR spectrum of ATRA loaded mPEG-phthaloylchitosan nanoparticles. (PPLC, DMSO deuterated with 0.05% trifluoroacetic acid).

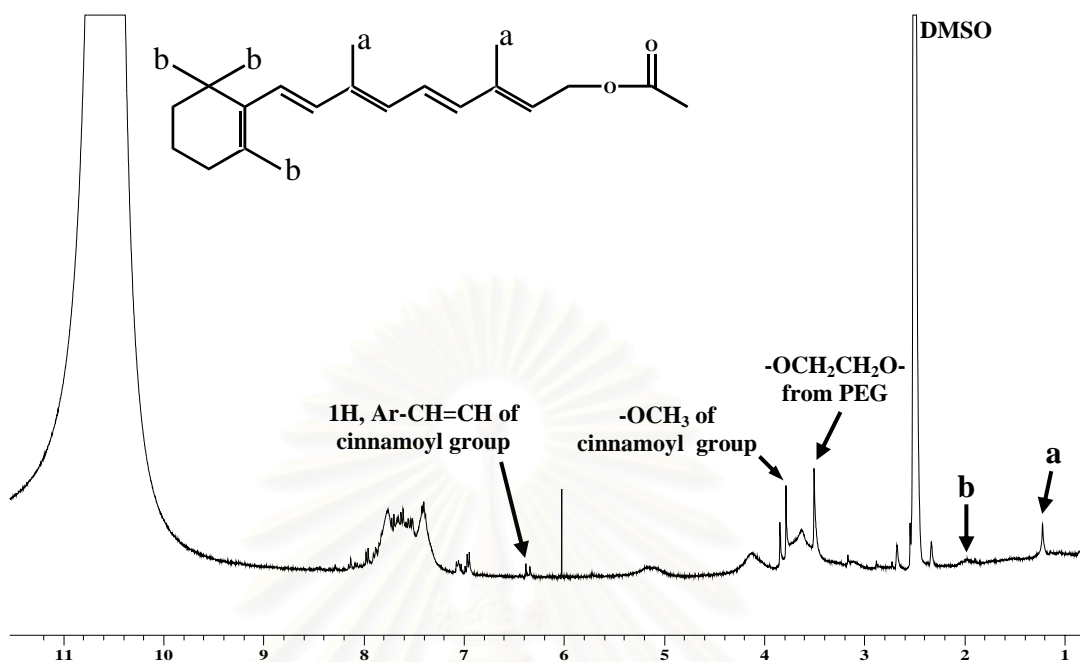


**Figure 3.17** NMR spectrum of ATRA loaded mPEG-4-methoxycinnamoyl phthaloylchitosan nanoparticles. (PCPLC, DMSO deuterated with 0.05% trifluoroacetic acid).

The amount of ATRA loaded into nanoparticles was determined by quantitating ATRA in the washing ethanol and the dialysate, using UV absorption spectrophotometry at 325 nm with the aid of calibration curve. The % drug loading were calculated using equation (1)

$$\% \text{ drug loading} = \frac{\text{weight of drug in nanoparticle}}{\text{weight of nanoparticle}} \times 100 \quad (2)$$

The % EE of all the processes used to encapsulate ATRA into PPLC and PCPLC nanoparticles are ~ 97% (Table 3.2 and see Appendix A for calculation). The drug loading percentage of 9.62%, 24.35% and 48.29% could be obtained from the experiments performed using 10%, 25% and 50% (w/w) of ATRA during the encapsulation into PPLC nanoparticle. In case of the PCPLC nanoparticles, the drug loading percentages of 7.93%, 22.05% and 46.14% could be obtained from the experiments performed using 10%, 25% and 50% (w/w) of ATRA during the encapsulation into PCPLC nanoparticle (Table 3.2). These data indicate that the PPLC and PCPLC nanoparticles are excellent carrier for ATRA.

**Table 3.2** Drug loading (% loading) and encapsulation efficiency percentages (%EE) of 600 ppm ATRA-encapsulated PPLC and PCPLC nanoparticles.

ATRA:Polymer use in the experiment (% w/w)	PPLC nanoparticles		PCPLC nanoparticles	
	% EE	% loading	% EE	% loading
10	96.22	9.62	79.32	7.93
25	97.42	24.35	88.19	22.05
50	96.58	48.29	92.28	46.14

### 3.5 Differential scanning calorimetry

DSC analyses of the PPLC (non-nanostructured) and the PPLC nanoparticle also confirm the nanostructure of the latter. The thermal decomposition of empty nanoparticles began at a little lower temperature (162.5 °C) than that of the non-nanostructured polymer (188 °C). The nanoparticles are more easily thermal degraded because their nanometric size makes the superficial area larger comparing to the non-nanostructured polymer.

The thermograms of PPLC nanoparticle and the ATRA-loaded-PPLC nanoparticle show initial broad endothermic peaks at 40-125 °C and higher exothermic peaks at 203.9 and 212.7 °C, respectively (see in Appendix B, Figure B.6 and B.8). The broad endothermic peaks are correlated with loss of water associated to hydrophilic groups of the PPLC polymer while the exothermic peaks result from breaking of the interactions those hold the nanospherical structures and degrading of the polymer. The shift of the exothermic peak to the higher temperature value after ATRA encapsulation indicates that the ATRA-encapsulated PPLC nanoparticle is a little more stable than the empty PPLC particles. The DSC study did not detect any crystalline ATRA in the ATRA-loaded nanoparticles sample; the endothermic peak of ATRA at 54.7 °C which corresponds to the melting temperature, was absent. Thus, it can be concluded that ATRA incorporated into the nanoparticles was in an amorphous or disorderd-crystalline phase of a molecular dispersion or a solid solution state in the polymer matrix.

The thermograms of PCPLC nanoparticle and the ATRA-loaded-PCPLC nanoparticle show initial broad endothermic peaks at 25-125 °C which correlated with



loss of water associated to hydrophilic groups of the nanoparticles. The endothermic peaks of PCPLC nanoparticle and the ATRA-loaded-PCPLC nanoparticle were 167.6 and 153.9 °C, respectively (see in Appendix B, Figure B.9 and B.10) which corresponds to the melting temperature. Thus both particles exhibit some crystalline phase. This crystalline phase is probably caused by the presence of 4-methoxycinnamoyl moieties in the polymer chains. The decreased in this melting temperature after ATRA encapsulation may be a result of ATRA-4-methoxycinnamoyl reaction. Thus, actually indicates interaction between ATRA and 4-methoxycinnamoyl moieties thus confirming that 4-methoxycinnamoyl moieties are positioned inside the sphere. The starting decomposition temperature of ATRA-loaded PCPLC nanoparticles (177 °C) was higher temperature than the bare particles (167.6 °C). It indicates the influence of strong interactions of ATRA and hydrophobic groups of this interaction increases the stability of the encapsulate product nanoparticles.

**Table 3.3** Thermal properties of chitosan (CS), mPEG-phthaloylchitosan (PPLC), mPEG-4-methoxycinnamoylphthaloylchitosan (PCPLC), and their ATRA-loaded and unloaded nanoparticles.

Sample	T <sub>g</sub> (°C)	T <sub>m</sub> (°C)	Starting decomposition temperature (°C)
Chitosan (CS)	63.1	-	275
PPLC non-nanostructured	61.5	-	188
PPLC nanoparticle	62.7	-	160
ATRA-loaded PPLC nanoparticles	53.6	-	176
PCPLC non-nanostructured	48.2	153.9	153.9
PCPLC nanoparticle	51.5	167.6	167.6
ATRA-loaded PCPLC nanoparticles	54.5	-	177
ATRA	-	54.7	100

The result agrees well with previous works done by Camer and coworker (2006). They investigated the thermogram of poly(*N*-vinylimidazole) grafted chitosan

(at 49% and 145% substitution). The initial decomposition of the grafted product was lower than that of the chitosan. The observed shift in the initial decomposition temperature was parallel to the increase in percent grafting [124]. The results of the grafted chitosans (PPLC and PCPLC) show lower initial decomposition temperature than chitosan (275 °C, Table 3.3). The grafting may result in the breaking of intramolecular hydrogen bonds of the chitosan chains thus lower its decomposition temperature. This result is consistent with improved solubility of grafted products (PPLC and PCPLC) in DMF and DMSO.

### 3.6 Morphology, size distribution and zeta potential of chitosan nanoparticles

Morphology of unencapsulated chitosan nanoparticles (PPLC and PCPLC) and ATRA-encapsulated nanoparticles were analyzed with scanning electron microscope (SEM) and transmission electron microscope (TEM). The mPEG-phthaloylchitosan (PPLC) and mPEG-4-methoxycinnamoylphthaloylchitosan (PCPLC) nanoparticles and ATRA-encapsulated nanoparticles are all spherical (Figure 3.16 and 3.17). The size distribution of the PPLC nanoparticles and ATRA-loaded-PPLC nanoparticles were measured by dynamic laser light scattering (Figure 3.22). The mean diameter of bare PPLC nanoparticles was  $53.34 \pm 0.16$  (PDI=0.24) nm while the diameters of 10%, 25% and 50% ATRA-loaded PPLC nanoparticles were  $111.23 \pm 1.71$  (PDI=0.13),  $98.24 \pm 0.64$  (PDI=0.32) and  $91.57 \pm 1.02$  (PDI=0.13) nm, respectively. The PCPLC nanoparticles showed the mean particle size of  $61.43 \pm 0.33$  (PDI=0.17) nm. The mean particle sizes of 10%, 25% and 50% ATRA-loaded PCPLC nanoparticles were  $78.23 \pm 0.80$  (PDI=0.19),  $78.20 \pm 0.28$  (PDI=0.32) and  $76.64 \pm 0.38$  (PDI=0.37) nm. Both bare and ATRA-loaded PPLC and PCPLC nanoparticles, gave quite narrow size distribution. All encapsulated particles are bigger than their corresponding bare particles. To our surprise when comparing 10%, 25% and 50% ATRA-loaded particles the diameter very slightly decreased with an increase in the weight ratio of ATRA to polymer. However, the result agrees well with previous works done by Opanasopit *et al.* [119]. They prepared amphiphilic grafted copolymer Phthalolchitosan-grafted poly(ethylene glycol) methyl ether (PLC-g-mPEG) using chitosan with four different degrees of deacetylations (DD) (80, 85, 90 and 95%).

They investigate the effect of different degrees of deacetylation on the size of all-*trans* retinoic acid incorporation into PLC-g-mPEG micelle. They shows that polymer

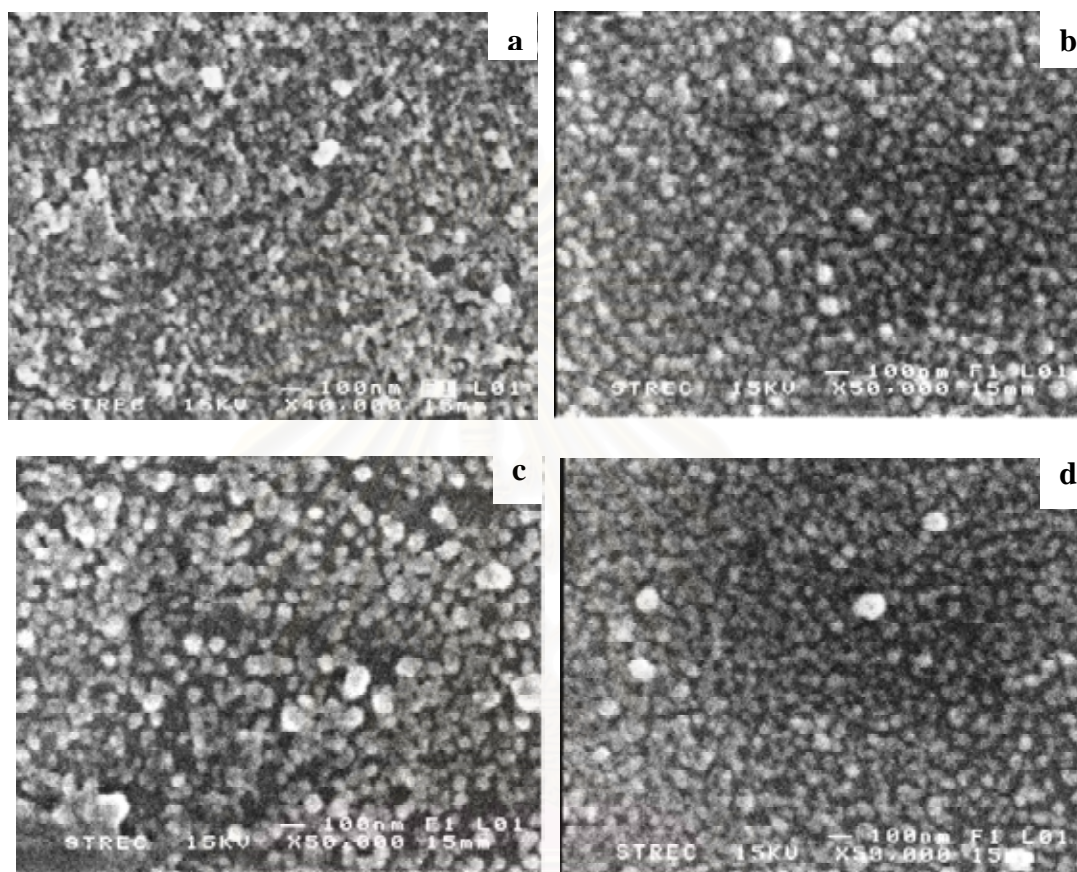


**Figure 3.18** SEM photographs of unencapsulated PPLC nanoparticle (a), 10% ATRA-loaded PPLC nanoparticle (b), 25% ATRA-loaded PPLC nanoparticle (c) and 50% ATRA-loaded PPLC nanoparticle (d) at 600 ppm.

with 95% DD gave nanoparticles with similar size nor matter of how much retinoic acids were encapsulated. In our work, the chitosan used was 99% DD and its derivatives gave particles with similar size nor matters of how much ATRA were encapsulated. SEM picture of PPLC and PCPLC revealed the dented spherical shape of the particles, therefore, it was speculate that there might be some void volume within the particles with lower amount of ATRA.

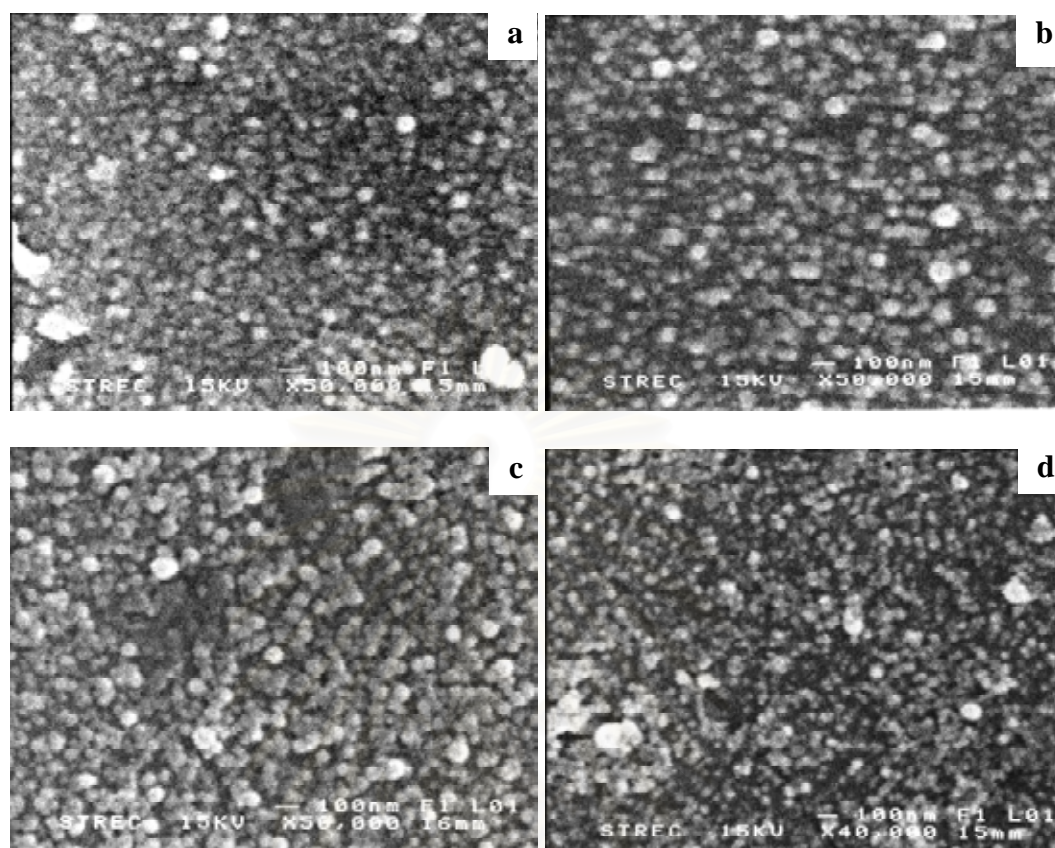


**Figure 3.19** SEM photographs of unencapsulated PCPLC nanoparticle (a), 10% ATRA-loaded PCPLC nanoparticle (b), 25% ATRA-loaded PCPLC nanoparticle (c) and 50% ATRA-loaded PCPLC nanoparticle (d) at 600 ppm.

The zeta potential, that is, surface charge, can greatly influence particle stability in suspension through the electric repulsion between particles. Zeta potential values for the unloaded PPLC ( $-23.61 \pm 1.23$  mV) and PCPLC ( $-26.40 \pm 0.48$  mV) nanoparticles indicate that the surfaces of the nanoparticles are negatively charged. The zeta potential of the 10%, 25% and 50% ATRA-loaded PPLC nanoparticles were  $-26.86 \pm 0.49$  mV,  $-26.25 \pm 0.27$  mV and  $-26.96 \pm 1.01$  mV, respectively. The zeta potential of 10%, 25% and 50% of ATRA-loaded PCPLC nanoparticles were  $-28.70 \pm 0.76$  mV,  $-26.59 \pm 0.65$  mV and  $-30.5 \pm 0.41$  mV, respectively. The zeta potential of ATRA-encapsulated PPLC and PCPLC nanoparticles are a little more negatively charged than unencapsulated nanoparticles. The results agree with the work reported by Kim and coworkers (2006). They prepared retinol-encapsulated chitosan nanoparticles with ultrasonication. The authors suggested that retinol was

encapsulated into chitosan nanoparticles by ion complex. The zeta potential of the particles increased after retinol encapsulation [114].

Furthermore, the effect of high temperature and pressure on morphology and particles size of chitosan nanoparticles were analyzed with SEM. The result indicated that chitosan nanoparticles were stable under the temperature of 110 °C at the pressure of 1 bar/sq inch for 10 minute (autoclaved condition). The particle size and morphology of autoclaved PPLC and PCPLC nanoparticles are similar (Figure 3.23 and 3.24).

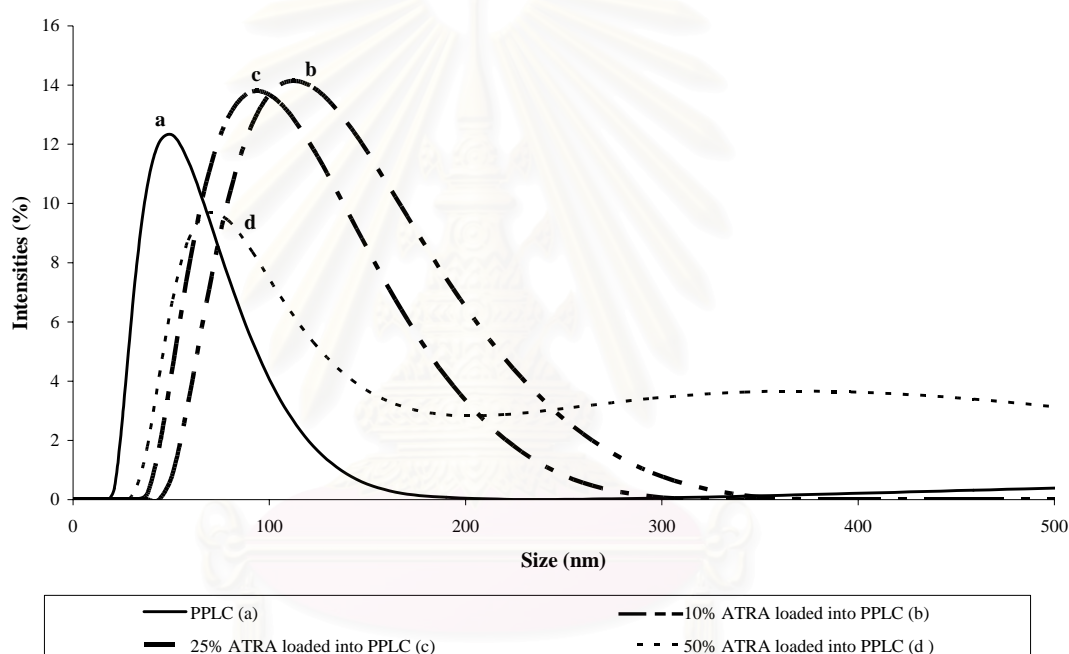


**Figure 3.20** Size distribution profiles of mPEG-phthaloylchitosan (PPLC) nanoparticles and 10%, 25% and 50% ATRA-loaded PPLC nanoparticles at 600 ppm.

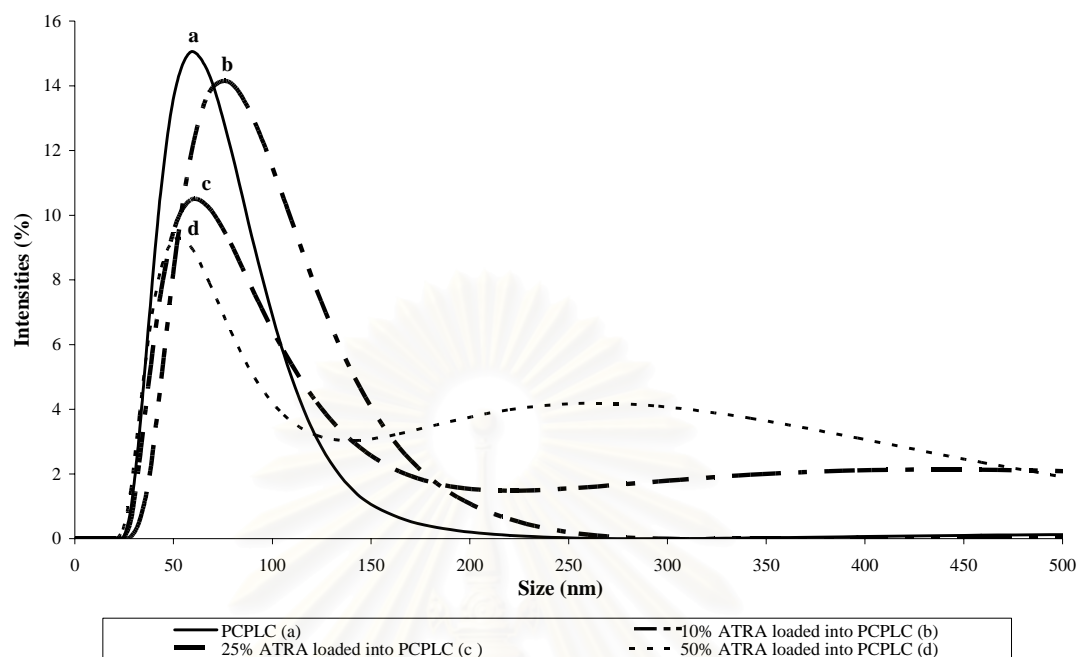


**Figure 3.21** Size distribution profiles of mPEG-4-methoxycinnamoyl phthaloylchitosan (PCPLC) nanoparticles and 10%, 25% and 50% ATRA-loaded PPLC nanoparticles at 600 ppm.

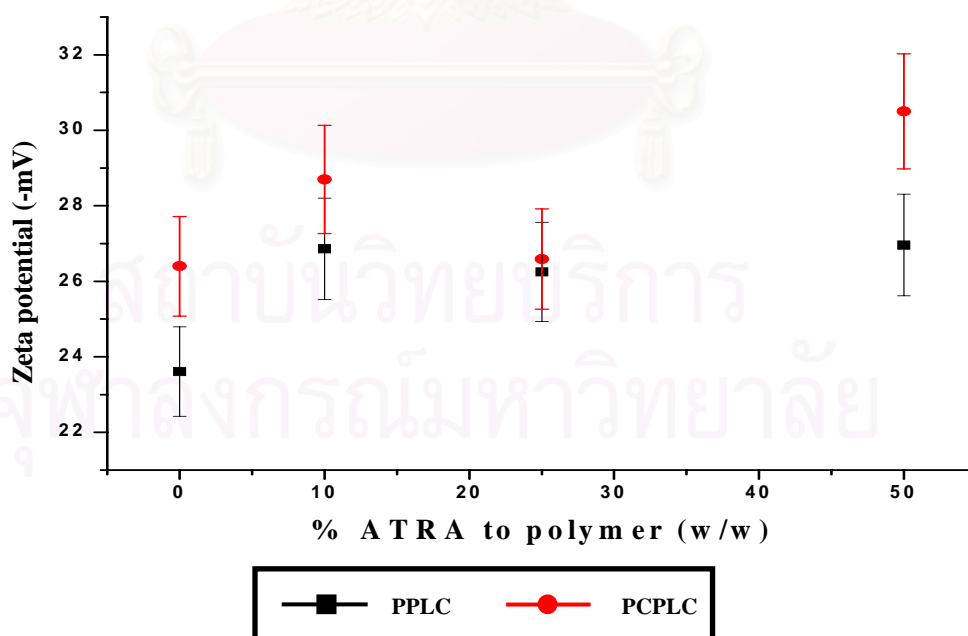


**Figure 3.22** Zeta potential profiles of mPEG-phthaloylchitosan (PPLC) and mPEG-4-methoxycinnamoyl phthaloylchitosan (PCPLC) nanoparticles at 600 ppm.

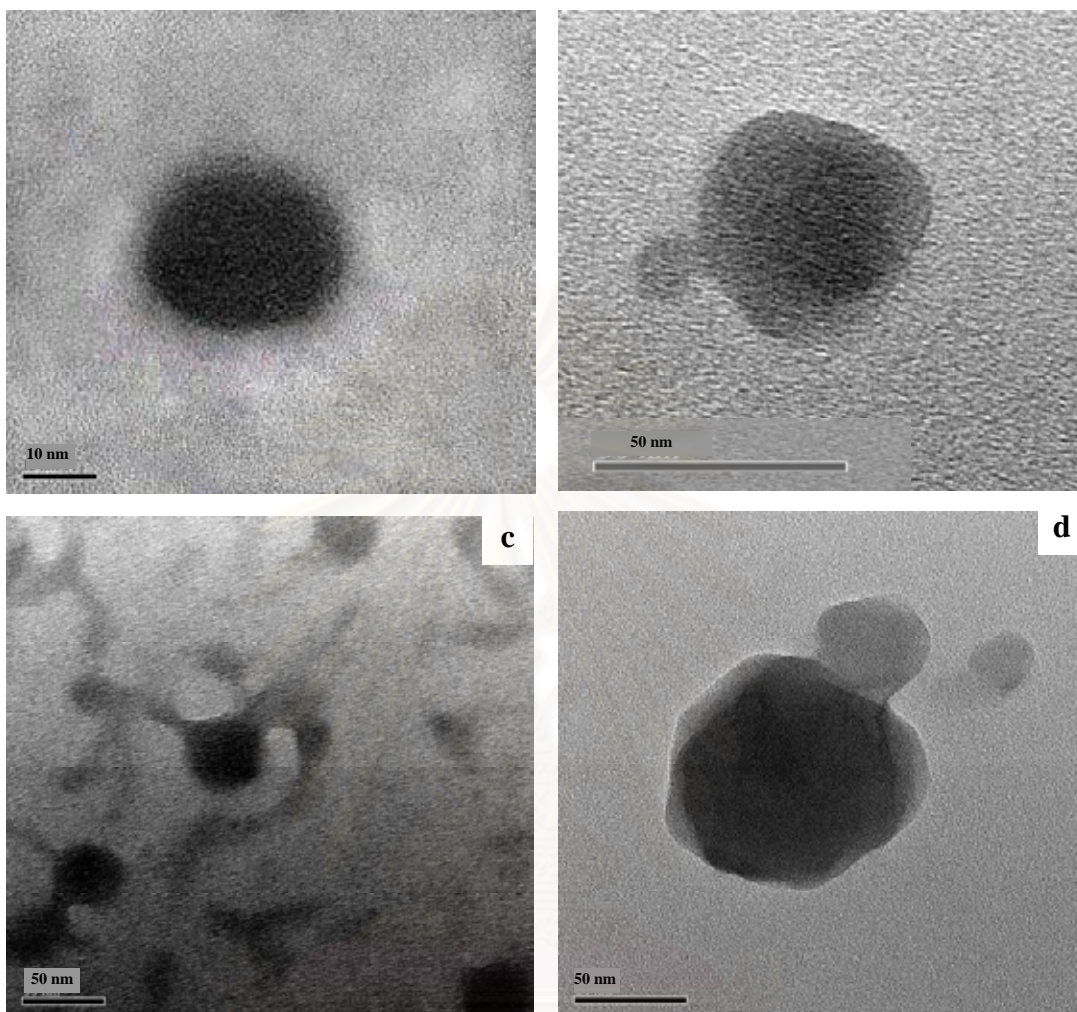


**Figure 3.23** TEM photograph of PPLC before (a) and after 10% ATRA (b), 25% ATRA (c) and 50% ATRA (d) to polymer encapsulation at 600 ppm

สภานิติบัญญัติ  
จุฬาลงกรณ์มหาวิทยาลัย

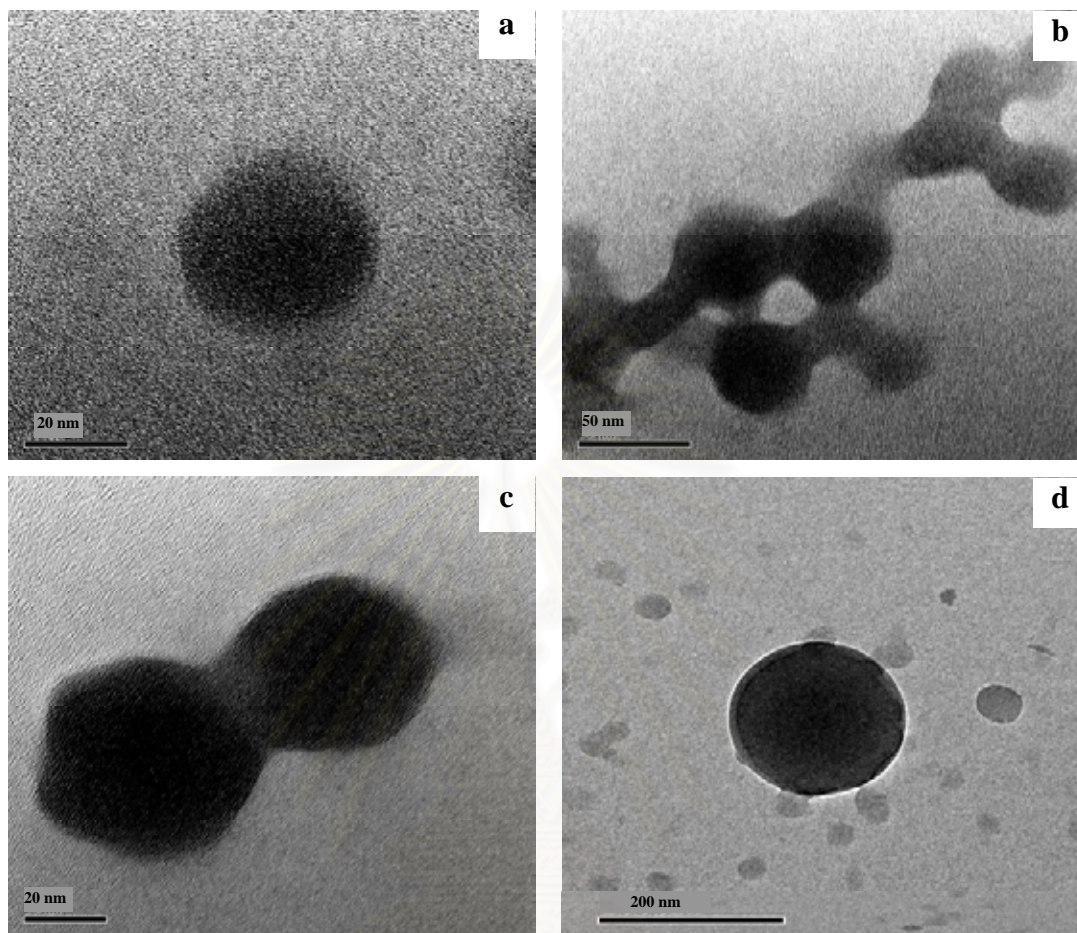


**Figure 3.24** TEM photograph of PCPLC before (a) and after 10% ATRA (b), 25% ATRA (c) and 50% ATRA (d) to polymer encapsulation at 600 ppm.

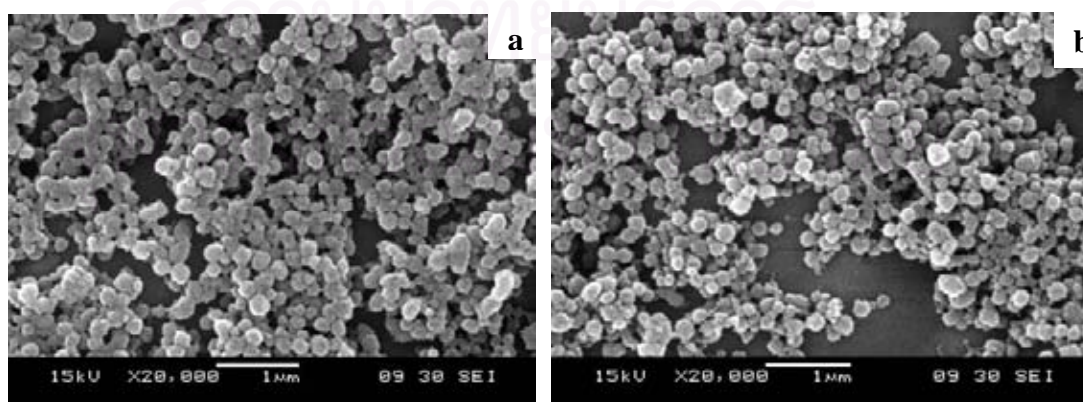


**Figure 3.25** Size and morphology of 10,000 ppm PLLC nanoparticles: a) before and b) after autoclave at 110 °C, 10 minute, 1 bar/sq inch.



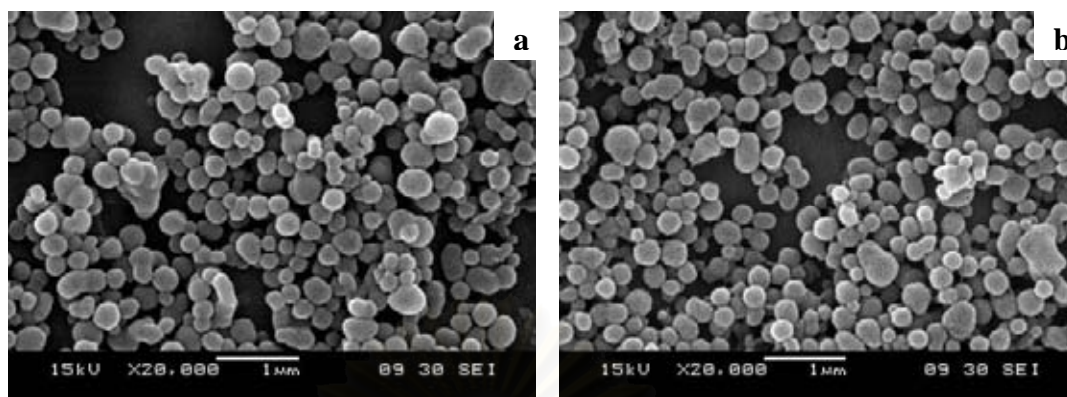


**Figure 3.26** Size and morphology of 10,000 ppm PCPLC: a) before and b) after autoclave at 110 °C, 10 minute, 1 bar/sq inch.

### 3.7 *In vitro* release

A dialysis method was used to perform the *in vitro* release test of all batches of ATRA-loaded PPLC and ATRA-loaded PCPLC nanoparticles. *In vitro* drug release tests of nanoparticles were carried out in phosphate buffer at pH 4, 7 and 10 for 72 h. During the experiments, the medium (3 mL) were withdrawn to determine the amounts of ATRA released from the nanoparticles using UV-absorption spectroscopy with the aid of calibration curve. It should be noted here that standards used for calibration curve constructions were prepared in phosphate buffer medium. Figure 3.25 and 3.26 show the release curves of ATRA-encapsulated PPLC and ATRA-encapsulated PCPLC nanoparticles at the three pH values. At pH 10 the ATRA was released slowly and only 20.80% of the loaded ATRA could be released after 30 h. While at pH 4 and pH 7, at 30 h, 52.49% and 63.88% of the ATRA were released from PPLC nanoparticle, respectively (Figure 3.25). The initial release rate (0-30 h) of ATRA from PPLC nanoparticles at pH 4, 7 and 10 at 30 h. were 0.052, 0.064 and 0.021 mg/h, respectively (Table 3.4). At pH 10, 20.90% of the ATRA was released from PCPLC nanoparticles within the first 30 h. While at pH 4 and pH 7, the amounts of ATRA release reached about 54.00%, and 62.63%, at 30 h, respectively.

The release rates of ATRA from PCPLC nanoparticle at pH 4, 7 and 10 were 0.054, 0.063 and 0.021 mg/h, respectively at 30 h (Table 3.5). As can be seen in Figure 3.25 and 3.26, the release rates of ATRA are maximized at neutral pH. This

result may suggest the pH-dependent swelling of PPLC and PCPLC affected the rate of drug release. Another explanation on this is that the solubilities of ATRA in the medium of different pH are different. However, our test showed that at the concentration used, ATRA can be solubilized equally well in all these medium. This result agrees well with previous works done by Ramesh *et al.* [127]. They investigated the pH-sensitivity of the *N,N'*-dimethylacrylamide chitosan microsphere. Chrolthiazide drug was loaded into microspheres and their release behaviors were studied. Cumulative release data indicate that by increasing the pH from 1.2 to 7.4, a considerable increase in the cumulative release is observed.

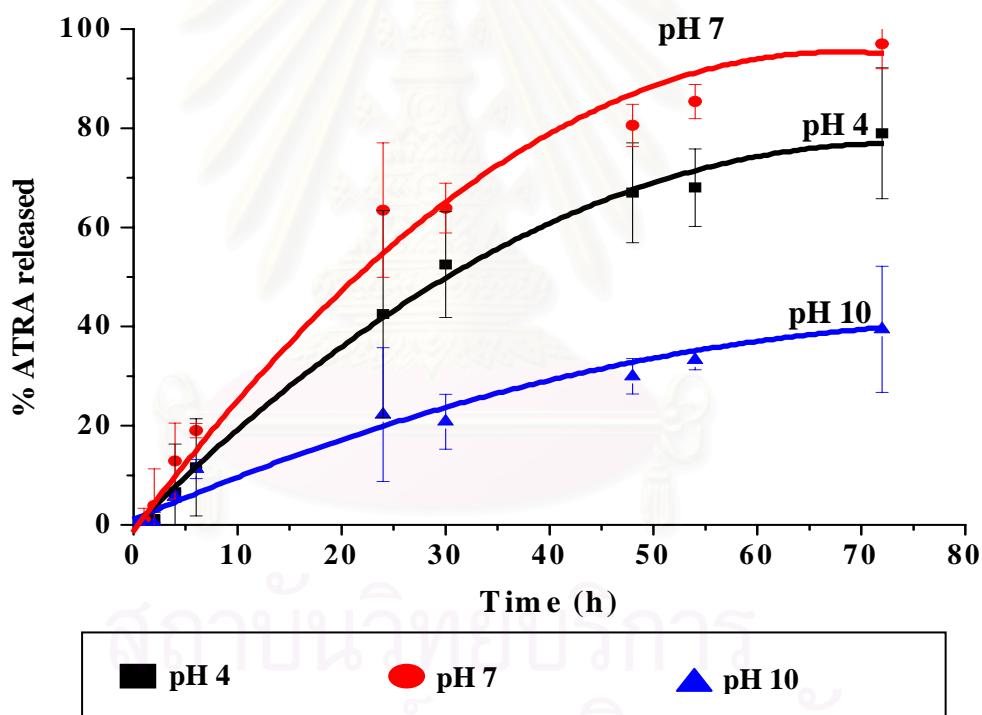


**Figure 3.27** *In vitro* release profile of ATRA from the PPLC nanoparticles in PBS at pH 4, pH 7 and pH 10 for 72 h (error bar represents maximum value-minimum value of the amount ATRA released).

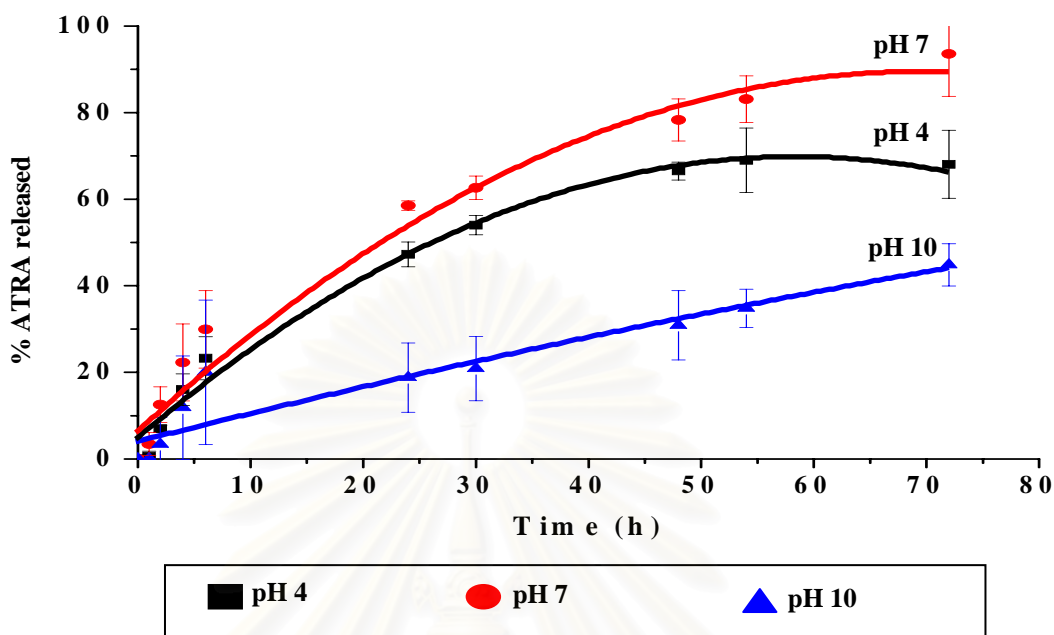


**Figure 3.28** *In vitro* release profile of ATRA from the PCPLC nanoparticles in PBS at pH 4, pH 7 and pH 10 for 72 h (error bar represents maximum value-minimum value of the amount ATRA released).

**Table 3.4** The percentage of ATRA released total and release rate of ATRA from PPLC nanoparticles.

Time (h)	% release total			Released rate (mg/h)		
	pH 4	pH 7	pH 10	pH 4	pH 7	pH 10
0	0	0	0	0	0	0
1	0	1.12	0	0	0.034	0
2	1.11	3.86	0.15	0.017	0.058	0.002
4	6.56	12.98	5.62	0.049	0.097	0.042
6	11.60	19.02	11.24	0.058	0.095	0.056
24	42.52	63.47	22.24	0.053	0.079	0.028
30	52.49	63.88	20.80	0.052	0.064	0.021
48	66.98	80.55	29.95	0.042	0.050	0.019
54	68.02	85.38	33.21	0.038	0.047	0.018
72	78.97	96.96	29.46	0.033	0.040	0.016

**Table 3.5** The percentage of ATRA released total and release rate of ATRA from PCPLC nanoparticles.

Time (h)	% release total			Released rate (mg/h)		
	pH 4	pH 7	pH 10	pH 4	pH 7	pH 10
0	0	0	0	0	0	0
1	0.60	3.45	0.04	0.018	0.104	0.001
2	6.96	12.54	3.37	0.104	0.188	0.051
4	16.01	22.30	11.85	0.120	0.167	0.089
6	23.26	29.91	19.99	0.116	0.150	0.100
24	47.25	58.52	18.77	0.059	0.073	0.023
30	54.00	62.63	20.90	0.054	0.063	0.021
48	66.51	78.31	30.86	0.042	0.049	0.019
54	68.99	83.11	34.81	0.038	0.046	0.019
72	68.04	93.54	44.84	0.028	0.039	0.019

## CHAPTER IV

### CONCLUSION

In this work, chitosan-nanoparticles with UV absorption property were prepared. Phthaloylchitosan (PLC) was firstly prepared by phthaloylation of chitosan (MW 110,000) to improve solubility property of the polymer. Grafting of mPEG-COOH and 4-methoxycinnamic acid onto phthaloylchitosan was carried out using 1-ethyl-3-(3-dimethylaminopropyl) carbodiimide, hydrochloride (EDCI) as a coupling agent and 1-hydroxy benzotriazole (HOBt) a catalyst. The substitution of the phthalimido group onto chitosan was 220%. Grafting of mPEG-COOH (MW 5,000) onto phthaloylchitosan gave mPEG-phthaloylchitosan (PPLC) with degree of mPEG substitution of 8.70%. Grafting of mPEG-COOH and 4-methoxycinnamic acid onto phthaloylchitosan gave mPEG-4-methoxycinnamoylphthaloylchitosan (PCPLC) with degree of substitution of 0.55% and 13.33% for mPEG and 4-methoxycinnamoyl moieties, respectively. Nanoparticles were then obtained from self-assembly of the prepared chitosan derivatives by solvent displacement method. Nanoparticles from PPLC and PCPLC were both spherical. The PPLC nanoparticles gave the average size of  $53.34 \pm 0.16$  nm. The zeta potential of PPLC particles indicated that the surfaces of the particles were negatively charge ( $-23.61 \pm 1.23$  mV). The PCPLC had the average size and zeta potential values of  $61.43 \pm 0.33$  nm and  $-26.40 \pm 0.48$  mV, respectively.

All-*trans* retinyl acetate (ATRA) were encapsulated into PPLC and PCPLC nanoparticles at various ATRA:polymer weight ratios. The encapsulation efficiency of ATRA into PPLC and PCPLC nanoparticles could be successfully done with % encapsulation efficiency (%EE) of > 96 and 79%, respectively. Furthermore, *in vitro* release behavior of ATRA from the nanoparticles was investigated by dialysis method under three pH conditions (pH 4, 7 and 10). The results indicated that the drug release was maximum at neutral pH.

In addition, some biological properties of chitosan nanoparticles were investigated. The mPEG-phthaloylchitosan and mPEG-4-methoxycinnamoyl phthaloylchitosan nanoparticles could inhibit the growth of both *Staphylococcus aureus* ATCC 25923 and *Escherichia coli* ATCC 25922. Both particles are

bacteriostatic against those two bacteria. These chitosan derivative nanoparticles showed stronger antimicrobial activity on Gram-positive bacteria than Gram-negative bacteria. Antimicrobial activity of mPEG-phthaloylchitosan nanoparticles was more pronounced than that of mPEG-4-methoxycinnamoylphthaloylchitosan nanoparticles. Both mPEG-phthaloylchitosan and mPEG-4-methoxycinnamoylphthaloylchitosan nanoparticles were subjected to melanoma A-375 cell cytotoxicity study and the results indicated that both compounds were not harmful to the human melanoma skin cell lines. Viability of melanoma cell lines treated with either nanoparticles was more than 85%.

This work thus demonstrates potential application of chitosan nanoparticles as drug or cosmetic active carrier.



สถาบันวิทยบริการ  
จุฬาลงกรณ์มหาวิทยาลัย

## REFERENCES

- [1] Shi, C., Zhu, Y., Ran, X., Wang, M., Su, Y., and Cheng, T. Therapeutic Potential of Chitosan and Its Derivatives in Regenerative Medicine. *Journal of Surgical Research*. **2006**, 113(2), 185-192.
- [2] Rinaudo, M. Chitin and chitosan: Properties and applications. *Progress in Polymer Science*. **2006**, 31, 603-632.
- [3] Xie, Y., Liu, X., and Chen, Q. Synthesis and characterization of water-soluble chitosan derivative and its antibacterial activity. *Carbohydrate Polymers*. **2007**, 69, 142-147.
- [4] Wang, Q., Zhang, N., Hu, X., Yang, J., and Du, Y. Chitosan/starch fibers and their properties for drug controlled release. *European Journal of Pharmaceutics and Biopharmaceutics*. **2007** (in press)
- [5] Herman, J., Remon, J.P., and De velder, J. Modified starches as hydrophilic matrices for controlled oral delivery1: Production and Characterization of thermally modified starches. *International Journal of Pharmaceutics*. **1989**, 56(1), 51-63.
- [6] Kurita, K. Chemistry and application of chitin and chitosan. *Polymer Degradation and Stability*. **1998**, 59, 117-120.
- [7] Prashanth, K.V., and Tharanathan, R.N. Chitin/chitosan: modification and their unlimited application potential-an overview. *Food Science Technology*. **2007**, 18, 117-131.
- [8] Satoh, T., Kano, H., Nakatani, M., Sakairi, N., Shinkai, S., and Nagasaki, T. 6-Amino-6-deoxy-chitosan sequential chemical modifications at the C-6 positions of N-phthaloylchitosan and evaluation as a gene carrier. *Carbohydrate Research*. **2006**, 341, 2406-2413.
- [9] Bahadur, R., Aryal, S., Bhattarai, N., and Kim, H.Y. Ceramic modification of N-acetylated chitosan stabilized gold nanoparticles. *Scripta Materialia*. **2006**, 54, 2029-2034.
- [10] Cravotto, G., Taglia, P.S., Robaldo, B. and Trotta, M. Chemical modification of chitosan under high-intensity ultrasound. *Ultrasonics Sonochemistry*. **2005**,

- 12, 95-98.
- [11] Jayakumar, R., Prabakaran, M., Ries, R.L., and Mano, J.F. Graft copolymerized chitosan—present status and applications. *Carbohydrate Polymers*. **2005**, 62, 142-158.
- [12] Liu, W., Zang, X., Sun, S.J., Sun, G.J., Yao, K.D., and Liang, D.C., *N*-alkylated chitosan as a potential nonviral vector for gene transfection. *Bioconjugate Chemistry*. **2003**, 14, 782–9.
- [13] Gallo, J.M., and Hassan, E.E., Receptor-mediated magnetic carriers: basis for targeting. *Pharmaceutical Research*. **1988**, 5, 300–304.
- [14] Doares, S.H., Syrovets, T., Weiler, E.W., and Ryan, C.A. Oligogalacturonides and chitosan activate plant defensive genes through the octadecanoid pathway. *Proceedings of National Academy of Sciences*. **1995**, 92, 4095–4098.
- [15] Fujii, S., Kumagai, H., and Noda, M. Preparation of poly(acyl)-chitosans. *Carbohydrate Research*. **1980**, 83, 389-393.
- [16] Loubaki, E., Sicsic, S., and Le Goffic, F. Chemical modification of chitosan by glycidyl trimethylammonium chloride. *European Polymer Journal*. **1989**, 25, 397-400.
- [17] Eli, W., Chen, W., and Xue, Q. The association of anionic surfactants with  $\beta$ -cyclodextrins. An isothermal titration calorimeter study. *Journal of Chemical Thermodynamics*. **1999**, 31, 1283–1296.
- [18] Rekharsky, M.V., and Inoue, Y. Complexation thermodynamics of cyclodextrins. *Chemical Reviews*. **1998**, 98, 1875–1917.
- [19] Kriz, Z., Koca, J., Imbert, A., Charlot, A., and Auzely-Velty, R. Investigation of the complexation of (+)-catechin by  $\beta$ -cyclodextrin by combination of NMR, microcalorimetry and molecular modelling techniques. *Organic and Biomolecular Chemistry*. **2003**, 1, 2590–2595.
- [20] Chen, S., and Wang, Y. Study of  $\alpha$ -cyclodextrin grafting with chitosan and slow release of its inclusion complex with radioactive iodine. *Journal of Applied Polymer Science*. **2001**, 82, 2414–2421.
- [21] Blair, H.S., Guthrie, J., Law, T., and Turkington, P. Chitosan and modified chitosan membranes I: preparation and characterization. *Journal of Applied Polymer Science*. **1987**, 33, 641–656.



- [22] Kurita, K., Yosihida, A., and Koyama, Y. Studies on chitin 13. New polysaccharide/polypeptide hybrid material based on chitin and poly( $\gamma$ -methyl-L-glutamate). *Macromolecules*. **1988**, 21, 1579–1583.
- [23] Yalpani, M., Marchessault, R.H., Morin, F.G., and Monasterios, C.J. Synthesis of poly(3-hydroxyalkanoate) (PHA) conjugates: PHA carbohydrate and PHA-synthetic polymer conjugates. *Macromolecules* **1991**, 24, 6046–6049.
- [24] Harris, J.M., Struk, E.C., Case, M.G., Paley, M.S., Yalpani, M., Van Alstin, J.M., and Brooks, D.E. Synthesis and Characterization of Poly(ethylene Glycol) Derivatives. *Journal of Polymer Science Part A: Polymer Chemistry Editor*. **1984**, 22, 341–352
- [25] Morimoto, M., Saimoto, H., and Shigemasu, Y. Control of functions of chitin and chitosan by chemical modifications. *Trends in Glycoscience and Glycotechnology*. **2002**, 14, 205–222.
- [26] Heras, A., Rodriguez, N.M., Ramos, V.M., and Agullo, E. N-methylene phosphonic chitosan: a novel soluble derivative. *Carbohydrate Polymer*. **2000**, 44, 1–8.
- [27] Ramos, V.M., Rodriguez, N.M., Diaz, M.F., Rodriguez, M.S., Heras, A., and Agullo, E. N-methylene phosphonic chitosan: effect of preparation methods on its properties. *Carbohydrate Polymer*. **2003**, 52, 39–46.
- [28] Ramos, V.M., Rodriguez, N.M., Rodriguez MS, Heras A, and Agullo E. Modified chitosan carrying phosphonic and alkyl groups. *Carbohydrate Polymer*. **2003**, 51, 425–429.
- [29] Holme, K.R., and Hall, L.D. Chitosan derivatives bearing C-10-alkyl glycoside branches: a temperature induced gelling polysaccharide. *Macromolecules*. **1991**, 24, 3828–3833.
- [30] Hall, L.D., and Yalpani, M. Formation of branched-chain, soluble polysaccharides from chitosan. *J. Chem Soc Chem Commun*. **1980**, 1153–1154.
- [31] Yalpani M, Hall LD. Some chemical and analytical aspects of polysaccharide modifications. 3. Formation of branchedchain, soluble chitosan derivatives. *Macromolecules*. **1984**, 17, 272–81.
- [32] Nishimura, S., Ikeuchi, Y., and Tokura, S. The adsorption of bovine blood

- proteins onto the surface of O-(carboxymethyl)chitin. *Carbohydrate Research*. **1984**, 134, 305–312.
- [33] Trujillo, R. Preparation of carboxymethyl chitin. *Carbohydrate Research*. **1968**, 7, 483–485.
- [34] Carolan, C.A., Blair, H.S., Allen, S.J., and McKay, G. *N,O*-Carboxymethyl chitosan, a water soluble derivative and potential ‘Green’ food preservative. *Chemical Engineering Research and Design*. **1991**, 69, 195–196.
- [35] Rinaudo, M., Dung, P.L., Gey, C., Milas, M., and Mariotti, S. Substituent distribution on O, N-carboxymethylchitosans by  $^1\text{H}$  and  $^{13}\text{C}$  NMR. *International Journal of Biological Macromolecules*. **1992**, 14, 122–128.
- [36] Muzzarelli, R.A.A, Tanfani, F., Emanuelli, M., and Mariotti, S. *N*-(carboxymethylidene)chitosans and *N*-(carboxymethyl)chitosans: Novel chelating polyampholytes obtained from chitosan glyoxylate. *Carbohydrate Research*. **1982**, 107, 199–214.
- [37] Delben, F., and Muzzarelli, R.A.A. Thermodynamic study of the interaction of *N*-Carboxymethyl chitosan with divalent metal ions. *Carbohydrate Polymer*. **1989**, 11, 221–232.
- [38] Dobetti, L., and Delben, F. Binding of metal cations by *N*-carboxymethyl chitosans in water. *Carbohydrate Polymer*. **1992**, 18, 273–283.
- [39] Muzzarelli, R.A.A., Tanfani, F., and Emanuelli, M. Sulfated *N*-(carboxymethyl)chitosans: Novel blood anticoagulants. *Carbohydrate Research*. **1984**, 126, 225–231.
- [40] Sashiwa, H., and Aiba, S.I. Chemically modified chitin and chitosan as biomaterials. *Progress in Polymer Science*. **2004**, 29, 887–908.
- [41] Chung, Y.C., Wang, H.L., Chen Y.M., and Li, S.L. Effect of abiotic factors on the antibacterial activity of chitosan against waterborne pathogens. *Bioresource Technology*. **2003**, 88(3), 179–184.
- [42] Liu, X. F., Guan, Y. L., Yang, D. Z., Li, Z., and Yao, K. D. Antibacterial action of chitosan and carboxymethylated chitosan. *Journal of Applied Polymer Science*. **2001**, 79(7), 1324–1335.
- [43] Sun, L., Du, Y., Fan, L., Chen, X., and Yang, J. Preparation, characterization and

- antimicrobial activity of quaternized carboxymethyl chitosan and application as pulp-cap. *Polymer*. **2006**, 14(6), 1796-1804.
- [44] Chen, S., Wu, G., and Zeng, H. Preparation of high antimicrobial activity thiourea chitosan-Ag<sup>+</sup> complex. *Carbohydrate Polymer*. **2005**, 60, 33-38.
- [45] Lehr, C. M., Bowstra, J. A., Schacht, E. H., and Jungiger, H. E. *In vitro* evaluation of mucoadhesive properties of chitosan and some other natural polymers. *International Journal of Pharmaceutics*. **1992**, 78(1), 43–48.
- [46] Chayed, S., and Winnik, F.M. In vitro evaluation of the mucoadhesive properties of polysaccharide-based nanoparticulate oral drug delivery systems. *European Journal of Pharmaceutics and Biopharmaceutics*. **2007**, 65(3), 363–370.
- [47] Gomes, P., Gomes, C.A.R., Batista, M.K.S., Pinto, L.F., and Silva, A.P.P. Synthesis, structural characterization and properties of water-soluble N-( $\gamma$ -propanoyl-amino acid)-chitosans. *Carbohydrate Polymers*. **2007**. (in press).
- [48] Charlton, S.T., Davis, S.S. and Illum, L. Evaluation of bioadhesive polymers as delivery systems for nose to brain delivery: In vitro characterisation studies. *Journal of Controlled Release*. **2007**, 118(2), 225–234.
- [49] Grenha, A. Grainger, C.I., Dailey, L.A., Seijo, B., Martin, G.P. Remuñán-López, C. and Forbes, B. Chitosan nanoparticles are compatible with respiratory epithelial cells in vitro. *European Journal of Pharmaceutical Sciences*. **2007**, 31(2), 73–84.
- [50] Cui, F., Qian, F., and Yin, C. Preparation and characterization of mucoadhesive polymer-coated nanoparticles. *International Journal of Pharmaceutics*. **2006**, 316(1-2), 154-161.
- [51] Dornish, M., Arnold, M., and Skaugrud, Q. Alginate and chitosan: Biodegradable biopolymers in drug delivery systems. *European Journal of Pharmaceutical Sciences*. **1996**, 1, S153.
- [52] Bangham, A.D., Standish, M.M., and Watkins, J.C. Diffusion of univalent ions across the lamellae of swollen phospholipids. *Journal of Molecular Biology*. **1965**, 13, 238-252.
- [53] Koo, Q.M., Rubinstein, I. and Onyuksel, H. Role of nanotechnology in targeted drug delivery and imaging: a concise review *Nanomedicine, Nanotechnology, Biology, and Medicine*. **2005**, 1 193– 212

- [54] Gregoradis, G. Liposome preparation and related techniques. *Liposome Technology*. **1993**, 1, 1–63.
- [55] Vemuri, S., and Rhodes, C.T. Preparation and characterization of liposomes as therapeutic delivery systems: a review. *Pharm Acta Helvetiae*. **1995**, 70, 95–111.
- [56] Watve, R.M., and Bellare, J.R. Manufacture of liposomes: a review. *Current Science*. **1995**, 68, 715–724.
- [57] Sethi, V., Onyuksel, H., and Rubinstein, I. Liposomal vasoactive intestinal peptide. *Methods Enzymological*. **2005**, 391, 377- 395.
- [58] Dijkstra, J., Galen, W.J.M., Regts, J., and Scherphof, G.L. Uptake and processing of liposomal phospholipids by Kupffer cells in vitro. *European Journal of Biochemistry*. **1985**, 148, 391–397.
- [59] Pain, D., Das, P.K., Ghosh, P.C., and Bachhawat, B.K. Increased circulatory half-life of liposomes after conjugation with dextran. *Journal of Biosciences*. **1984**, 6, 811-816.
- [60] Allen, T.M., and Chonn, A. Large unilamellar liposomes with low uptake into the reticuloendothelial system. *FEBS Letters*. **1987**, 223, 42-46.
- [61] Papahadjopoulos, D., Allen, T.M., Gabizon, A., Mayhew, E., Matthay, K., and Huang, S.K. Sterically stabilized liposomes: improvements in pharmacokinetics and antitumor therapeutic efficacy. *Proceedings of National Academy of Sciences*. **1991**, 881, 1460-1464.
- [62] Lasic, D.D., Martin, F.J., Gabizon, A., Huang, S.K., and Papahadjopoulos, D. Sterically stabilized liposomes: a hypothesis on the molecular origin of the extended circulation times. *Biochimica et Biophysica Acta*. **1991**, 1070, 187-192.
- [63] Torchilin, V.P., Levchenko, T.S., Whiteman, K.R., Yaroslavov, A.A., Tsatsakis, A.M., and Rizo, A.K. Amphiphilic poly-N-vinylpyrrolidones: synthesis, properties and liposome surface modification. *Biomaterials*. **2001**, 22, 3035-3044.
- [64] Takeuchi, H., Kojima, H., Yamamoto, H., and Kawashima, Y. Evaluation of circulation profiles of liposomes coated with hydrophilic polymers having

- different molecular weights in rats. *Journal of Controlled Release*. **2001**, 75, 83 - 91.
- [65] Sharma, A., and Sharma U.S. Liposomes in drug delivery: progress and limitations. *International Journal of Pharmaceutics*. **1997**, 154, 123-140.
- [66] Brime, B., Frutos, P., Bringas, P., Nieto, A., Ballesteros, M.P., Frutos, G. Comparative pharmacokinetics and safety of a novel lyophilized amphotericin B lecithin-based oil-water microemulsion and amphotericin B deoxycholate in animal models. *Journal of Antimicrobial Chemotherapy*. **2003**, 52, 103- 109.
- [67] He, L., Wang, G.L., and Zhang, Q. An alternative paclitaxel microemulsion formulation: hypersensitivity evaluation and pharmacokinetic profile. *International Journal of Pharmaceutics*. **2003**, 250, 45-50.
- [68] Seki, J., Sonoke, S., Saheki, A., Fukui, H., Sasaki, H., and Mayumi, T. A nanometer lipid emulsion, lipid nano-sphere (LNS), as a parenteral drug carrier for passive drug targeting. *International Journal of Pharmaceutics*. **2004**, 273, 75-83.
- [69] Santos-Magalhaes, N.S., Pontes, A., Pereira, V.M., and Caetano, M.N. Colloidal carriers for benzathine penicillin G: nanoemulsions and nanocapsules. *International Journal of Pharmaceutics*. **2000**, 208, 71-80.
- [70] Tadros, T., Izquierdo, P., Esquena, J., and Solans, C. Formation and stability of nano-emulsions. *Advances in Colloid and Interface Science*. **2004**, 108-109, 303 -318.
- [71] Junping, W., Takayama, K., Nagai, T., and Maitani, Y. Pharmacokinetics and antitumor effects of vincristine carried by microemulsions composed of PEG-lipid, oleic acid, vitamin E and cholesterol. *International Journal of Pharmaceutics*. **2003**, 251, 13-21.
- [72] Kang, B.K., Chon, S.K., Kim, S.H., Jeong, S.Y., Kim, M.S., and Cho, S.H. Controlled release of paclitaxel from microemulsion containing PLGA and evaluation of anti-tumor activity in vitro and in vivo. *International Journal of Pharmaceutics* **2004**, 286, 147-156.
- [73] Kreuter, J., and Speiser, P.P. New adjuvants on a polymethylmethacrylate base. *Infection and Immunity*. **1976**, 13, 204-210.
- [74] Gessner, A., Waicz, R., Lieske, A., Paulke, B., Mader, K., and Muller R.H.

- Nanoparticles with decreasing surface hydrophobicities: influence on plasma protein adsorption. *International Journal of Pharmaceutics*. **2000**, 196, 245-249.
- [75] Zweers, M.L., Engbers, G.H., Grijpma, D.W., and Feijen, J. In vitro degradation of nanoparticles prepared from polymers based on dlactide, glycolide and poly(ethylene oxide). *Journal of Controlled Release*. **2004**, 100, 347-356.
- [76] Leo, E., Brina, B., Forni F., and Vandelli, M.A. In vitro evaluation of PLA nanoparticles containing a lipophilic drug in water-soluble or insoluble form. *International Journal of Pharmaceutics*. **2004**, 278, 133-141.
- [77] Sinha, V.R., Bansal, K., Kaushik, R., Kumria, R., and Trehan, A. Poly-epsilon-caprolactone microspheres and nanospheres: an overview. *International Journal of Pharmaceutics*. **2004**, 278, 1-23.
- [78] Csaba, N., Gonzalez, L., Sanchez, A., and Alonso, M.J. Design and characterisation of new nanoparticulate polymer blends for drug delivery. *Journal of Biomaterial Science Polymer Edition*. **2004**, 15, 1137-1151.
- [79] Birnbaum, D.T., and Brannon-Peppas, L. Molecular weight distribution changes during degradation and release of PLGA nanoparticles containing epirubicin HCl. *Journal of Biomaterial Science Polymer Edition*. **2003**, 14, 87-102.
- [80] Panyam, J., Williams, D., Dash, A., Leslie-Pelecky, D., and Labhasetwar, V. Solid-state solubility influences encapsulation and release of hydrophobic drugs from PLGA/PLA nanoparticles. *Journal of Pharmaceutical Science*. **2004**, 93, 1804-1814.
- [81] Shenoy, D.B., and Amiji, M.M. Poly(ethylene oxide)-modified poly(epsilon-caprolactone) nanoparticles for targeted delivery of tamoxifen in breast cancer. *International Journal of Pharmaceutics*. **2005**, 293, 261-270.
- [82] Molpeceres, J., Chacon, M., Guzman, M., Berges, and Aberturas, M. A polycaprolactone nanoparticle formulation of cyclosporin-A improves the prediction of area under the curve using a limited sampling strategy. *International Journal of Pharmaceutics*. **1999**, 187, 101-113.
- [83] Radwan, M.A., Zaghloul, I.Y., and Aly, Z.H. In vivo performance of parenteral theophylline-loaded polyisobutylcyanoacrylate nanoparticles in rats. *European Journal of Pharmaceutical Sciences*. **1999**, 8, 95-98.

- [84] Jain, R.A. The manufacturing techniques of various drug loaded biodegradable poly(lactide-co-glycolide) (PLGA) devices. *Biomaterials*. **2000**, 21, 2475-2490.
- [85] Shiraishi, S., Imai, T., and Otagiri, M. Controlled release of indomethacin by chitosan–polyelectrolyte complex: optimization and in vivo/in vitro evaluation. *Journal of Controlled Release*. **1993**, 25, 217–225.
- [86] Mi, F.L., Wong, T.B., and Shyu, S.S. Sustained-release of oxytetracycline from chitosan microspheres prepared by interfacial acylation and spray hardening methods. *Journal of Microencapsulation*. **1997**, 14, 577–591.
- [87] Al-Helw, A.A., Al-Angary, A.A., Mahrous, G.M., and Al-Dardari, M.M., Preparation and evaluation of sustained release cross-linked chitosan microspheres containing phenobarbitone. *Journal of Microencapsulation*. **1998**, 15, 373–382.
- [88] Genta, I., Perugini, P., Pavanetto, F., Different molecular weight chitosan microspheres: influence on drug loading and drug release. *Drug Development and Industrial Pharmacy*. **1998**, 24, 779–784.
- [89] Nishioka, Y., Kyotani, S., Okamura, M., Miyazaki, M., Okazaki, K., Ohnishi, S., Yamamoto, Y., and Ito, K. Release characteristics of cisplatin chitosan microspheres and effect of containing chitin. *Chemical and Pharmaceutical Bulletin(Tokyo)*. **1990**, 38, 2871–2873.
- [90] Bayomi, M.A., al-Suwayeh, S.A., el-Helw, A.M., and Mesnad, A.F., Preparation of casein–chitosan microspheres containing diltiazem hydrochloride by an aqueous coacervation technique. *Pharmaceutical Acta Helvetiae*. **1998**, 73, 187–192.
- [91] Akbuga, J., and Durmaz, G. Preparation and evaluation of crosslinked chitosan microspheres containing furosemide. *International Journal of Pharmaceutics*. **1994**, 111, 217–222.
- [92] Bodmeier, R., Oh, K.H., and Pramdar, Y. Preparation and evaluation of drug-containing chitosan beads. *Drug Development and Industrial Pharmacy*. **1989**, 15, 1475–1494.
- [93] Jameela, S.R., Kumary, T.V., Lal, A.V., and Jayakrishnan, A. Progesterone-

- loaded chitosan microspheres: a long acting biodegradable controlled delivery system. *Journal of Controlled Release*. **1998**, 52, 17–24.
- [94] Jameela, S.R., and Jayakrishnan, A. Glutaraldehyde crosslinked chitosan microspheres as a long acting biodegradable drug delivery vehicle: studies on the in vitro release of mitoxantrone and in vivo degradation of microspheres in rat muscle. *Biomaterials*. **1995**, 16, 769–775.
- [95] Ko, J.A., Park, H.J., Hwang, S.J., Park, J.B., and Lee, J.S. Preparation and characterization of chitosan microparticles intended for controlled drug delivery. *International Journal of Pharmaceutics*. **2002**, 249, 165–174.
- [96] Bollag, W., and Holdener, E.E. Retinoids in cancer prevention and therapy. *Annals of Oncology*. **1992**, 3, 513-526.
- [97] Lane, M.A., and Bailey, S.J. Role of retinoid signalling in the adult brain. *Progress in Neurobiology*. **2005**, 75, 275–293.
- [98] Maden, M. Retinoid signalling in the development of the central nervous system. *Nature Reviews Neuroscience*. **2002**, 3 (11), 843–853.
- [99] McCaffery, P.J., Adams, J., Maden, M., and Rosa-Molinar, E., Too much of a good thing: retinoic acid as an endogenous regulator of neural differentiation and exogenous teratogen. *European Journal of Neuroscience*. **2003**, 18(3), 457–472.
- [100] Mey, J., and McCaffery, P.J. Retinoic acid signaling in the nervous system of adult vertebrates. *Neuroscientist*. **2004**, 10, 409–421.
- [101] Bollag W. Vitamin A and retinoids: From nutrition to pharmacotherapy in dermatology and oncology. *Lancet*, **1983**, 1, 860-863.
- [102] Bollag W. The development of retinoids in experimental and clinical oncology and dermatology. *Journal of the American Academy of Dermatology*. **1983**, 9, 797-805.
- [103] Bollag W., and Hartmann H.R. Prevention and therapy of cancer with retinoids in animals and man. *Cancer Surveillance*. **1983**, 2, 293-314.
- [104] Moon R.C., and Itri L.M. Retinoids and cancer. In Sporn MB, Roberts AB, Goodman DS (eds): *The Retinoids*. Orlando: Academic Press. **1984**, 2, 327-371.
- [105] Lippman S.M., and Kessler J.F., and Meyskens, F.L. Retinoids as preventive



- and therapeutic anticancer agents (Part II). *Cancer Treatment Reports*. **1987**, 71, 493-515.
- [106] Lippman S.M., and Meyskens, F.L. Results of the use of vitamin A and retinoids in cutaneous malignancies. *Pharmaceutical Therapy*. **1989**, 40, 107-122.
- [107] Sun, S.Y., and Lotan, R., Retinoids and their receptors in cancer development and chemoprevention. *Critical Reviews Oncology/Hematology*. **2002**, 41, 41-55.
- [108] Chansri, N., Kawakami, S., Yamashita, F., and Hashida, M. Inhibition of liver metastasis by all-*trans* retinoic acid incorporated into O/W emulsions in mice. *International Journal of Pharmaceutics*. **2006**, 321, 42-49.
- [109] Jane, K.A., Fresneau, M.P., Marazuela, A., and Fabra, A. Chitosan nanoparticles as delivery systems for doxorubicin. *Journal of Controlled release*. **2001**, 73, 255-267.
- [110] Ko, J.A., Park, H.J., Hwang, S.J., Park, J.B., and Lee, J.S. Preparation and characterization of chitosan microparticles intended for controlled drug delivery *International Journal of Pharmaceutics*. **2002**, 249, 165-174.
- [111] Prego, C., Torres, D., Fernandez-Megia, E., Novoa-Carballal, R., Quiñoá, E., and Alonso M.J. Chitosan-PEG nanocapsules as new carriers for oral peptide delivery effect of chitosan pegylation degree. *Journal of Controlled Release*. **2006**, 111, 299-308.
- [112] Du, J., Dai, J., Liu, J.L. Theresa Dankovich. Novel pH-sensitive polyelectrolyte carboxymethyl Konjac glucomannan-chitosan beads as drug carriers. *Reactive & Functional Polymers*. **2006**, 66, 1055-1061
- [113] Opanasopit, P., Ngawhirunpat, T., Chaidedgumjorn, A., Rojanarata, T., Apirakaramwong, A., Phongying, S., Choochottiros, C., and Chirachanchai, S. Incorporation of camptothecin into N-phthaloyl chitosan-g-mPEG self-assembly micellar system. *European Journal of Pharmaceutics and Biopharmaceutics*. **2006**, 64, 269-276.
- [114] Kima, D.G., Jeong, Y.I., Choi, C., Roh, S.H., Kang, S.K., Jang, M.K., and Nah, J.W. Retinol-encapsulated low molecular water-soluble chitosan nanoparticles. *International Journal of Pharmaceutics*. **2006**, 319, 130-138.

- [115] Maestrelli, F., Garcia-Fuentes, M., Mura, P., and Alonso, M.J. A new drug nanocarrier consisting of chitosan and hydroxypropylcyclodextrin. *European Journal of Pharmaceutics and Biopharmaceutics*. **2006**, 63, 79–86.
- [116] Yuan, Y., Chesnutt, B.M., Utturkar, G., Haggard, W.O., Yang, Y., Ong, J.L., and Bumgardner, J.D. The effect of cross-linking of chitosan microspheres with genipin on protein release. *Carbohydrate Polymers*. **2007**, 68, 561–567.
- [117] Wang, Y.S., Liu, L.R., Jiang, Q., and Zhang, Q.Q. Self-aggregated nanoparticles of cholesterol-modified chitosan conjugate as a novel carrier of epirubicin. *European Polymer Journal*. **2007**, 43, 43–51.
- [118] Guo, B.L. and Gao, Q.Y. Preparation and properties of a pH/temperature-responsive carboxymethyl chitosan/poly(N-isopropylacrylamide)semi-IPN hydrogel for oral delivery of drugs. *Carbohydrate Research*. **2007**, (in press).
- [119] Opanasopit, P., Ngawhirunpat, T., Rojanarata, T., Choochottiros, C., and Chirachanchai, S. *N*-Phthaloylchitosan-g-mPEG design for all-*trans* retinoic acid-loaded polymeric micelles. *European journal of pharmaceutical sciences*. **2007**, 30, 424–431.
- [120] Qi, L., Xu, Z., Jiang, X., Hu, C., and Zou, X. Preparation and antibacterial activity of chitosan nanoparticles. *Carbohydrate Research*. **2004**, 339 2693–2700.
- [121] Yang, T.C., Chou, C.C., and Li, C.F. Antibacterial activity of *N*-alkylated disaccharide chitosan derivatives. *International Journal of Food Microbiology*. **2005**, 97, 237– 245.
- [122] Peng, Y., Han, B., Liua, W., and Xu, X. Preparation and antimicrobial activity of hydroxypropyl chitosan. *Carbohydrate Research*. **2005**, 340, 1846–1851.
- [123] Liu, N., Chen, X.G., Park, H.J., Liu, C.G. Liu, C.S. Meng, X.H., Yu, L.J. Effect of MW and concentration of chitosan on antibacterial activity of *Escherichia coli*. *Carbohydrate Polymers*. **2006**, 64, 60–65.
- [124] Caner, H. Yilmaz, E., and Yilmaz, O. Synthesis, characterization and antibacterial activity of poly(N-vinylimidazole) grafted chitosan. *Carbohydrate Polymers*. **2007**, 69, 318-325.
- [125] Zhou, N.L., Liu, Y., Li, L., Meng, N., Huang, Y.X. Zhang, J., Wei, S.H., and

- Shen, J. A new nanocomposite biomedical material of polymer/Clay–Cts–Ag nanocomposites. *Current Applied Physics*. **2007**, 7S1, e58–e62.
- [126] Liu, H., Du, Y., Yang, J., and Zhu, H. Structural characterization and antimicrobial activity of chitosan/betaine derivative complex. *Carbohydrate Polymers*. **2004**, 55, 291–297.
- [127] Babu, V.R., Hosamani, K.M., and Aminabhavi, T.M. Preparation and *in-vitro* release of chlorothiazide novel pH-sensitive chitosan-N,N'-dimethylacrylamide semi-interpenetrating network microspheres. *Carbohydrate Polymers*. **2007**. (in press).
- [128] Qi, L., Xu, Z., Jiang, X., Li, Y. and Wang, M. Cytotoxic activities of chitosan nanoparticles and copper-loaded nanoparticles. *Bioorganic & Medicinal Chemistry Letters*. **2005**, 15, 1397–1399.
- [129] Je, J.Y., Cho, .S., and Kim, S.K. Cytotoxic activities of water-soluble chitosan derivatives with different degree of deacetylation. *Bioorganic & Medicinal Chemistry Letters*. **2006**, 16, 2122–2126.



**APPENDICES**

สถาบันวิทยบริการ  
จุฬาลงกรณ์มหาวิทยาลัย

## APPENDIX A

### I % drug loading and % encapsulation efficiency of all-*trans* retinyl acetate loaded into chitosan nanoparticles

#### 1.) mPEG-phthaloylchitosan (PPLC) nanoparticles.

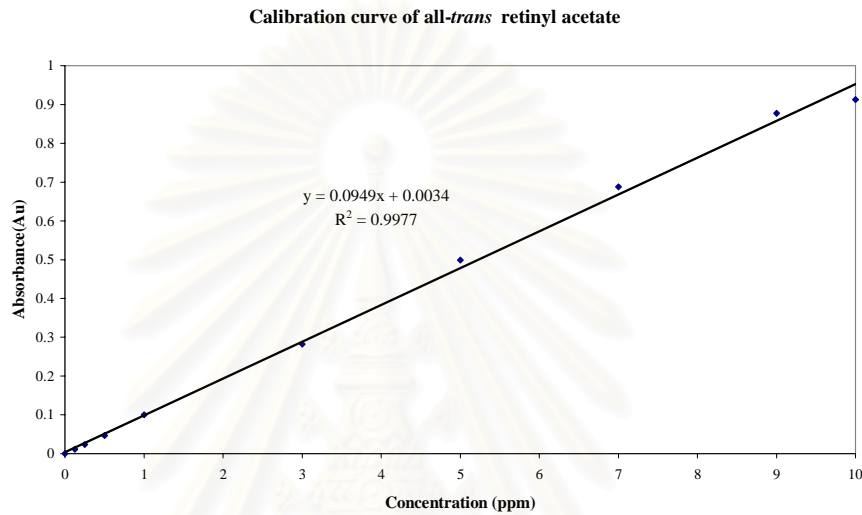


Figure A.1 Calibration curve of all-*trans* retinyl acetate in ethanol solution.

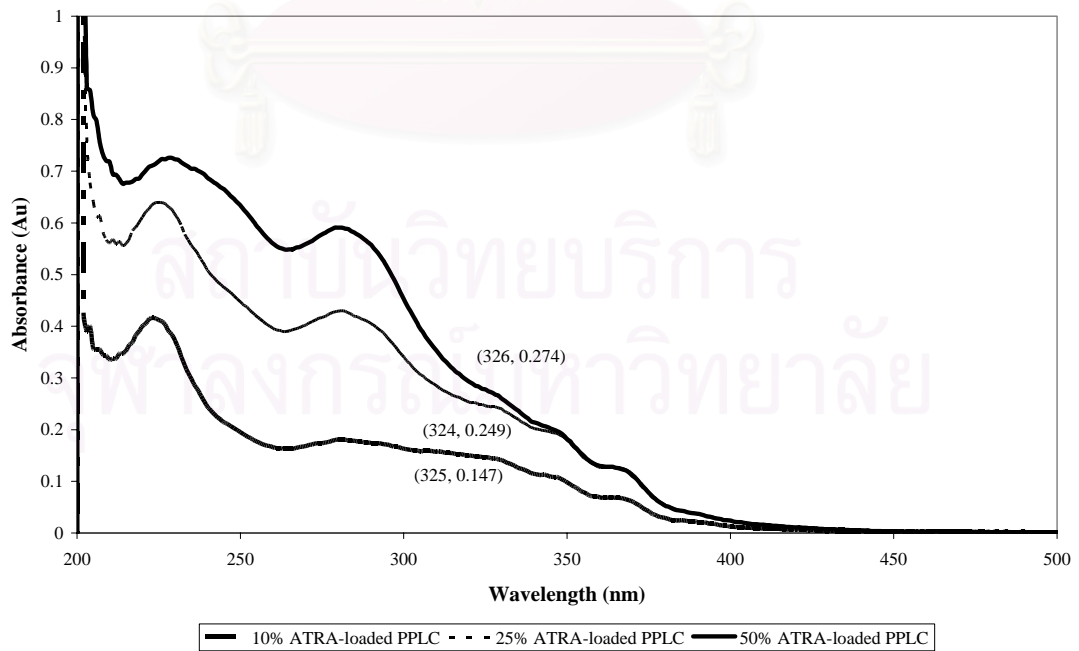


Figure A.2 UV absorption spectra of all-*trans* retinyl acetate were adhered at the outside of mPEG-phthaloylchitosan nanoparticle in ethanol solution.

From the equation of calibration curve;

$$Y = 0.0949x + 0.0034, R^2 = 0.9977 \quad (1)$$

### 1.1) 10% ATRA loaded PPLC nanoparticles

The amount of ATRA (10% ATRA to polymer) loaded adhered at the outside of particles was calculated by equation (1);

$$0.147 = 0.0949x + 0.0034$$

$$X = 1.513 \text{ ppm}$$

ppm  $\rightarrow$  mg/L

$$\therefore 1.513 \text{ ppm} = 1.513 \text{ mg/L}$$

$$\therefore \text{In volumetric 5 mL had all-trans retinyl acetate } (5 \times 1.513)/1000 = 0.0076 \text{ mg.}$$

Weight of the ATRA and mPEG-phthaloylchitosan (PPLC) were 0.2 and 2 mg in 5 mL.

$$\begin{aligned} \therefore \text{Weight of the ATRA loaded into particle} &= 0.2 - 0.0076 \text{ mg} \\ &= 0.1924 \text{ mg} \end{aligned}$$

$$\% \text{ drug loading} = \frac{\text{weight of drug in nanoparticle}}{\text{weight of nanoparticle}} \times 100 \quad (2)$$

$$\begin{aligned} &= (0.1924/2) \times 100 \\ &= 9.62 \% \end{aligned}$$

$$\% \text{ encapsulation efficiency (\%EE)} = \frac{\text{total amount of ATRA- free ATRA}}{\text{total amount of ATRA}} \times 100 \quad (3)$$

$$\begin{aligned} &= [(0.2-0.0076)/0.2] \times 100 \\ &= 96.22 \% \end{aligned}$$

Therefore, % drug loading and % EE of ATRA (10% ATRA to polymer) loaded into mPEG-phthaloylchitosan nanoparticle were 9.62 and 96.22%, respectively.

### 1.2) 25% ATRA loaded PPLC nanoparticles

The amount of ATRA (25% ATRA to polymer) adhered at the outside of particles was calculated by equation (1);

$$0.249 = 0.0949x + 0.0034$$

$$X = 2.588 \text{ ppm}$$

$$\therefore 2.588 \text{ ppm} = 2.588 \text{ mg/L}$$

$\therefore$  In volumetric 5 mL had all-*trans* retinyl acetate  $(5 \times 2.588)/1000 = 0.0129 \text{ mg}$ .

Weight of the ATRA and mPEG-phthaloylchitosan (PPLC) were 0.5 and 2 mg in 5 mL.

$$\begin{aligned} \therefore \text{Weight of the ATRA loaded into particle} &= 0.5 - 0.0129 \text{ mg} \\ &= 0.4871 \text{ mg} \end{aligned}$$

% drug loading and % EE were calculated by equations (2) and (3), respectively;

$$\begin{aligned} \% \text{ drug loading} &= (0.4871/2) \times 100 \\ &= 24.35 \% \end{aligned}$$

$$\begin{aligned} \% \text{ encapsulation efficiency (\%EE)} &= [(0.5-0.0129)/0.5] \times 100 \\ &= 97.42 \% \end{aligned}$$

Therefore, % drug loading and % EE of ATRA (25% ATRA to polymer) loaded into mPEG-phthaloylchitosan nanoparticle were 24.35 and 97.42%, respectively.

### 1.3) 50% ATRA loaded PPLC nanoparticles

The amount of ATRA (50% ATRA to polymer) adhered at the outside of particles was calculated by equation (1);

$$0.274 = 0.0949x + 0.0034$$

$$X = 2.851 \text{ ppm}$$

Since the ATRA diluted three-fold with ethanol, so the amount of ATRA was  $(2.851 \times 3) = 8.554 \text{ ppm}$ .

$$\therefore 8.554 \text{ ppm} = 8.554 \text{ mg/L}$$

$\therefore$  In volumetric 5 mL had all-*trans* retinyl acetate  $(5 \times 8.554)/1000 = 0.0428 \text{ mg}$ .

Weight of the ATRA and mPEG-phthaloylchitosan (PPLC) were 1.25 and 2.5 mg in 5 mL.

$$\begin{aligned} \therefore \text{Weight of the ATRA loaded into particle} &= 1.25 - 0.0428 \text{ mg} \\ &= 1.2072 \text{ mg} \end{aligned}$$

% drug loading and % EE were calculated by equations (2) and (3), respectively;

$$\begin{aligned} \% \text{ drug loading} &= (1.2072/2.5) \times 100 \\ &= 48.28 \% \end{aligned}$$

$$\begin{aligned} \% \text{ encapsulation efficiency (\%EE)} &= [(1.25-0.0428)/1.25] \times 100 \\ &= 96.58 \% \end{aligned}$$

Therefore, % drug loading and % EE of ATRA (50% ATRA to polymer) loaded into mPEG-phthaloylchitosan nanoparticle were 48.28 and 96.58%, respectively.

## 2.) mPEG-4-methoxycinnamoylphthaloylchitosan nanoparticles

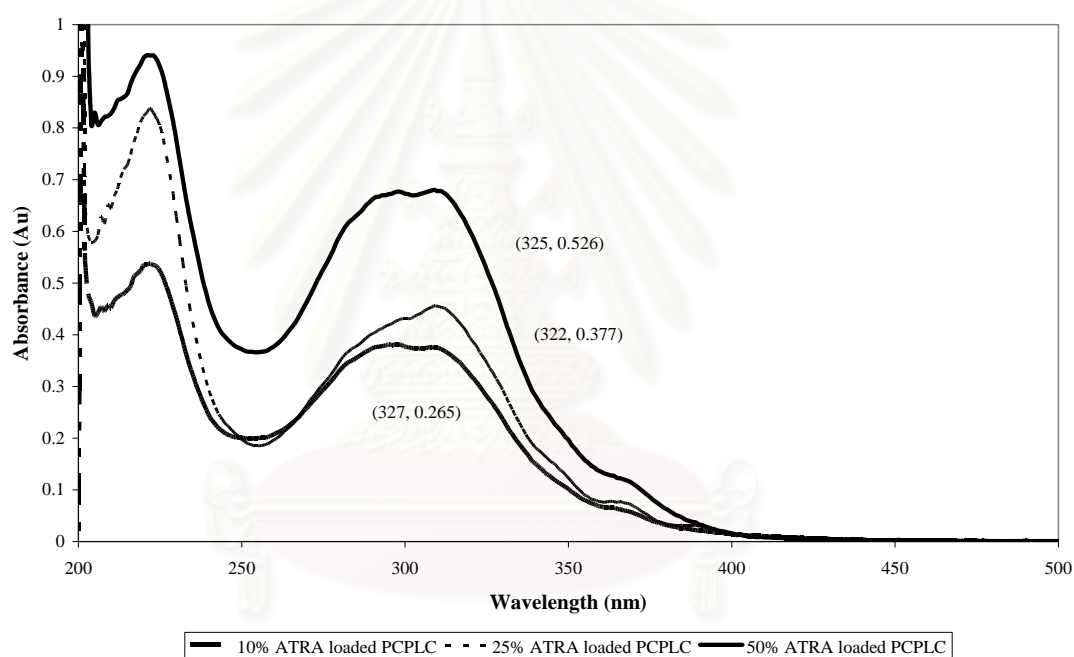


**Figure A.3** UV absorption spectra of all-*trans* retinyl acetate were adhered at the outside of mPEG-4-methoxycinnamoylphthaloylchitosan nanoparticle in ethanol solution.



### 2.1) 10% ATRA loaded PCPLC nanoparticles

The amount of ATRA (10% ATRA to polymer) loaded adhered at the outside of mPEG-4-methoxycinnamoylphthaloylchitosan particles was calculated by equation (1);

$$0.265 = 0.0949x + 0.0034$$

$$X = 2.757 \text{ ppm}$$

Since the ATRA diluted three-fold with ethanol, so the amount of ATRA was  $(2.757 \times 3) = 8.271 \text{ ppm}$ .

$$\therefore 8.271 \text{ ppm} = 8.271 \text{ mg/L}$$

$$\therefore \text{In volumetric 5 mL had all-trans retinyl acetate } (5 \times 8.271)/1000 = 0.0414 \text{ mg.}$$

Weight of the ATRA and mPEG-4-methoxycinnamoylphthaloylchitosan (PCPLC) were 0.2 and 2 mg in 5 mL.

$$\begin{aligned} \therefore \text{Weight of the ATRA loaded into particle} &= 0.2 - 0.0414 \text{ mg} \\ &= 0.1586 \text{ mg} \end{aligned}$$

$$\begin{aligned} \% \text{ drug loading} &= \frac{\text{weight of drug in nanoparticle}}{\text{weight of nanoparticle}} \times 100 & (2) \\ &= (0.1586/2) \times 100 \\ &= 7.93 \% \end{aligned}$$

$$\begin{aligned} \% \text{ encapsulation efficiency (\%EE)} &= \frac{\text{total amount of ATRA- free ATRA}}{\text{total amount of ATRA}} \times 100 & (3) \\ &= [(0.2-0.0414)/0.2] \times 100 \\ &= 79.32 \% \end{aligned}$$

Therefore, % drug loading and % EE of ATRA (10% ATRA to polymer) loaded into mPEG-4-methoxycinnamoylphthaloylchitosan nanoparticle were 7.93 and 79.32%, respectively.

### 2.2) 25% ATRA loaded PCPLC nanoparticles

The amount of ATRA (25% ATRA to polymer) adhered at the outside of mPEG-4-methoxycinnamoylphthaloylchitosan particles was calculated by equation (1);

$$0.377 = 0.0949x + 0.0034$$

$$X = 3.937 \text{ ppm}$$

Since the ATRA diluted three-fold with ethanol, so the amount of ATRA was  $(3.937 \times 3) = 11.811$  ppm.

$$\therefore 11.811 \text{ ppm} = 11.811 \text{ mg/L}$$

$\therefore$  In volumetric 5 mL had all-*trans* retinyl acetate  $(5 \times 11.811)/1000 = 0.0591$  mg.

Weight of the ATRA and mPEG-4-methoxycinnamoylphthaloylchitosan (PCPLC) were 0.5 and 2 mg in 5 mL.

$$\begin{aligned} \therefore \text{Weight of the ATRA loaded into particle} &= 0.5 - 0.0591 \text{ mg} \\ &= 0.4409 \text{ mg} \end{aligned}$$

% drug loading and % EE were calculated by equations (2) and (3), respectively;

$$\begin{aligned} \% \text{ drug loading} &= (0.4409/2) \times 100 \\ &= 22.05 \% \end{aligned}$$

$$\begin{aligned} \% \text{ encapsulation efficiency (\%EE)} &= [(0.5-0.0591)/0.5] \times 100 \\ &= 88.19 \% \end{aligned}$$

Therefore, % drug loading and % EE of ATRA (25% ATRA to polymer) loaded into mPEG-4-methoxycinnamoylphthaloylchitosan nanoparticle were 22.05 and 88.19%, respectively.

### 2.3) 50% ATRA loaded PCPLC nanoparticles

The amount of ATRA (50% ATRA to polymer) adhered at the outside of mPEG-4-methoxycinnamoylphthaloylchitosan particles was calculated by equation (1);

$$0.526 = 0.0949x + 0.0034$$

$$X = 5.507 \text{ ppm}$$

Since the ATRA diluted three-fold with ethanol, so the amount of ATRA was  $(5.507 \times 3) = 16.521$  ppm.

$$\therefore 16.521 \text{ ppm} = 16.521 \text{ mg/L}$$

$\therefore$  In volumetric 5 mL had all-*trans* retinyl acetate  $(5 \times 16.521)/1000 = 0.0826$  mg.

Weight of the ATRA and mPEG-phthaloylchitosan (PPLC) were 1.07 and 2.14 mg in 5 mL.

$$\begin{aligned} \therefore \text{Weight of the ATRA loaded into particle} &= 1.07 - 0.0826 \text{ mg} \\ &= 0.9874 \text{ mg} \end{aligned}$$

% drug loading and % EE were calculated by equations (2) and (3), respectively;

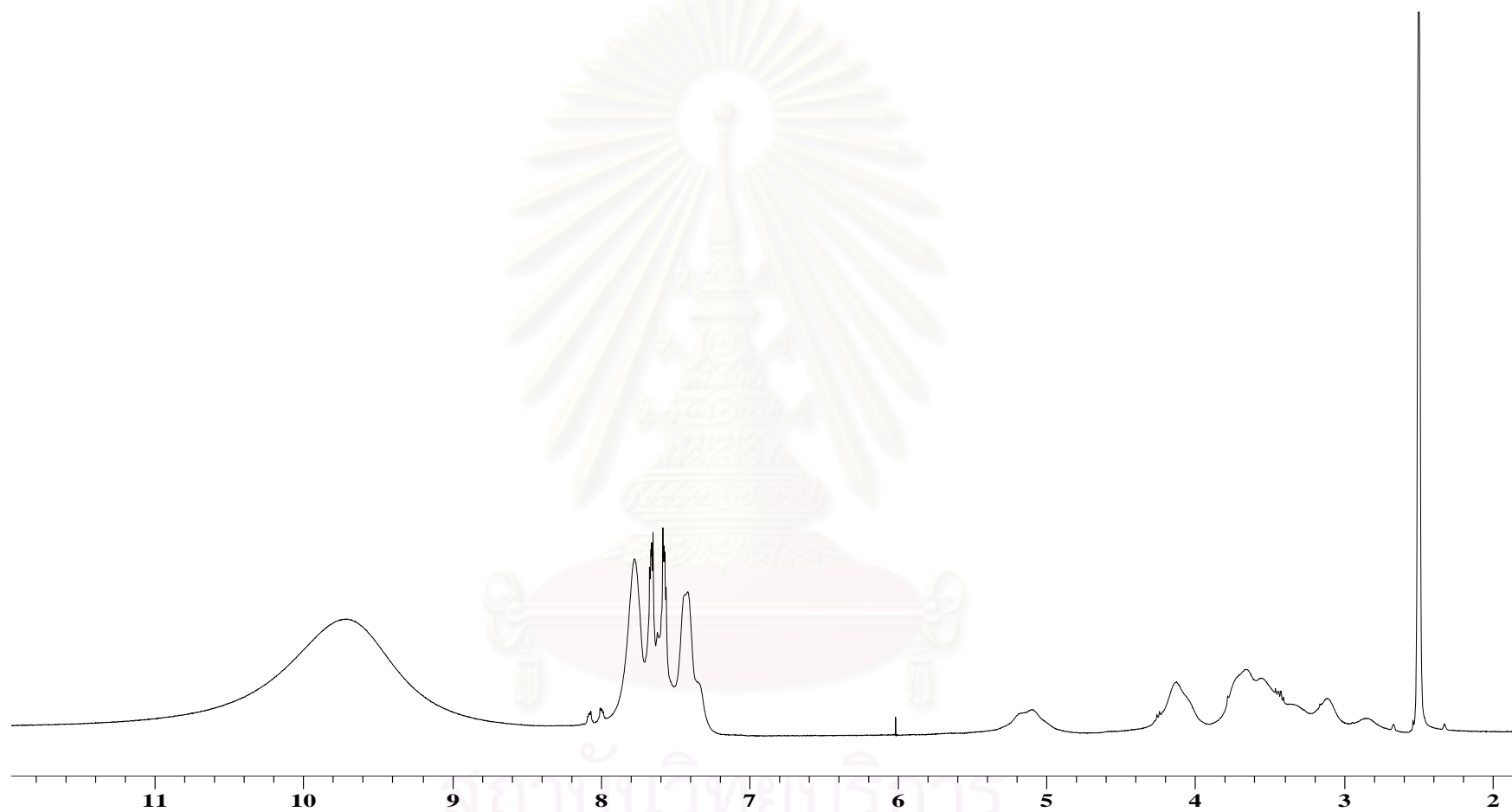
$$\begin{aligned}\% \text{ drug loading} &= (0.9874/2.14) \times 100 \\ &= 46.14\%\end{aligned}$$

$$\begin{aligned}\% \text{ encapsulation efficiency (\%EE)} &= [(1.07 - 0.0826)/1.07] \times 100 \\ &= 92.28 \%\end{aligned}$$

Therefore, % drug loading and % EE of ATRA (50% ATRA to polymer) loaded into mPEG-4-methoxycinnamoylphthaloylchitosan nanoparticle were 46.14 and 92.28%, respectively.



สถาบันวิทยบริการ  
จุฬาลงกรณ์มหาวิทยาลัย

**APPENDIX B**

**Figure B.1** NMR spectrum of phthaloylchitosan (DMSO deuterated with 0.05% trifluoroacetic acid).

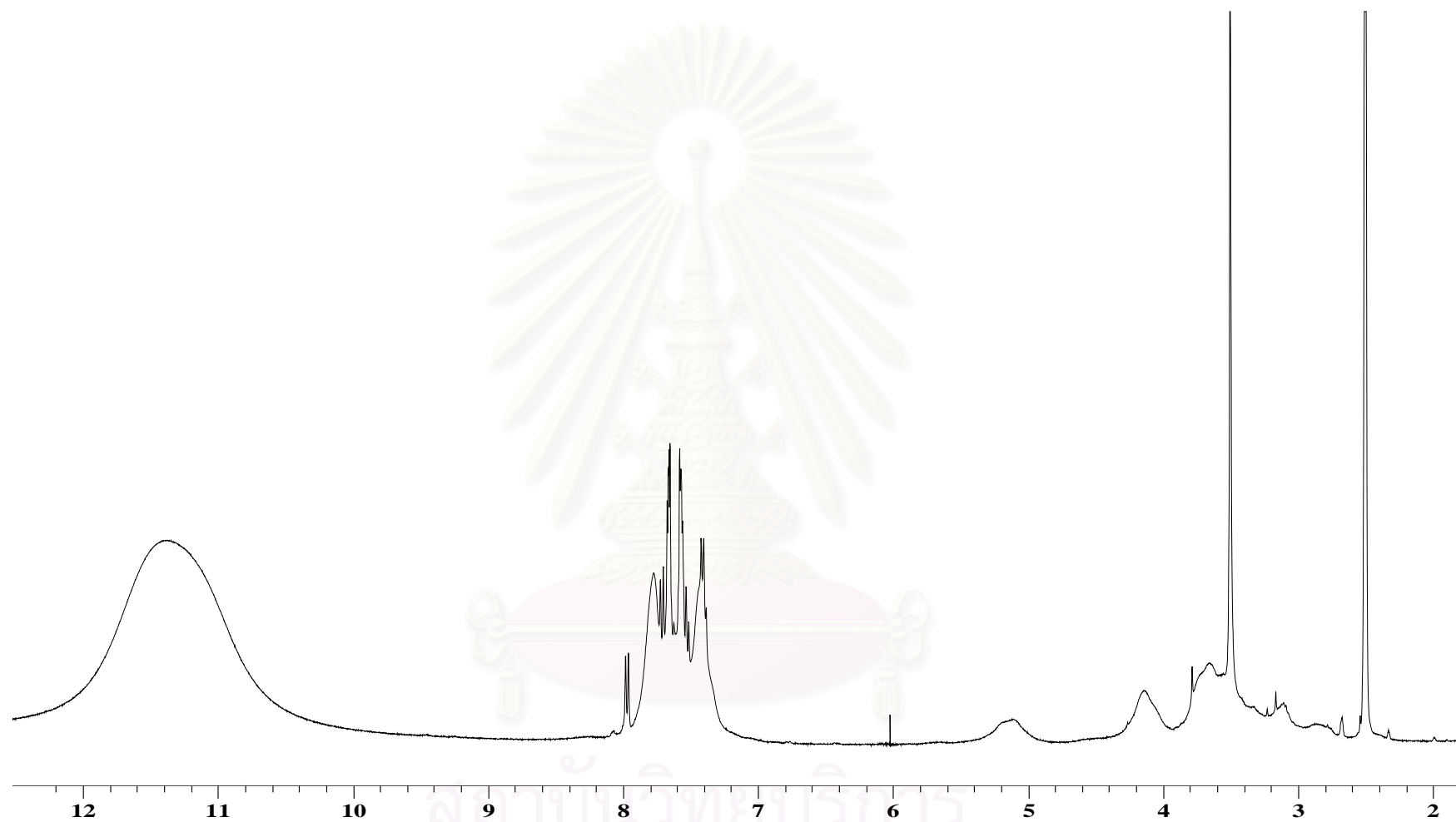


**Figure B.2** NMR spectrum of mPEG-phthaloylchitosan (DMSO deuterated with 0.05% trifluoroacetic acid).

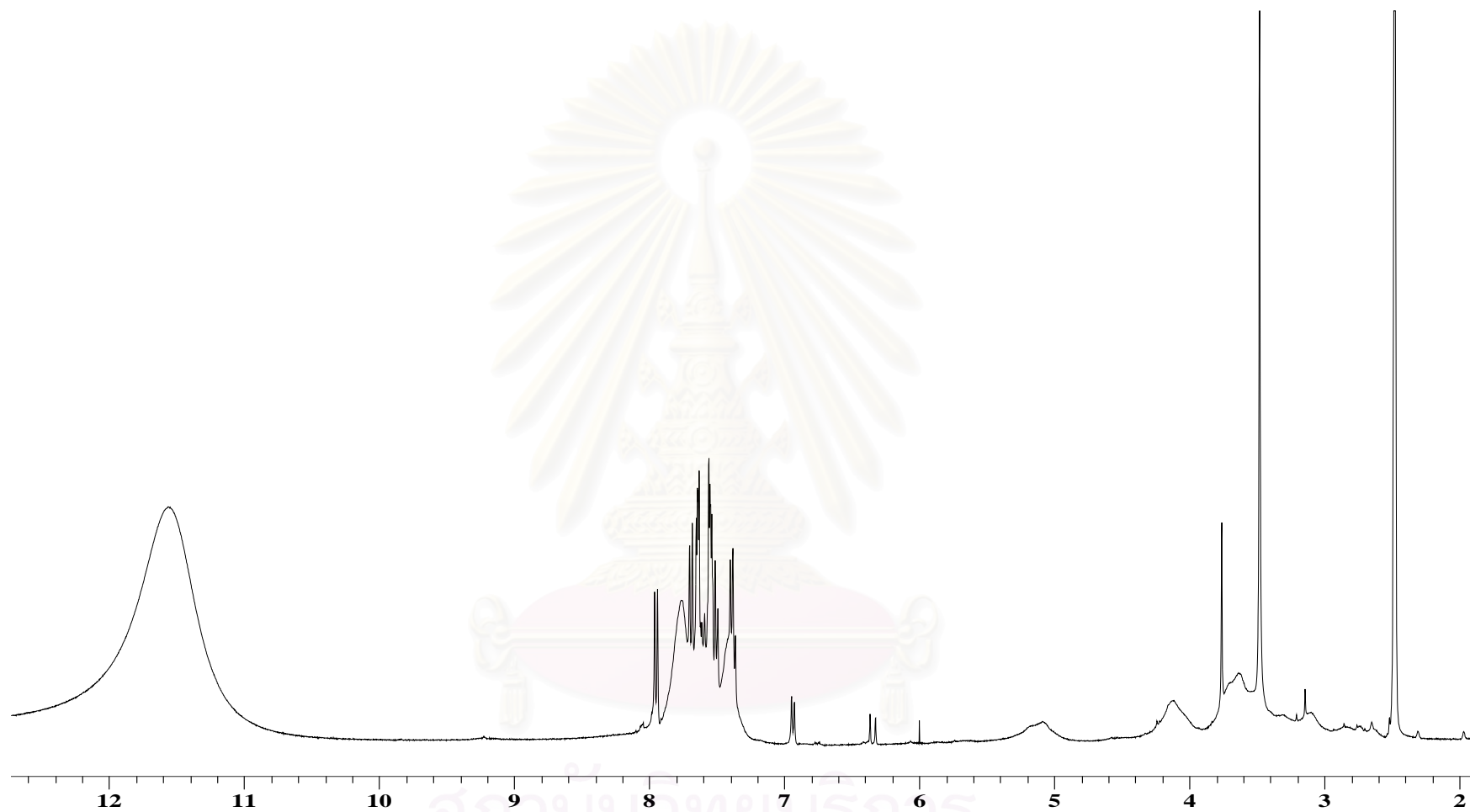


**Figure B.3** NMR spectrum of mPEG-4-methoxycinnamoylphthaloylchitosan (DMSO deuterated with 0.05% trifluoroacetic acid).

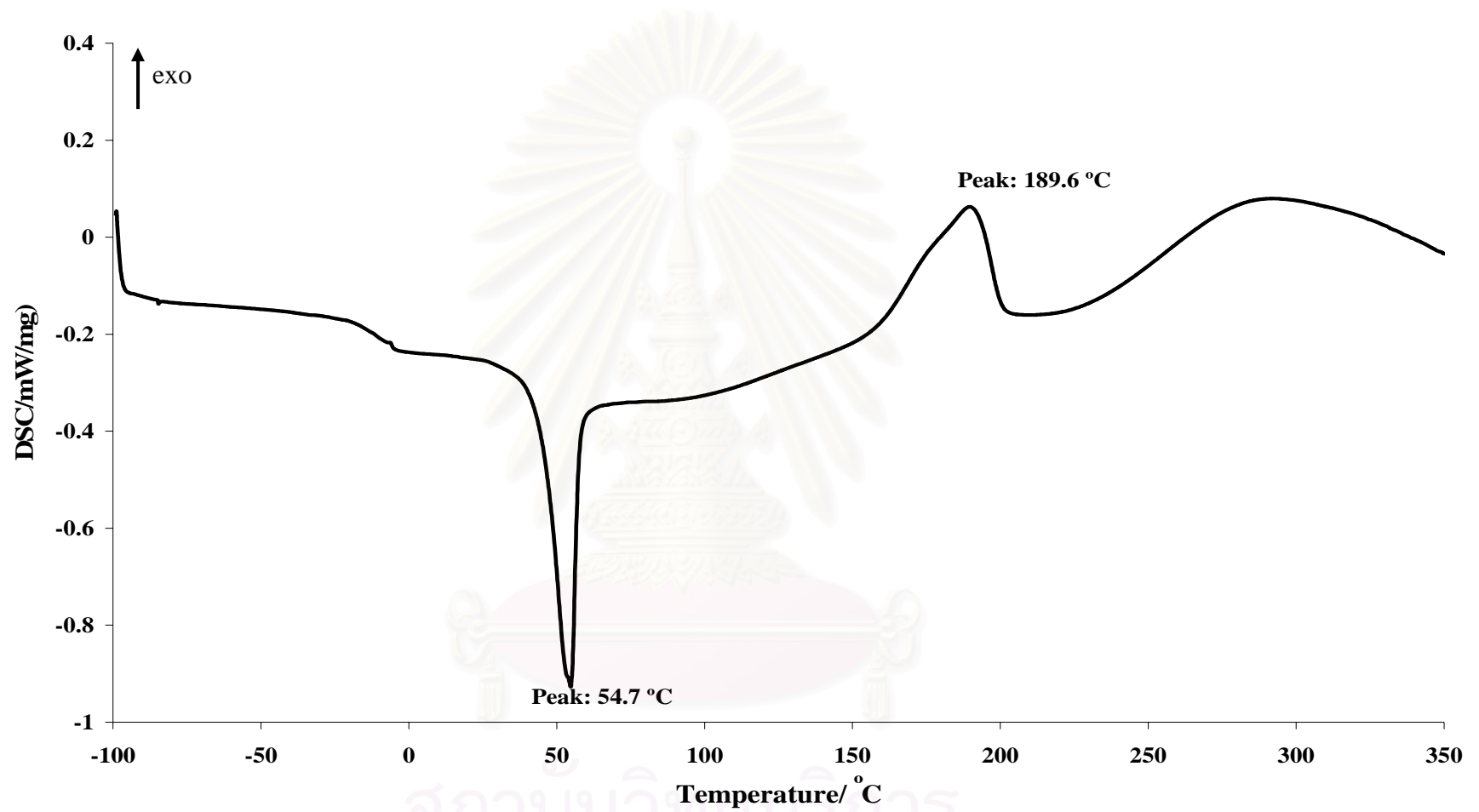


**Figure B.4** First run differential scanning calorimetry (DSC) curve of all-*trans* retinyl acetate.

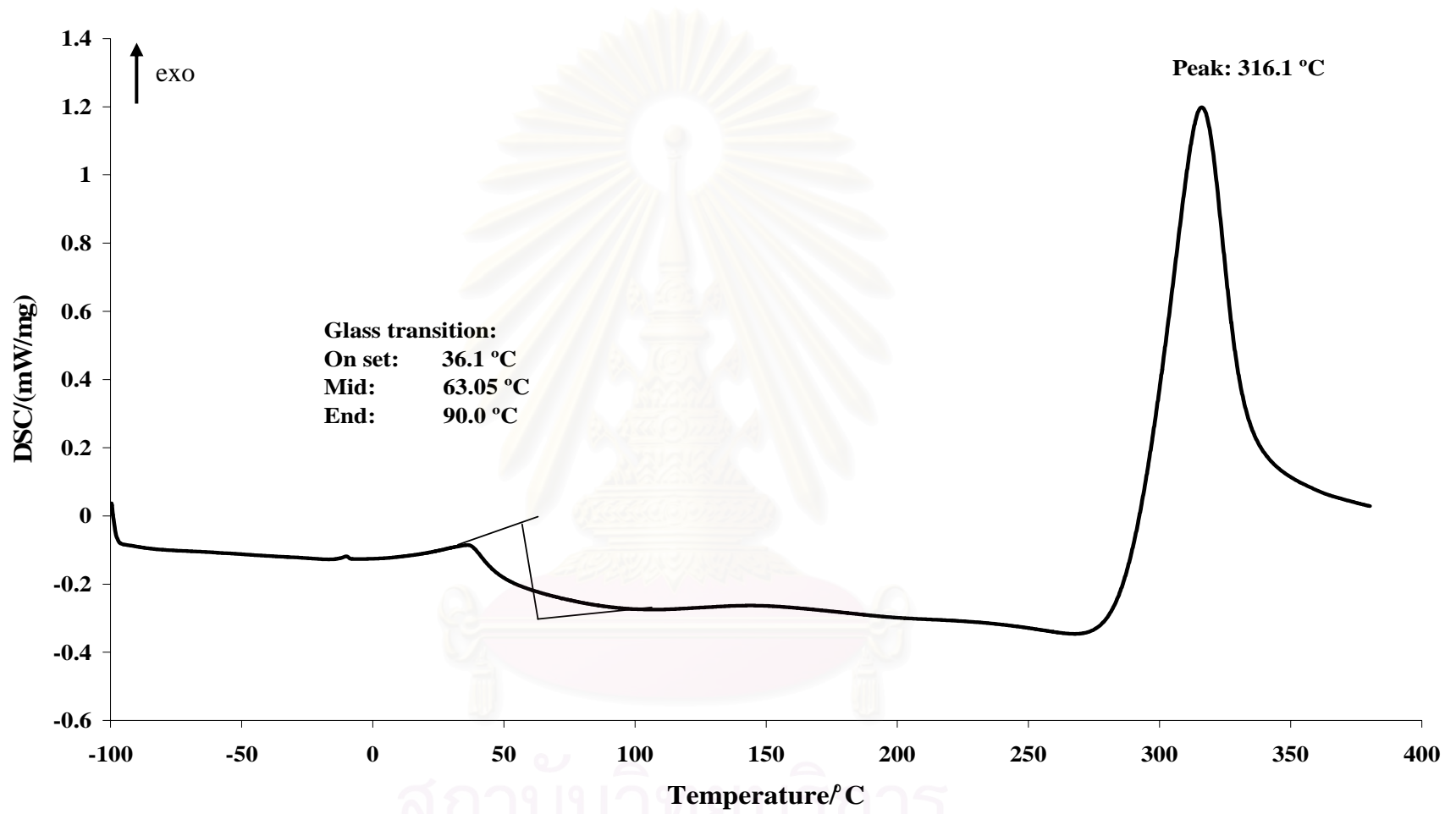
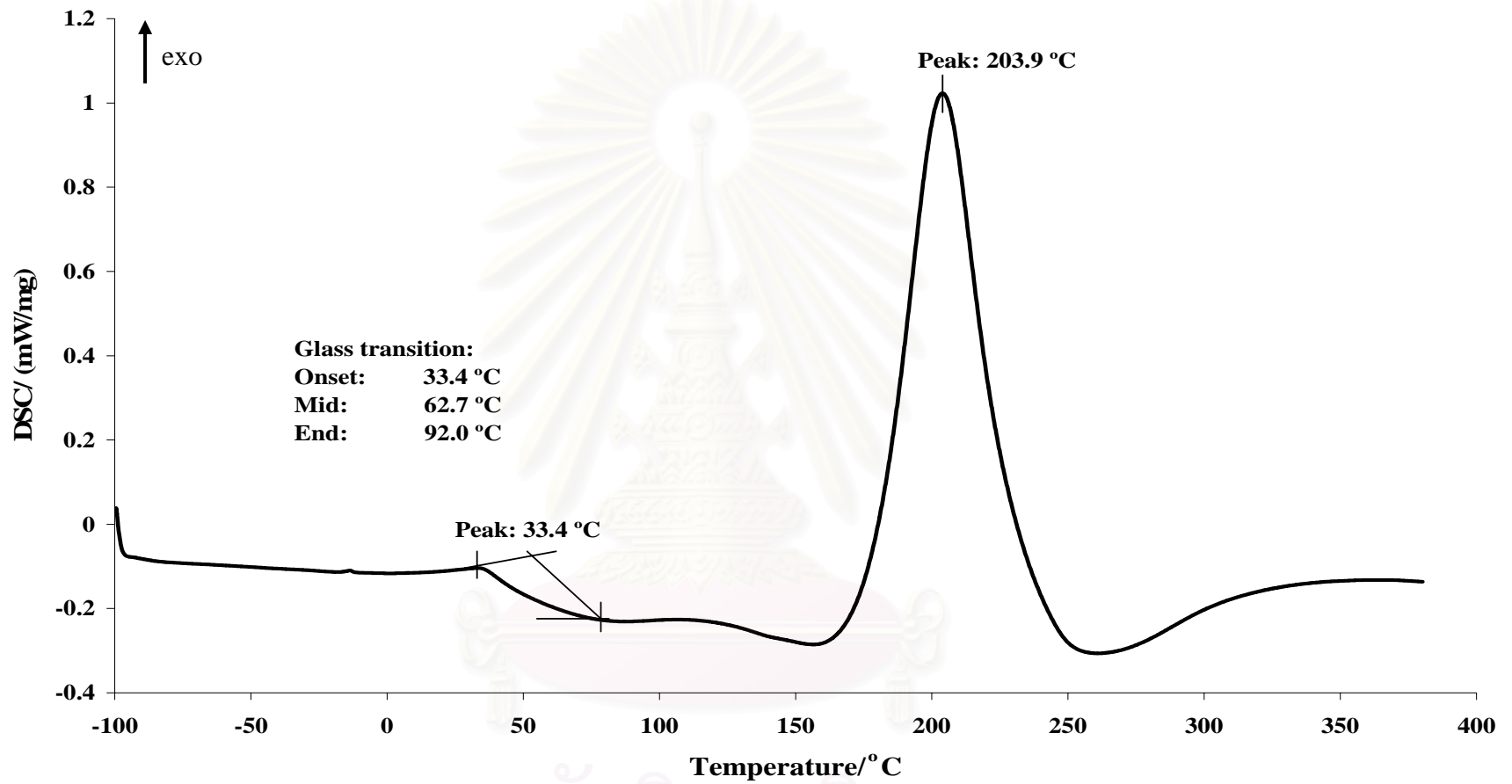


Figure B.5 Second run differential scanning calorimetry (DSC) curve of chitosan.





**Figure B.6** Second run differential scanning calorimetry (DSC) curve of mPEG-phthaloylchitosan nanoparticle.

สถาบันวิทยบริการ  
จุฬาลงกรณ์มหาวิทยาลัย

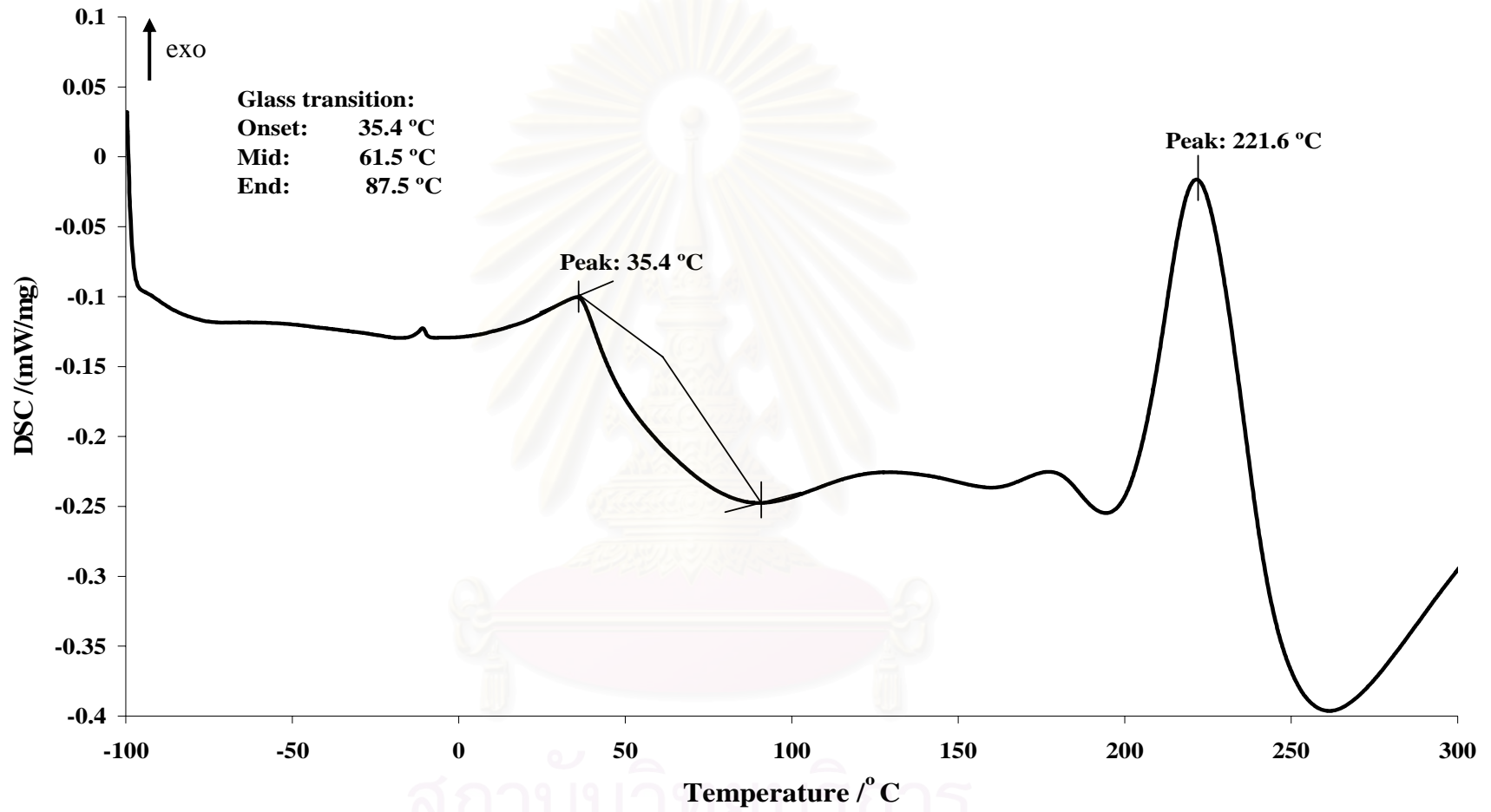


**Figure B.7** Second run differential scanning calorimetry (DSC) curve of mPEG-phthaloylchitosan non-nanostructure.

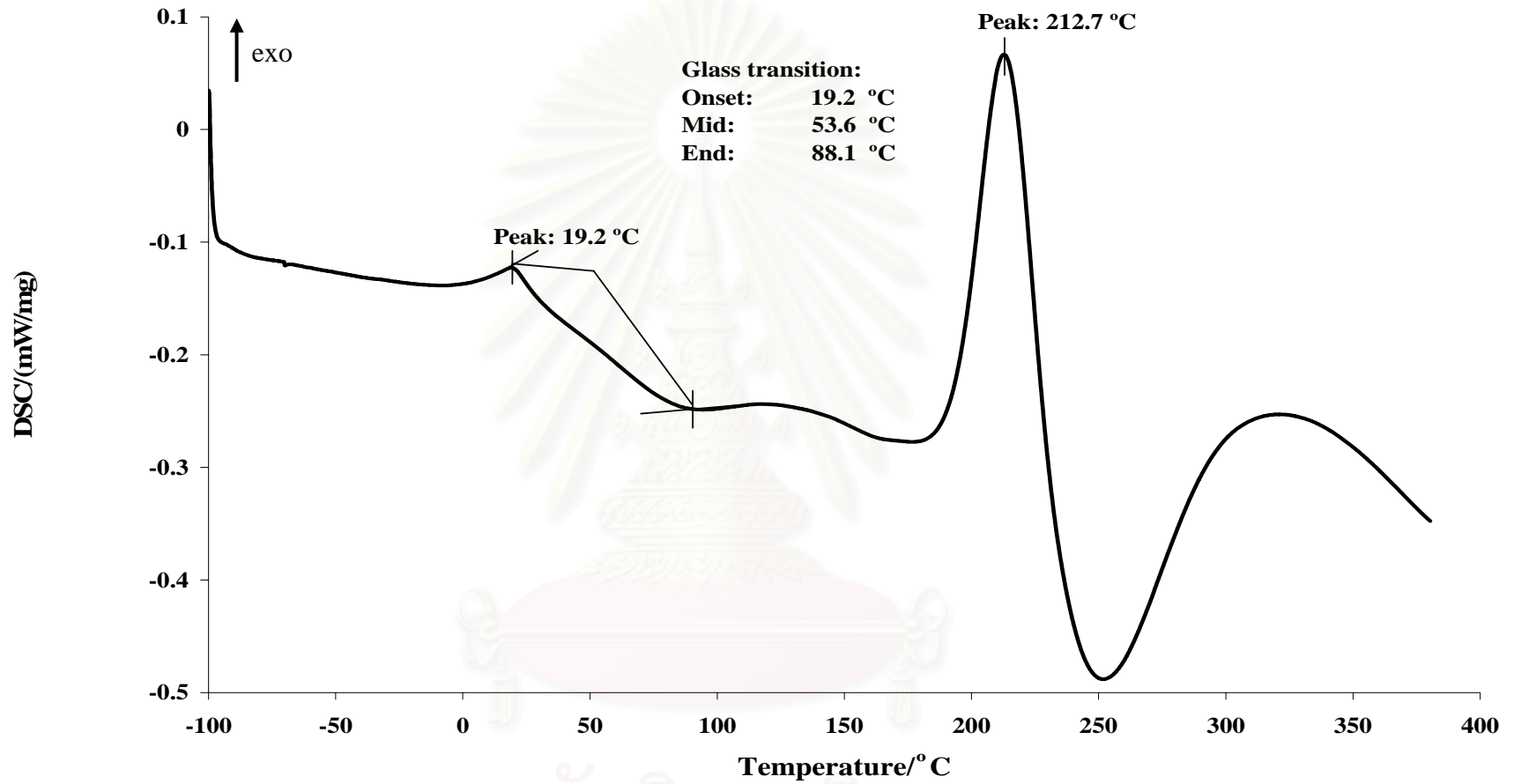


**Figure B.8** Second run differential scanning calorimetry (DSC) curve of ATRA-encapsulated mPEG-phthaloylchitosan nanoparticle.

สถาบันวิทยบริการ  
จุฬาลงกรณ์มหาวิทยาลัย

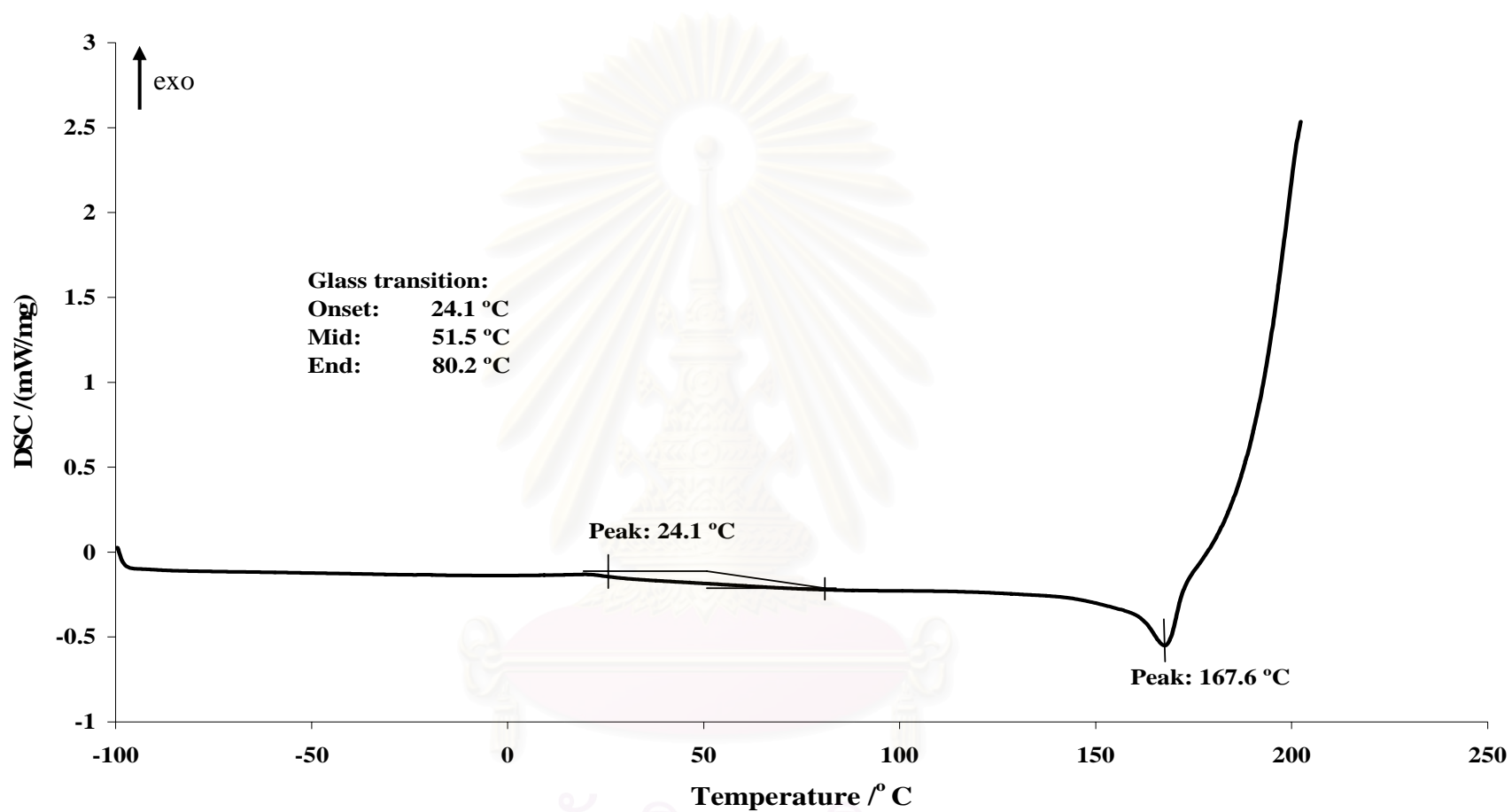


**Figure B.9** Second run differential scanning calorimetry (DSC) curve of mPEG-4-methoxycinnamoylphthaloylchitosan nanoparticle.

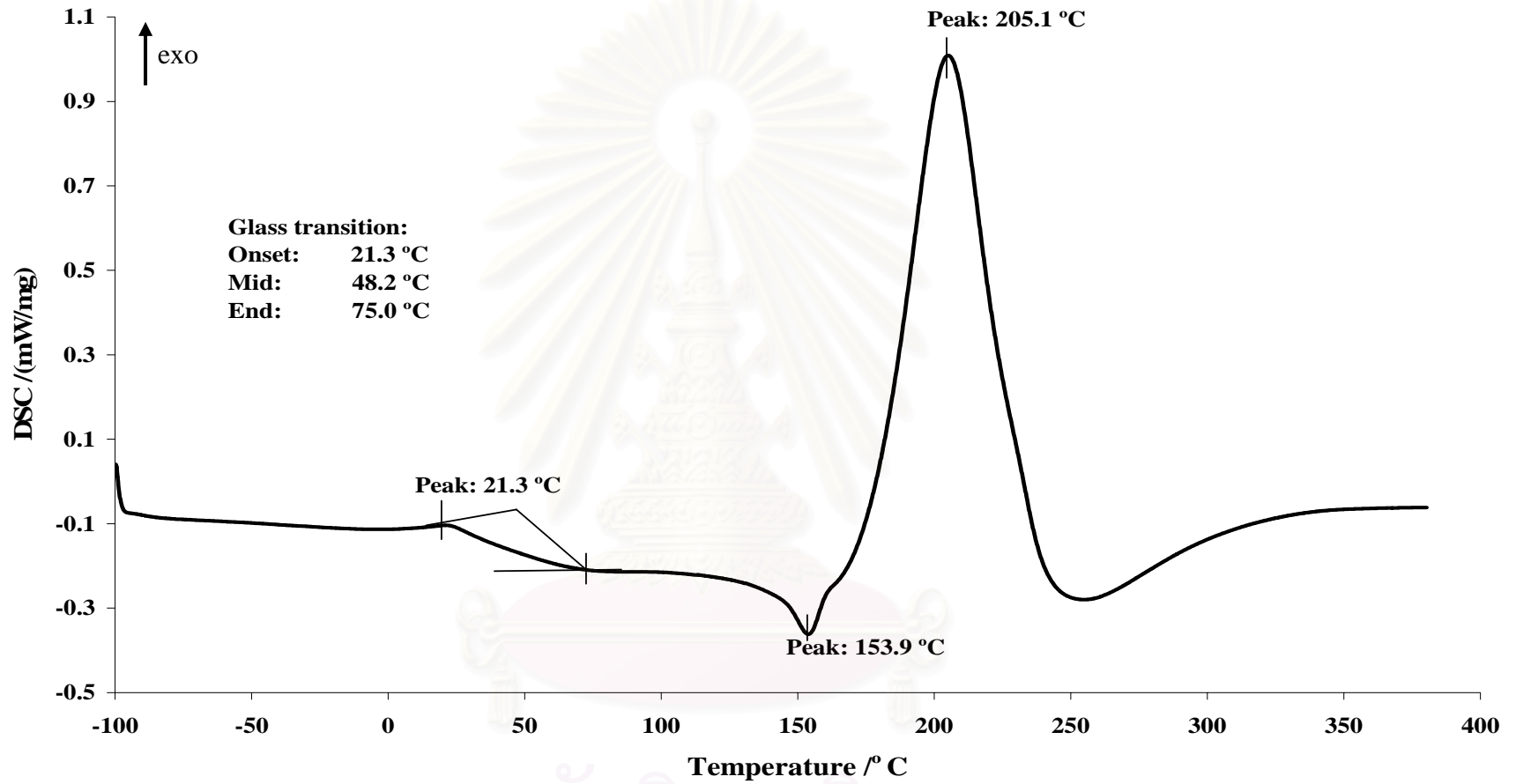


**Figure B.10** Second run differential scanning calorimetry (DSC) curve of mPEG-4-methoxycinnamoylphthaloylchitosan non-nanostructured.

จุฬาลงกรณ์มหาวิทยาลัย

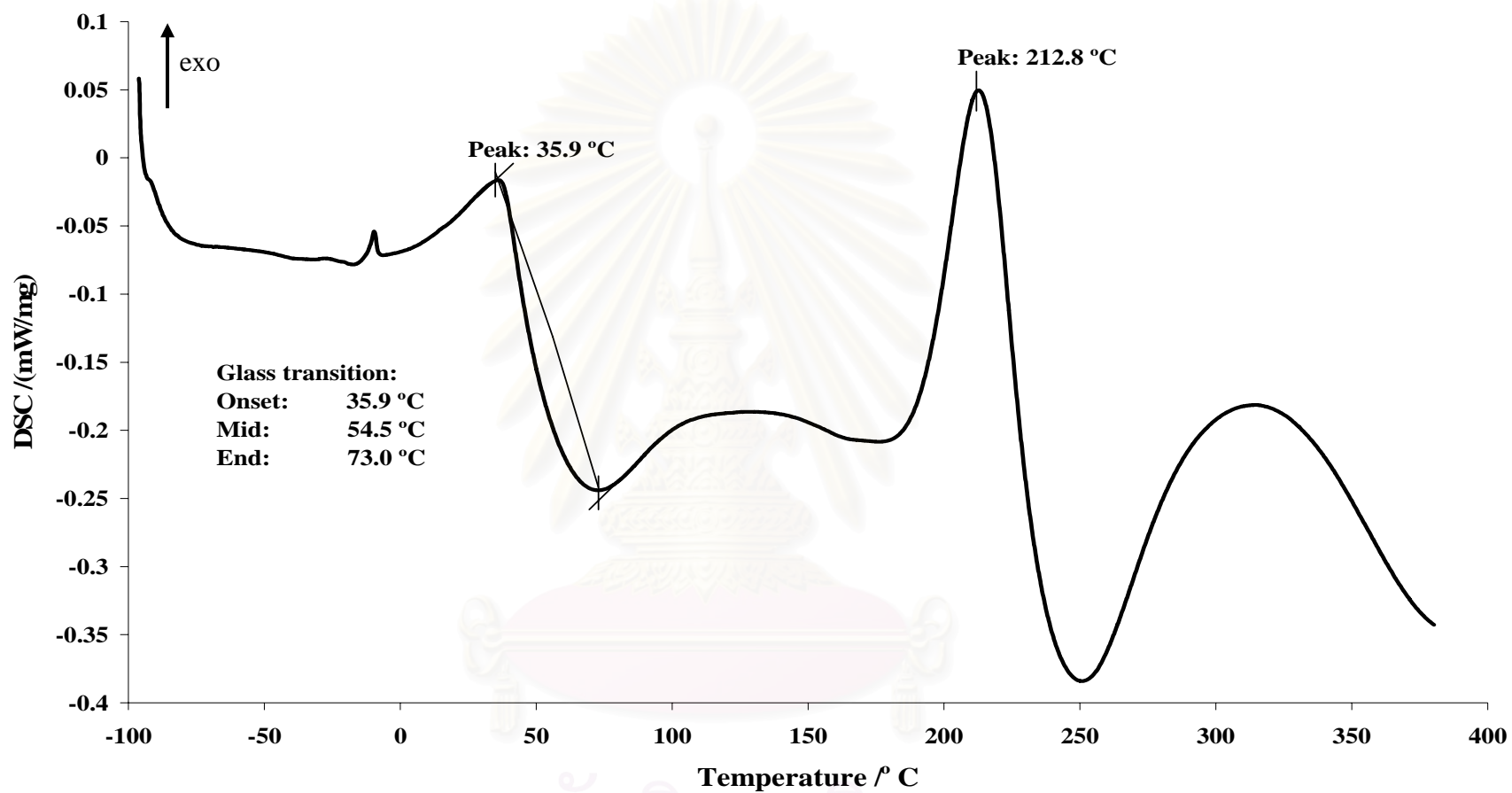


**Figure B.11** Second run differential scanning calorimetry (DSC) curve of ATRA-encapsulated mPEG-4-methoxycinnamoylphthaloylchitosan nanoparticle.

## APPENDIX C

**Table C.1** Growth rate of Gram-positive bacteria *Staphylococcus aureus* ATCC 25923 in Tryptic soy broth.

Time(h)	Absorbance at 600 nm			Average
	Replicate1 (Rep1)	Replicate 2 (Rep2)	Replicate 3 (Rep3)	
0	0.001	0.003	0.004	0.003
2	0.003	0.004	0.004	0.004
4	0.014	0.013	0.019	0.015
5	0.101	0.099	0.110	0.103
6	0.369	0.353	0.359	0.360
6.5	0.492	0.463	0.488	0.481
7	0.709	0.665	0.699	0.691
7.5	0.980	0.930	0.957	0.956
8	1.212	1.181	1.214	1.202
8.5	1.400	1.393	1.411	1.401
9	1.502	1.484	1.501	1.496
9.5	1.572	1.553	1.580	1.568
10	1.619	1.610	1.632	1.620

สถาบันวิทยบริการ  
จุฬาลงกรณ์มหาวิทยาลัย

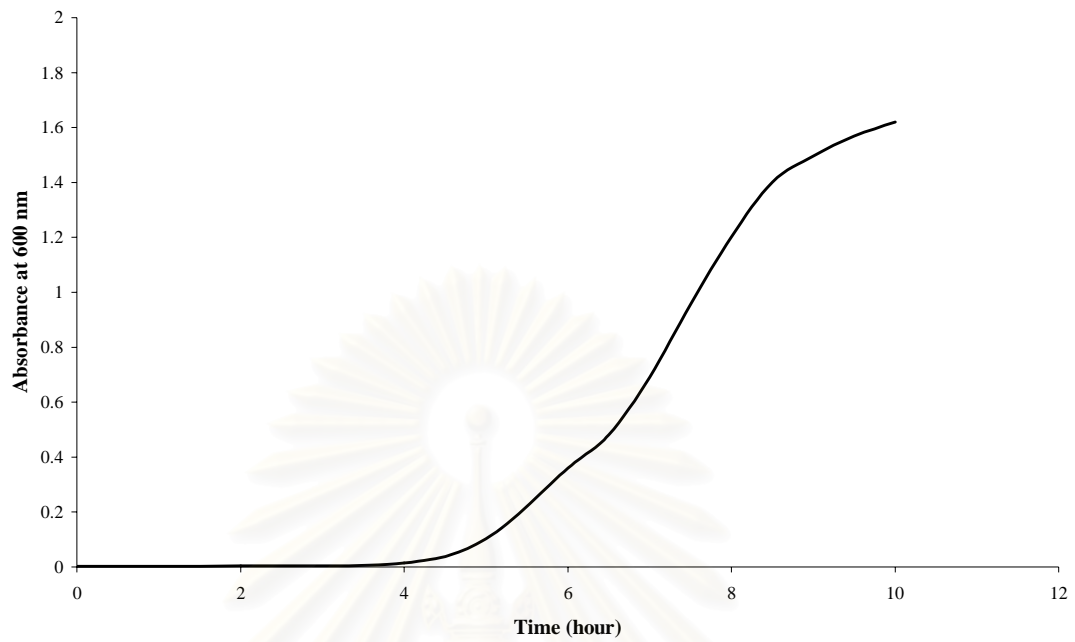


**Figure C.1** Growth curve of Gram-positive bacteria *Staphylococcus aureus* ATCC 25923 in Tryptic soy broth.

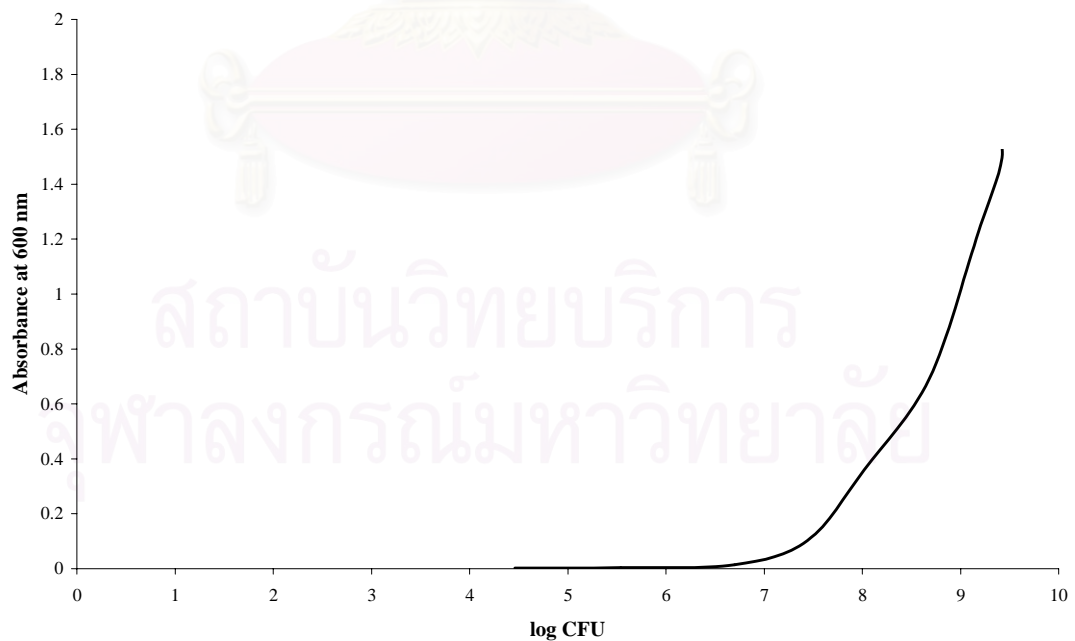


**Figure C.2** Log CFU of Gram-positive bacteria, *Staphylococcus aureus* ATCC 25923 in Tryptic soy agar.



**Table C.2** Growth rate of Gram-negative bacteria, *Escherichia coli* ATCC 25922 in Tryptic soy broth.

Time(h)	Absorbance at 600 nm			Average
	Replicate1 (Rep1)	Replicate 2 (Rep2)	Replicate 3 (Rep3)	
0	0.000	0.000	0.000	0.000
2	0.000	0.000	0.000	0.000
4	0.007	0.004	0.009	0.007
5	0.050	0.054	0.073	0.059
5.5	0.115	0.128	0.171	0.138
6	0.244	0.273	0.349	0.289
6.5	0.461	0.495	0.535	0.497
7	0.732	0.740	0.860	0.777
7.5	0.963	0.982	1.074	1.006
8	1.135	1.144	1.125	1.135
8.5	1.227	1.213	1.320	1.253
9	1.293	1.295	1.382	1.323
9.5	1.327	1.338	1.436	1.367
10	1.374	1.376	1.487	1.412

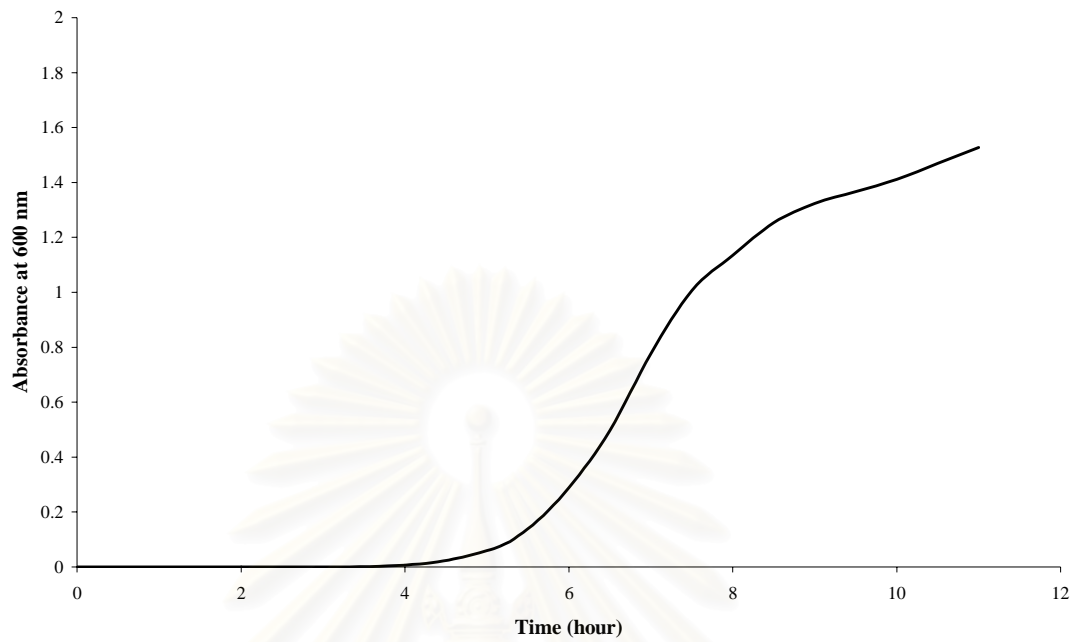


**Figure C.3** Growth curve of Gram-negative bacteria, *Escherichia coli* ATCC 25922 in Tryptic soy broth.

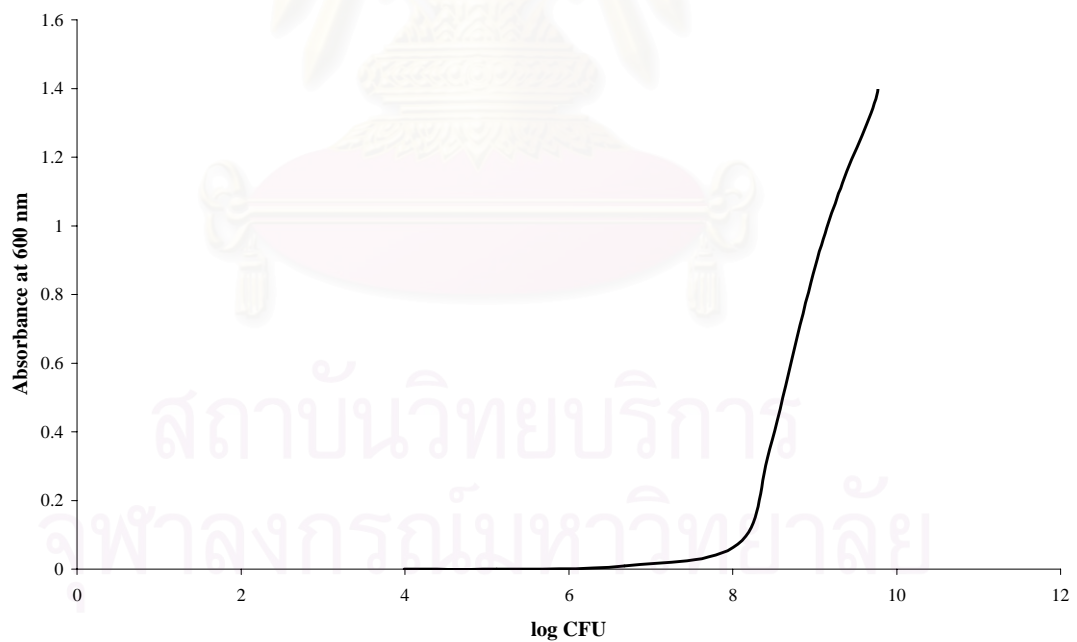


**Figure C.4** Log CFU of Gram-negative bacteria, *Escherichia coli* ATCC 25922 in Tryptic soy agar.

**Table C.3** Growth of Gram-positive bacteria, *Staphylococcus aureus* ATCC 25923 after treated with mPEG-phthaloylchitosan nanoparticle (PPLC) for 24 h at various concentrations.

concentration ( $\mu\text{g/mL}$ )	Absorbance at 600 nm					Absorbance difference between 0 h and 24 h
	0 h	3 h	6 h	12 h	24 h	
2500	2.034	2.000	2.025	2.078	2.096	0.062
1250	1.399	1.447	1.602	1.677	1.797	0.398
625	0.764	0.874	1.139	1.329	1.466	0.702
312	0.384	0.593	0.933	1.152	1.289	0.905
156	0.169	0.392	0.679	1.035	1.250	1.081
78	0.104	0.403	0.819	1.041	1.200	1.096
39	0.057	0.301	0.845	0.998	1.213	1.156
20	0.041	0.365	0.751	1.008	1.162	1.121

**Table C.4** Growth of Gram-positive bacteria, *Staphylococcus aureus* ATCC 25923 after treated with mPEG-4-methoxycinnamoylphthaloylchitosan nanoparticle (PCPLC) for 24 h at various concentrations.

concentration ( $\mu\text{g/mL}$ )	Absorbance at 600 nm					Absorbance difference between 0 h and 24 h
	0 h	3 h	6 h	12 h	24 h	
2500	1.141	1.299	1.417	1.650	1.763	0.622
1250	0.652	0.992	1.226	1.552	1.804	1.152
625	0.342	0.779	1.086	1.446	1.700	1.358
312	0.182	0.606	0.943	1.332	1.446	1.264
156	0.103	0.617	1.009	1.370	1.683	1.580
78	0.059	0.521	0.888	1.282	1.396	1.337
39	0.041	0.562	0.974	1.318	1.471	1.430
20	0.027	0.475	0.789	1.225	1.313	1.286

**Table C.5** Growth of Gram-positive bacteria, *Staphylococcus aureus* ATCC 25923 after treated with chitosan for 24 h at various concentrations.

concentration ( $\mu\text{g/mL}$ )	Absorbance at 600 nm					Absorbance difference between 0 h and 24 h
	0 h	3 h	6 h	12 h	24 h	
2500	0.245	0.042	0.042	0.045	0.038	-0.207
1250	0.954	0.352	0.253	0.215	0.130	-0.824
625	0.949	0.732	0.627	0.530	0.317	-0.632
312	0.672	0.596	0.595	0.536	1.121	0.449
156	0.360	0.420	0.457	0.809	1.357	0.997
78	0.204	0.346	0.185	0.914	1.553	1.349
39	0.112	0.467	0.929	1.397	1.547	1.435
20	0.071	0.561	1.042	1.335	1.465	1.394

**Table C.6** Growth of Gram-positive bacteria, *Staphylococcus aureus* ATCC 25923 after treated with clindamycin for 24 h at various concentrations.

concentration ( $\mu\text{g/mL}$ )	Absorbance at 600 nm					Absorbance difference between 0 h and 24 h
	0 h	3 h	6 h	12 h	24 h	
500	0.005	0.006	0.011	0.017	0.020	0.015
250	0.014	0.020	0.025	0.028	0.037	0.023
125	0.009	0.021	0.027	0.031	0.042	0.033
63	0.008	0.029	0.036	0.040	0.052	0.044
32	0.011	0.024	0.029	0.034	0.093	0.082
16	0.009	0.034	0.037	0.043	0.071	0.062
8	0.015	0.056	0.118	0.259	0.742	0.727
4	0.015	0.153	0.391	0.854	1.056	1.041

**Table C.7** Growth of untreated Gram-positive bacteria, *Staphylococcus aureus* ATCC 25923 after incubated for 24 h.

Control	Time (hour)					Absorbance difference between 0 h and 24 h
	0 h	3 h	6 h	12 h	24 h	
Absorbance at 600 nm	0.008	0.292	0.698	0.970	1.130	1.122

**Table C.8** Growth of *Staphylococcus aureus* ATCC 25923 after tested with mPEG-phthaloylchitosan by a loopful on Tryptic soy agar.

Concentration ( $\mu\text{g/mL}$ )	Rep 1	Rep2	Rep3
2500	✓	✓	✓
1250	✓	✓	✓
625	✓	✓	✓
312	✓	✓	✓
156	✓	✓	✓
78	✓	✓	✓
39	✓	✓	✓
20	✓	✓	✓

**Noted** Symbol ✓ : Bacteria growth was observed

✗ : No bacteria growth was observed

**Table C.9** Growth of *Staphylococcus aureus* ATCC 25923 after tested with mPEG-4-methoxycinnamoylphthaloylchitosan by a loopful on Tryptic soy agar.

Concentration (µg/mL)	Rep 1	Rep2	Rep3
2500	✓	✓	✓
1250	✓	✓	✓
625	✓	✓	✓
312	✓	✓	✓
156	✓	✓	✓
78	✓	✓	✓
39	✓	✓	✓
20	✓	✓	✓

**Noted** Symbol ✓ : Bacteria growth was observed

✗ : No bacteria growth was observed

**Table C.10** Growth of *Staphylococcus aureus* ATCC 25923 after tested with chitosan by a loopful on Tryptic soy agar.

Concentration (µg/mL)	Rep1	Rep2	Rep3
2500	✗	✗	✗
1250	✗	✗	✗
625	✓	✓	✓
312	✓	✓	✓
156	✓	✓	✓
78	✓	✓	✓
39	✓	✓	✓
20	✓	✓	✓

**Noted** Symbol ✓ : Bacteria growth was observed

✗ : No bacteria growth was observed

**Table C.11** Growth of *Staphylococcus aureus* ATCC 25923 after tested with clindamycin by a loopful on Tryptic soy agar.

concentration ( $\mu\text{g/mL}$ )	Rep1	Rep2	Rep3
500	×	×	×
250	×	×	×
125	✓	✓	✓
63	✓	✓	✓
32	✓	✓	✓
16	✓	✓	✓
8	✓	✓	✓
4	✓	✓	✓

**Noted** Symbol ✓ : Bacteria growth was observed

× : No bacteria growth was observed

**Table C.12** Growth of Gram-negative bacteria, *Escherichia coli* ATCC 25922 after treated with mPEG-phthaloylchitosan nanoparticle (PPLC) for 24 h at various concentrations.

concentration ( $\mu\text{g/mL}$ )	Absorbance at 600 nm					Absorbance difference between 0 h and 24 h
	0 h	3 h	6 h	12 h	24 h	
5000	2.384	2.388	2.415	2.445	2.479	0.095
2500	1.834	1.929	1.993	1.986	2.027	0.193
1250	1.110	1.429	1.617	1.652	1.674	0.564
625	0.586	1.069	1.361	1.399	1.441	0.855
312	0.298	0.833	1.156	1.227	1.276	0.978
156	0.160	0.764	1.147	1.203	1.258	1.098
78	0.091	0.699	1.092	1.161	1.210	1.119
39	0.056	0.647	1.092	1.165	1.200	1.144
20	0.041	0.653	1.066	1.134	1.167	1.126
10	0.033	0.686	1.107	1.193	1.226	1.193

**Table C.13** Growth of Gram-negative bacteria, *Escherichia coli* ATCC 25922 after treated with mPEG-4-methoxycinnamoylphthaloylchitosan nanoparticle (PCPLC) for 24 h at various concentrations.

concentration ( $\mu\text{g/mL}$ )	Absorbance at 600 nm					Absorbance difference between 0 h and 24 h
	0 h	3 h	6 h	12 h	24 h	
5000	1.958	2.010	2.033	2.071	2.150	0.192
2500	1.251	1.575	1.768	1.833	2.002	0.751
1250	0.736	1.308	1.516	1.640	1.769	1.033
625	0.423	1.153	1.377	1.454	1.664	1.241
312	0.241	1.055	1.319	1.402	1.493	1.252
156	0.134	0.996	1.150	1.248	1.370	1.236
78	0.087	0.938	1.136	1.257	1.363	1.276
39	0.071	0.935	1.144	1.304	1.447	1.376
20	0.056	0.922	1.139	1.295	1.412	1.356
10	0.043	0.935	1.145	1.284	1.410	1.367

**Table C.14** Growth of Gram-negative bacteria, *Escherichia coli* ATCC 25922 after treated with chitosan for 24 h at various concentrations.

concentration ( $\mu\text{g/mL}$ )	Absorbance at 600 nm					Absorbance difference between 0 h and 24 h
	0 h	3 h	6 h	12 h	24 h	
5000	0.215	0.219	0.215	0.206	0.209	-0.006
2500	0.228	0.082	0.078	0.074	0.03	-0.145
1250	0.659	0.350	0.312	0.237	0.196	-0.463
625	0.975	0.782	0.702	0.592	0.479	-0.496
312	0.716	0.634	0.589	0.519	0.447	-0.269
156	0.438	0.384	0.358	0.292	0.241	-0.197
78	0.245	0.204	0.200	0.804	1.358	1.113
39	0.158	0.285	0.586	1.150	1.149	0.991
20	0.114	0.760	1.068	1.157	1.205	1.091
10	0.076	0.744	0.988	1.046	1.066	0.990



**Table C.15** Growth of Gram-negative bacteria, *Escherichia coli* ATCC 25922 after treated with clindamycin for 24 h at various concentrations.

concentration ( $\mu\text{g/mL}$ )	Absorbance at 600 nm					Absorbance difference between 0 h and 24 h
	0 h	3 h	6 h	12 h	24 h	
5000	0.010	0.012	0.015	0.023	0.025	0.015
2500	0.015	0.013	0.014	0.018	0.019	0.004
1250	0.015	0.016	0.019	0.021	0.021	0.006
500	0.012	0.013	0.016	0.021	0.024	0.012
250	0.016	0.034	0.069	0.184	0.296	0.280
125	0.020	0.091	0.224	0.506	0.583	0.563
63	0.023	0.216	0.477	0.760	1.031	1.008
32	0.026	0.448	0.765	1.066	1.176	1.150
16	0.026	0.555	0.886	1.136	1.248	1.222
8	0.026	0.632	0.934	1.139	1.259	1.233

**Table C.16** Growth of untreated Gram-negative bacteria, *Escherichia coli* ATCC 25922 after incubated for 24 h.

Control	Time (hour)					Absorbance difference between 0 h and 24 h
	0 h	3 h	6 h	12 h	24 h	
Absorbance at 600 nm	0.019	0.610	1.011	1.132	1.218	1.199

**Table C.17** Growth of *Escherichia coli* ATCC 25922 after tested with mPEG-phthaloylchitosan by a loopful on Tryptic soy agar.

Concentration (µg/mL)	Rep 1	Rep2	Rep3
5000	✓	✓	✓
2500	✓	✓	✓
1250	✓	✓	✓
625	✓	✓	✓
312	✓	✓	✓
156	✓	✓	✓
78	✓	✓	✓
39	✓	✓	✓
20	✓	✓	✓
10	✓	✓	✓

**Noted** Symbol ✓ : Bacteria growth was observed

✗ : No bacteria growth was observed

**Table C.18** Growth of *Escherichia coli* ATCC 25922 after tested with mPEG-4-methoxycinnamoylphthaloylchitosan by a loopful on Tryptic soy agar.

Concentration (µg/mL)	Rep 1	Rep2	Rep3
5000	✓	✓	✓
2500	✓	✓	✓
1250	✓	✓	✓
625	✓	✓	✓
312	✓	✓	✓
156	✓	✓	✓
78	✓	✓	✓
39	✓	✓	✓
20	✓	✓	✓
10	✓	✓	✓

**Noted** Symbol ✓ : Bacteria growth was observed

✗ : No bacteria growth was observed

**Table C.19** Growth of *Escherichia coli* ATCC 25922 after tested with chitosan by a loopful on Tryptic soy agar.

Concentration (µg/mL)	Rep 1	Rep2	Rep3
5000	×	×	×
2500	×	×	×
1250	×	×	×
625	✓	✓	✓
312	✓	✓	✓
156	✓	✓	✓
78	✓	✓	✓
39	✓	✓	✓
20	✓	✓	✓
10	✓	✓	✓

**Noted** Symbol ✓ : Bacteria growth was observed

× : No bacteria growth was observed

**Table C.20** Growth of *Escherichia coli* ATCC 25922 after tested with clindamycin by a loopful on Tryptic soy agar.

Concentration (µg/mL)	Rep 1	Rep2	Rep3
5000	×	×	×
2500	×	×	×
1250	✓	✓	✓
500	✓	✓	✓
250	✓	✓	✓
125	✓	✓	✓
63	✓	✓	✓
32	✓	✓	✓
16	✓	✓	✓
8	✓	✓	✓

**Noted** Symbol ✓ : Bacteria growth was observed

× : No bacteria growth was observed

### Survival cell count

#### 1. *Staphylococcus aureus* ATCC 25923

**Table C.21** Growth of Gram-positive bacteria, *Staphylococcus aureus* ATCC 25923 after treated with mPEG-phthaloylchitosan nanoparticle (PPLC) for 24 h at concentration 2500  $\mu\text{g/mL}$ .

Sam Rep	Absorbance at 600 nm					Absorbance difference between 0 h and 24 h
	0 hr.	3 hr.	6 hr.	12 hr.	24 hr.	
Rep1	2.048	2.050	2.067	2.075	2.112	
Rep2	2.029	2.041	2.051	2.063	2.099	
Rep3	2.036	2.034	2.048	2.056	2.084	
Average	2.038	2.042	2.055	2.065	2.098	0.060

**Table C.22** Growth of Gram-positive bacteria, *Staphylococcus aureus* ATCC 25923 after treated with mPEG-4-methoxycinnamoylphthaloylchitosan nanoparticle (PCPLC) for 24 h at concentration 2500  $\mu\text{g/mL}$ .

Sam Rep	Absorbance at 600 nm					Absorbance difference between 0 h and 24 h
	0 hr.	3 hr.	6 hr.	12 hr.	24 hr.	
Rep1	1.261	1.256	1.243	1.305	1.569	
Rep2	1.238	1.182	1.260	1.294	1.554	
Rep3	1.234	1.189	1.228	1.321	1.579	
Average	1.244	1.209	1.244	1.307	1.567	0.323

**Table C.23** Growth of Gram-positive bacteria, *Staphylococcus aureus* ATCC 25923 after treated with clindamycin for 24 h at concentration 250 µg/mL.

Sam Rep	Absorbance at 600 nm					Absorbance difference between 0 h and 24 h
	0 hr.	3 hr.	6 hr.	12 hr.	24 hr.	
Rep1	0.007	0.003	0.007	0.003	0.004	
Rep2	0.004	0.000	0.001	0.000	0.000	
Rep3	0.005	0.000	0.003	0.000	0.000	
average	0.005	0.001	0.004	0.001	0.001	-0.004

**Table C.24** Growth of untreated Gram-positive bacteria, *Staphylococcus aureus* ATCC 25923 after incubated for 24 h.

Sam Rep	Absorbance at 600 nm					Absorbance difference between 0 h and 24 h
	0 hr.	3 hr.	6 hr.	12 hr.	24 hr.	
Rep1	0.000	0.000	0.004	0.656	0.986	
Rep2	0.000	0.000	0.007	0.749	1.011	
Rep3	0.000	0.000	0.002	0.816	1.129	
Average	0.000	0.000	0.004	0.740	1.042	1.042

**Table C.25** Log CFU/mL of Gram-positive bacteria, *Staphylococcus aureus* ATCC 25923 after treated with mPEG-phthaloylchitosan nanoparticle (PPLC) at concentration 2500 µg/mL for 24 h.

No. of Replicate	Rep 1	Rep 2	Rep 3
		$3.72 \times 10^8$	$2.99 \times 10^8$
Average	$3.36 \times 10^8$		

**Table C.26** Log CFU/mL of Gram-positive bacteria, *Staphylococcus aureus* ATCC 25923 after treated with mPEG-4-methoxycinnamoylphthaloylchitosan nanoparticle (PCPLC) at concentration 2500  $\mu\text{g/mL}$  for 24 h.

No. of Replicate	Rep 1	Rep 2	Rep 3
	$2.67 \times 10^{10}$	$3.45 \times 10^{10}$	$4.17 \times 10^{10}$
<b>Average</b>	$3.43 \times 10^{10}$		

**Table C.27** Log CFU/mL of Gram-positive bacteria, *Staphylococcus aureus* ATCC 25923 after treated with clindamycin at concentration 250  $\mu\text{g/mL}$  for 24 h.

No. of Replicate	Rep 1	Rep 2	Rep 3
	0	0	0
<b>Average</b>	0		

**Table C.28** Log CFU/mL of untreated Gram-positive bacteria, *Staphylococcus aureus* ATCC 25923 after incubated for 24 h.

No. of Replicate	Rep 1	Rep 2	Rep 3
	$2.76 \times 10^{14}$	$2.5 \times 10^{14}$	$4.49 \times 10^{14}$
<b>Average</b>	$3.25 \times 10^{14}$		

## 2. *Escherichia coli* ATCC 25922

- Starting number of bacteria was  $8.37 \times 10^5$

**Table C.29** Growth of Gram-negative bacteria, *Escherichia coli* ATCC 25922 after treated with mPEG-phthaloylchitosan nanoparticle (PPLC) for 24 h at concentration 5000  $\mu\text{g/mL}$ .

Sam Rep	Absorbance at 600 nm					Absorbance difference between 0 h and 24 h
	0 hr.	3 hr.	6 hr.	12 hr.	24 hr.	
Rep1	2.358	2.374	2.353	2.431	2.441	
Rep2	2.340	2.358	2.350	2.420	2.438	
Rep3	2.345	2.339	2.346	2.400	2.429	
average	2.348	2.357	2.350	2.420	2.436	0.088

**Table C.30** Growth of Gram-negative bacteria, *Escherichia coli* ATCC 25922 after treated with mPEG-4-methoxycinnamoylphthaloylchitosan nanoparticle (PCPLC) for 24 h at concentration 5000  $\mu\text{g/mL}$ .

Sam Rep	Absorbance at 600 nm					Absorbance difference between 0 h and 24 h
	0 hr.	3 hr.	6 hr.	12 hr.	24 hr.	
Rep1	1.918	1.921	1.935	2.008	2.136	
Rep2	1.853	1.848	1.838	1.971	2.130	
Rep3	1.883	1.867	1.868	1.999	2.142	
average	1.885	1.879	1.880	1.993	2.136	0.251

**Table C.31** Growth of Gram-negative bacteria, *Escherichia coli* ATCC 25922 after treated with clindamycin for 24 h at concentration 2500 µg/mL.

Sam Rep	Absorbance at 600 nm					Absorbance difference between 0 h and 24 h
	0 hr.	3 hr.	6 hr.	12 hr.	24 hr.	
Rep1	0.000	0.000	0.000	0.000	0.000	
Rep2	0.000	0.002	0.000	0.003	0.003	
Rep3	0.000	0.000	0.000	0.000	0.000	
average	0.000	0.000	0.000	0.001	0.001	0.001

**Table C.32** Growth of untreated Gram-negative bacteria, *Escherichia coli* ATCC 25922 after incubated for 24 h.

Sam Rep	Absorbance at 600 nm					Absorbance difference between 0 h and 24 h
	0 hr.	3 hr.	6 hr.	12 hr.	24 hr.	
Rep1	0.000	0.000	0.053	0.896	1.130	
Rep2	0.000	0.000	0.056	0.897	1.142	
Rep3	0.000	0.000	0.050	0.899	1.163	
Average	0.000	0.000	0.053	0.897	1.145	1.145

**Table C.33** Log CFU/mL of untreated Gram-negative bacteria, *Escherichia coli* ATCC 25922 after treated with mPEG-phthaloylchitosan nanoparticle (PPLC) at concentration 5000 µg/mL for 24 h.

No. of Replicate	Rep 1	Rep 2	Rep 3
		4.06 x 10 <sup>9</sup>	3.95 x 10 <sup>9</sup>
Average	3.40 x 10 <sup>9</sup>		



**Table C.34** Log CFU/mL of untreated Gram-negative bacteria, *Escherichia coli* ATCC 25922 after treated with mPEG-4-methoxycinnamoylphthaloylchitosan nanoparticle (PCPLC) at concentration 5000 µg/mL for 24 h.

No. of Replicate	Rep 1	Rep 2	Rep 3
	$3.84 \times 10^{10}$	$2.16 \times 10^{10}$	$3.96 \times 10^{10}$
<b>Average</b>	$3.32 \times 10^{10}$		

**Table C.35** Log CFU/mL of untreated Gram-negative bacteria, *Escherichia coli* ATCC 25922 after treated with clindamycin at concentration 2500 µg/mL for 24 h.

No. of Replicate	Rep 1	Rep 2	Rep 3
	0	0	0
<b>Average</b>	0		

**Table C.36** Log CFU/mL of untreated Gram-negative bacteria, *Escherichia coli* ATCC 25922 after incubated for 24 h.

No. of Replicate	Rep 1	Rep 2	Rep 3
	$4.84 \times 10^{14}$	$5.31 \times 10^{14}$	$4.08 \times 10^{14}$
<b>Average</b>	$4.74 \times 10^{14}$		

สถาบันวิทยบริการ  
จุฬาลงกรณ์มหาวิทยาลัย

## VITA

Ms. Mayura Wittayasuporn was born on March 18, 1982 in Bangkok. She received a Bachelor's Degree of Science in Biology from Kasetsart University in 2004. After that, she started her graduate study on Master's degree of the Program in Biotechnology, Faculty of Science, Chulalongkorn University. This project was presented in German-Thai Symposium on Nanoscience and Nanotechnology (2007).

My address is 145 Magrood Road, Tumbol Sabarung, Amphur Muang, Pattani 94000.



สถาบันวิทยบริการ  
จุฬาลงกรณ์มหาวิทยาลัย